2022

Inhibition of de novo and the Prion-Like Spread of Amyloidogenesis Using in vitro and in vivo Disease Models

Johnson Anazoba Joseph
University of Denver

Inhibition of de novo and the Prion-Like Spread of Amyloidogenesis Using in vitro and in vivo Disease Models

Abstract

The aberrant fibrous, extracellular, and intracellular proteinaceous deposits in cells, organs and tissues are referred to as amyloids. These deposits are dominated by β-sheet structures that have been implicated in several neurodegenerative diseases and cancer. In this work, the types of amyloidosis studied include Parkinson's disease (PD) using UA196 and NL5901 strains of *Caenorhabditis elegans (C. elegans)*, Alzheimer's disease (AD) using GMC101 strain of *C. elegans*, and cancer-associated mutant p53 aggregation in MIA PaCa-2 mutant cells. Several molecules including SK-129, NS132, NS163, bexarotene, a polyphenol (-)-epi-gallocatechine gallate (EGCG), ADH40, RD148, and RD242 were screened *in vitro* and *in vivo* while studying the inhibition of the amyloid protein aggregation. Also, the prion-like spread of amyloid fibrils was studied (through secondary nucleation) in NL5901 strain of *C. elegans* using α-Synuclein (αS) preformed fibrils and in MIA-PaCa-2 cells using p53 preformed fibrils. Various techniques were used in this study including paralysis assay, Thioflavin T (ThT) assay, immunofluorescence (IF) assay, confocal imaging, Proteomics analysis, Western Blot (WB) analysis to study the locomotion of *C. elegans*, to determine the amyloid fibril content *in vitro* and *in vivo*, determine upregulated and downregulated proteins in cells, and identify target proteins through immunoblotting of cell lysates, respectively. Oligopyridylamides (OPs) and Oligoquinolines (OQs) displayed remarkable neuroprotective effects in DA neurons and rescued various PD phenotypes of *C. elegans*, including rescue of degeneration of DA neurons, improved motility rate, decreased reactive oxygen species, food-sensing behavioral deficits, and rescue of dopamine synthesis. Also, we demonstrated that OPs rescue PD phenotypes when administered to the post-disease-onset *C. elegans* model. The results from this study proposed that SK-129, NS132, NS163, bexarotene, EGCG, ADH40, RD148, and RD242 are potent antagonists for amyloid protein aggregation.

Document Type

Thesis

Degree Name

M.S.

Department

Chemistry and Biochemistry

First Advisor

Sunil Kumar

Second Advisor

Daniel Linseman

Third Advisor

Martin Margittai

Keywords

Alzheimer's disease, Amyloids, Caenorhabditis elegans, Cancer, Neurodegenerative diseases, Parkinson's disease

Inhibition of *de novo* and the prion-like spread of amyloidogenesis using *in vitro* and *in vivo* disease models

A Thesis

Presented to

the Faculty of the College of Natural Sciences and Mathematics

University of Denver

In Partial Fulfillment

of the Requirements for the Degree

Master of Science

by

Johnson Anazoba Joseph

August 2022

Advisor: Dr. Sunil Kumar, Ph.D.

Author: Johnson Anazoba Joseph
Title: Inhibition of *de novo* and the prion-like spread of amyloidogenesis using *in vitro* and *in vivo* disease models
Advisor: Dr. Sunil Kumar, Ph.D.
Degree Date: August 2022

Abstract

The aberrant fibrous, extracellular, and intracellular proteinaceous deposits in cells, organs and tissues are referred to as amyloids. These deposits are dominated by β-sheet structures that have been implicated in several neurodegenerative diseases and cancer. In this work, the types of amyloidosis studied include Parkinson's disease (PD) using UA196 and NL5901 strains of *Caenorhabditis elegans (C. elegans),* Alzheimer's disease (AD) using GMC101 strain of *C. elegans*, and cancer-associated mutant p53 aggregation in MIA PaCa-2 mutant cells. Several molecules including SK-129, NS132, NS163, bexarotene, a polyphenol (-)-epi-gallocatechine gallate (EGCG), ADH40, RD148, and RD242 were screened *in vitro* and *in vivo* while studying the inhibition of the amyloid protein aggregation. Also, the prion-like spread of amyloid fibrils was studied (through secondary nucleation) in NL5901 strain of *C. elegans* using α-Synuclein (αS) preformed fibrils and in MIA-PaCa-2 cells using p53 preformed fibrils. Various techniques were used in this study including paralysis assay, Thioflavin T (ThT) assay, immunofluorescence (IF) assay, confocal imaging, Proteomics analysis, Western Blot (WB) analysis to study the locomotion of *C. elegans*, to determine the amyloid fibril content *in vitro* and *in vivo*, determine upregulated and downregulated proteins in cells, and identify target proteins through immunoblotting of cell lysates, respectively. Oligopyridylamides (OPs) and Oligoquinolines (OQs) displayed remarkable neuroprotective effects in DA neurons and rescued various PD phenotypes of *C. elegans*, including rescue of degeneration of DA

neurons, improved motility rate, decreased reactive oxygen species, food-sensing behavioral deficits, and rescue of dopamine synthesis. Also, we demonstrated that OPs rescue PD phenotypes when administered to the post-disease-onset *C. elegans* model. The results from this study proposed that SK-129, NS132, NS163, bexarotene, EGCG, ADH40, RD148, and RD242 are potent antagonists for amyloid protein aggregation.

Acknowledgements

Special thanks to Dr. Sunil Kumar for offering me the opportunity to join his lab as a graduate student and for his enormous research advise and support on my professional career. I am honored to have worked with him. Thanks to the members of my research committee including Dr. Martin Margittai, Dr. Michelle Knowles, and Dr. Daniel Linseman for all their research advise and willingness to be part of my committee. Thanks to Dr. Daniel Paredes and Dr. Briony Catlow for all their research advise and support.

Additionally, special thanks to University of Colorado (CU) Anschutz Medical Campus, Mass Spectrometry Proteomics Core Facility for conducting the Proteomics experiment. Thanks to Dr. Ann Wehman for her contributions on the *C.elegans* studies including Stereo microscopy GFP fluorescence imaging of the animals and donation of SLE1 strain of bacteria for feeding the animals. Thanks to my lab mates especially Jemil Ahmed for his in-depth research advise; Alexandra Thomas, Apshara Siwakoti, Ryan Dohoney, Nick Stillman, Tessa Fitch, Courtney Donnelly, Viviana Martinez, Charles Baysah and Tyler Ball for their research support at various levels.

Finally, thanks to my Fiancée (Kaylee), my child (Bethany), my dad (Joseph) and my mom (Rose) of blessed memories for all their moral support and for training me to become resilient, and the best person I can be.

Table of Contents

Abstract …… ii
Acknowledgements …….. iv
Table of Contents ……. v
List of Figures …….. viii
Abbreviations ……... x

1. Inhibition of de novo and the prion-like spread of α-Synuclein using *in vivo* *C. elegans* disease models …….. 1
    1.1 Introduction …… 1
    1.2 Materials and Methods ……... 8
        1.2.1 Culture methods of *C. elegans* strains ……. 8
        1.2.2 Paralysis assay for NL5901 strain treated with Epigallocatechin gallate (EGCG) using 6 well plate ……... 9
        1.2.3 Paralysis assay for NL5901 strain treated with SK-129 using 6 well plate ……... 10
        1.2.4 Paralysis assay for NL5901 strain treated with SK-129 using 24 well plate ……. 10
        1.2.5 Paralysis assay for NL5901 strain treated with EGCG using 24 well plate ……. 11
        1.2.6 Paralysis assay for NL5901 strain treated with NS163 and NS132 using 24 well plate ……... 11
        1.2.7 Paralysis assay for NL5901 strain treated with SK-6 ……. 11
        1.2.8 Paralysis assay for UA196 strain treated with NS163 and NS132 ……... 11
        1.2.9 Dopamine dependent *C. elegans* (N2 and UA196) assay ….... 12
        1.2.10 Confocal microscopy of early stage treated *C. elegans* (NL5901 and UA196) …….. 12
        1.2.11 Confocal microscopy of post-disease onset PD model of *C. elegans* (UA196) …….. 13
        1.2.12 Chemotaxis assay for *C. elegans* (N2 and UA196) ……..... 13
        1.2.13 Measurement of intracellular Reactive Oxygen Species (ROS) of early stage treated *C. elegans* (UA196) under normal culture conditions ……. 14
        1.2.14 Measurement of intracellular ROS of post disease onset *C.elegans* (UA196) under normal culture conditions …….. 16
        1.2.15 Preparation and conjugation of αS preformed fibrils (PFFs) for prion-like studies …… 16
        1.2.16 Paralysis Assay for transfected NL5901 strain ……. 17
        1.2.17 Sample preparation for Total Proteome Measurements …… 17
            1.2.17.1 Desalting …… 19
            1.2.17.2 Mass spectrometry analysis …… 19
            1.2.17.3 Database Searching and Protein Identification ….. 20
    1.3 Results and discussions …….. 21

1.3.1 Effects of ligands on αS aggregation mediated PD phenotypes in *in vivo C. elegans* models ……. 21
1.3.2 Effect of OPs on the degeneration of DA neurons in a *C. elegans* PD model …… 26
1.3.3 Effect of OPs on the motility rate of UA196 strain …… 28
1.3.4 Effect of OPs on the dopamine level in UA196 strain of *C. elegans* …… 29
1.3.5 Effect of OPs on Behavioral deficits in UA196 strain of *C. elegans* …… 31
1.3.6 Effects of ligands (OPs) on the ROS level in *C. elegans* (N2 and UA196) …… 37
1.3.7 Extensive Proteome analysis during aging of *C. elegans* …… 40
1.3.8 Effects of OPs on the neurodegeneration in a post-disease onset PD model …… 42
1.3.9 Study of the prion-like spread of αS in *C. elegans* model 46
1.4 Conclusions and future work ……. 52

2. Investigation of small molecule inhibitors of amyloid-β (Aβ) aggregation using *C. elegans* models …… 53
2.1 Introduction …… 53
2.2 Materials and Methods ……... 55
2.2.1 Culture methods for *C. elegans* strains ……... 55
2.2.2 Paralysis Assay for GMC101 strain treated with EGCG using 6-well plate ……. 56
2.2.3 Paralysis Assay for GMC101 strain treated with Bexarotene using 6-well plate ……. 56
2.2.4 Paralysis Assay for GMC101 strain treated with EGCG using 24-well plate ……... 56
2.2.5 Paralysis Assay for GMC101 strain treated with Bexarotene using 24-well plate …… 56
2.2.6 Paralysis Assay for GMC101 strain treated with RD242 ….. 57
2.2.7 Staining of GMC101 with NIAD-4 dye …….. 57
2.2.8 Confocal microscopy of GMC101 strain of *C. elegans* ……... 57
2.2.9 Measurement of intracellular Reactive Oxygen Species (ROS) of *C. elegans* (GMC101 and N2 strains) under normal culture conditions ……. 57
2.3 Results and discussions …….. 58
2.3.1 High throughput assay for screening inhibitory molecules of Aβ42 aggregation ……. 58
2.4 Conclusions and future work ……. 65

3. Investigation of the prion-like spread of cancer-associated mutant p53 and its inhibition using MIA PaCa-2 mutant cells …… 66
3.1 Introduction …… 66

3.2 Materials and Methods 72
3.2.1 Cell Culture 72
3.2.2 Preparation of wild type p53 preformed fibrils (pWT PFF) and labeling 72
3.2.3 Thioflavin T (ThT)-based aggregation assay 73
3.2.4 Immunofluorescence assay (IFA) 74
3.2.5 Cell fractionation and western blot analysis 75
3.2.6 The 3-(4,5-dimethylthiazol-2-yl)-2,5-diphenyltetrazolium bromide (MTT)-Based Cytotoxicity Assay (MIA PaCa-2 cells) 76
3.2.7 Thioflavin S (ThS) assay 77
3.2.8 Preparation of peptide with Lipofectamine solution for transfection 78
3.3 Results and discussion 79
3.3.1 RD148 is a potent antagonist for of amyloid formation of the aggregation-nucleating sequence of p53 DBD in an *in vitro* ThT assay 79
3.3.2 RD148 causes selective cytotoxicity in cancer cells bearing mutant p53 82
3.3.3 Prion-like behavior of p53 amyloid aggregates 85
3.4 Conclusions and future work 88
References 91

List of Figures

Figure 1.1 Chemical structures, and molecular weight (MW) of OQ and OPs and reaction mechanism for peptide stapling 7
Figure 1.2 The intracellular inhibition of αS aggregation by SK-129 in NL5901 strain of *C. elegans* 24
Figure 1.3 The intracellular inhibition of αS aggregation by EGCG in NL5901 strain of *C. elegans* 30
Figure 1.4 The intracellular inhibition of αS aggregation by OPs in an *in vivo* PD model 32
Figure 1.5 The intracellular inhibition of αS aggregation by NS132 in an *in vivo* PD model 33
Figure 1.6 The intracellular inhibition of αS aggregation by stapled peptide (SK6) in an *in vivo* PD model 34
Figure 1.7 Neuroprotective effect of OPs on the degeneration of DA neurons 35
Figure 1.8 Chemotaxis assay for the behavior of UA196 in the absence and presence of ligands 38
Figure 1.9 Effect of OPs on the PD phenotypes in UA196 strain 39
Figure 1.10 The effect of ligands on the ROS level in UA196 strain 41
Figure 1.11 Total proteomics analysis of *C. elegans* in the absence and presence of ligands at day seven of adulthood 43
Figure 1.12 The post disease onset intracellular inhibition of αS aggregation in DA neurons by ligands in an *in vivo* PD model 47
Figure 1.13 The post disease onset intracellular inhibition of αS aggregation in DA neurons by ligands in an *in vivo* PD model 48
Figure 1.14 The effect of ligands on the ROS level for post disease onset UA196 strain of *C. elegans* 49
Figure 1.15 Prion-like spread of αS in NL5901 strain of *C. elegans* 51

Figure 2.1 Chemical structures and MW of small molecule potent antagonists of Aβ aggregation 54
Figure 2.2 The intracellular inhibition of Aβ42 aggregation by EGCG in GMC101 strain of *C. elegans* 60
Figure 2.3 The intracellular inhibition of Aβ42 aggregation by Bexarotene in GMC101 strain of *C. elegans* 62
Figure 2.4 The intracellular inhibition of Aβ42 aggregation by Bexarotene and RD242 in GMC101 strain of *C. elegans* 63
Figure 2.5 RD242 is a potent antagonist for the inhibition of Aβ42 aggregation in *C. elegans* models of Aβ42-mediated toxicity 64

Figure 3.1 Domain organization of p53 tumor suppressor protein 67
Figure 3.2 Chemical structures and MW of OPs 71

Figure 3.3 RD148 inhibits amyloid fibril formation of aggregation-prone region of p53 DBD …… 83
Figure 3.4 Confocal fluorescence microscopy images of MIA PaCa-2 cells stained with PAb 240-A647 ……... 86
Figure 3.5 ThS assay, Cell viability assay, and Western blot analysis for p53 inclusions in MIA PaCa-2 cells in the absence and presence of OPs …… 87
Figure 3.6 Prion-like spread of p53 in MIA PaCa-2 mutant cells …….. 89

Abbreviations

αS PFF–AF633	α-Synuclein preformed fibrils conjugated to Alexa fluor 633
αS	α-Synuclein
αS-YFP	α-Synuclein conjugated with yellow fluorescent protein
µl	Microliter
µM	Micromolar
2D-FAST	2-Dimensional Fragment-Assisted Structure-based Technique
AD	Alzheimer's disease
ADE	Anterior deirid
APP	Amyloid precursor protein
aPPIs	Aberrant protein-protein interactions
ATCC	American Type Culture Collection
Aβ	β-amyloid
BCA	Bicinchonimic acid
C. elegans	*Caenorhabditis elegans*
$CaCl_2$	Calcium chloride
cAMP	Cyclic adenosine monophosphate
CEP	Cephalic
CI	Chemotaxis Index
Cl^-	Chloride ion
CO_2	Carbom dioxide
COOH	Carboxylic acid group
CTX	Chemotaxis
Cu	Copper
DA	Dopaminergic
DBD	DNA-binding domain
DCF	Dichlorofluorescein
DMEM	Dulbecco-s Modified Eagle Medium
DMSO	Dimethylsulfoxide
DN	Dominant-negative
DNA	Deoxyribonucleic acid
DTT	Dithiothreitol
E. coli	*Escherichia coli*
ECL	Enhanced Chemiluminescence
EGCG	(-)-epi-gallocatechine gallate
EtOH	Ethanol
Fe	Iron
FUDR	Fluorodeoxyuridine
GFP	Green fluorescent protein
GoF	Gain-of-function
h	hour
H_2DCF-DA	2',7'-dichlorofluorescein diacetate
H_2O	Water
HFIP	1,1,1,3,3,3-hexafluoro-2-propanol
HRP	Horseradish peroxidase

HSP	Heat shock protein
HSQC	Heteronuclear single quantum coherence spectroscopy
HSR	Heat shock response
IAPP	Islet amyloid polypeptide
IF	Immunofluorescence
KH_2PO_4	Potassium dihydrogen phosphate
L4	Larva 4
LC-MS	Liquid chromatography- mass spectrometry
LoF	Loss-of-function
m/z	Mass-to-charge ratio
MDM2	Murine double minute 2
MDMX	Murine double minute X
$MgSO_4$	Magnesium sulfate
MS	Mass spectrometry
MS/MS	Tandem mass spectrometry
MTT	3- [4,5- dimethylthiazol-2-yl]-2,5-diphenyl tetrazolium bromide
MW	Molecular Weight
n	Number of experimental trials
Na^+	Sodium ion
Na_2HPO_4	Sodium hydrogen phosphate
NaCl	Sodium chloride
NGM	Nematode Growth Media
NIAD-4	[[5'-(4-Hydroxyphenyl)[2,2'-bithiophen]-5-yl]methylene] propanedinitrile
OD	Optical density
OPs	Oligopyridylamides
OQs	Oligoquinolines
pAb-240-AF647	p53 primary antibody conjugated with Alexa fluor 647 secondary Antibody
PAMPA	Parallel artificial membrane permeability assay
PBS	Phosphate buffered saline
PD	Parkinson's disease
Pen/Strep	Penicillin/Streptomycin
PFFs	Preformed fibrils
PrP	Prion protein
PrPc	Cellular prion protein
PrPSc	Scrapie-associated prion protein
PVDF	Polyvinylidene fluoride
pWT PFF-FITC	WT p53 DBD-derived preformed fibril conjugated to Fluorescein isothiocyanate
r.t.	room temperature
RIPA	RadioImmunoPrecipitation Assay
ROS	Reactive oxygen species
S.E.M	Standard error of the mean
SDS	Sodium dodecyl sulfate

SDS-PAGE	Sodium dodecyl sulfate - polyacrylamide gel
T2D	Type-2 diabetes
TBST	10x Tris-buffered saline and 0.1% Tween 20
TEAB	Triethylammonium bicarbonate
TEM	Transmission electron microscopy
ThS	Thioflavin S
ThT	Thioflavin T
WB	Western Blot
WT	Wild type
YFP	Yellow Fluorescent Protein
Zn	Zinc

1.Inhibition of *de novo* and the prion-like spread of α-Synuclein using *in vivo C. elegans* disease models

1.1 Introduction

Previous studies have shown that most neurodegenerative diseases involve the accumulation of irregular amyloid protein aggregates in the brain resulting in different types of amyloidosis[1,2]. One of these diseases is PD, the second most common neurodegenerative disorder after AD. In the United States, each year, there are about 60,000 new cases of PD and more than 23,000 deaths resulting to the fact that about 1.5 million people are affected by PD[3]. PD has been linked to the aggregation of αS and the formation of Lewy bodies over time. αS (originally expressed by the SNCA gene) is a neuronal protein primarily found in presynaptic nerve termini of the central nervous system[2,4]. αS is associated with the regulation of dopamine levels at the nerve termini (in the substantia nigra of the midbrain) for body movement. There are several established causes of PD including genetic mutations, environmental factors (such as heavy metals, and agricultural chemicals such as paraquat and rotenone)[5]. When αS misfolds, it can lead to its self-aggregation linked to PD[2]. Hence, PD is regarded as a neurological disorder due to the impairment of dopaminergic (DA) neurons in the brain. When an estimated 80% of

DA neurons become damaged, symptoms of PD can be seen in a patient including movement disorders (tremor, rigidity, bradykinesia, and postural instability), neuropsychiatric disturbances (mood, cognition, behavior or thought alterations), sensory and sleep difficulties. Synthesis of therapeutic drugs/molecules that can identify and target the sites or domains involved with αS aggregation can offer potent inhibition of the αS self-aggregation.

Previous studies have shown that small molecules can inhibit αS aggregation but those studies presented insufficient atomic-level data for understanding the ligand - αS interaction[6]. In this study, foldamer-based approach was used along with mutagenesis study for identification and validation of αS sequences as important therapeutic targets that are involved with the initiation of αS aggregation. Hence, foldamer-based molecules were synthesized for the inhibition of αS aggregation. Foldamers are artificially active ligands that can mimic the topography and the chemical space of proteins' secondary structures[7]. Foldamers may also be regarded as α-helix mimetics. It has been shown that Oligoquinoline (OQ)-based foldamers can be used to inhibit the self-assembly of islet amyloid polypeptide (IAPP)[8,9] and Aβ-peptide[10–12]; these amyloid protein aggregations have been linked with type-2 diabetes (T2D) and AD respectively.

SK-129 (Figure 1.1a) was synthesized using OQs as a potent inhibitor of αS aggregation in both *in vitro* and *in vivo* PD models[2]. The binding sites of SK-129 on αS were identified using 2D-NMR-based atomic level studies. These studies were validated using fluorescent polarization and mutation studies[2]. αS sequences were identified as important novel targets for the initiation of the amyloid aggregation. OQs were used to validate novel αS sequences by targeting these sequences with the OQs and rescuing PD

phenotypic readouts in cellular/neuronal and *in vivo* PD models. NL5901 and UA196 strains of *C.elegans* were used as PD models to test the efficacy of SK-129 (Figure 1.1a), NS163 (Figure 1.1c), NS132 (Figure 1.1b), SK6 (Figure 1.1e) and EGCG (Figure 2.1b) as potent antagonists for the inhibition of αS aggregation. SK-129 was synthesized by Dr. Sunil Kumar, and SK6 was designed by Dr. Sunil Kumar. NS163 and NS132 were synthesized by Nick Stillman in the Kumar Lab at University of Denver.

NS132 and NS163 are OPs and these are another class of synthetic protein mimetic ligands that can manipulate the aggregation of various amyloid proteins[13]. OPs have a large surface area and synthetically tunable side-chain functionalities that can support the topography and side-chain residues of proteins such as those present at interfaces of aberrant protein-protein interactions (aPPIs)[13] during the process of protein misfolding and aggregation. It was found that there were limitations for the synthesis of OP libraries including (1) The synthesis of OPs is difficult comprising of 3 chromatography steps to synthesize each monopyridyl with a side chain functionality; (2) The elongation of the OP backbone (mono- to di- to tripyridyl) requires column chromatography at each step and this leads to multiple synthetic and chromatography steps. As a result, a small number of side chains (~10) with limited chemical diversity were introduced on OPs; (3) OPs were pre-synthesized and screened and the product lacked a systematic optimization of OPs against the dynamic and transient nature of aPPIs such as those present during the protein aggregation. (4) All side chains (~10) where not efficiently utilized in the generation of OPs, otherwise, it should have been ~20 times OPs with 10 side chains (~1000 OPs instead of 50 OPs). A novel 2-Dimensional Fragment-Assisted Structure-based Technique (2D-FAST) was developed as an alternative and easier mechanism for the synthesis of OPs

compared to the traditional and vintage method. 2D-FAST combines the fragment and structure-based techniques into the OP scaffold to systematically optimize the antagonistic activity of a ligand against aPPIs. Fast has become a productive and efficient method for drug discovery where the weakly binding ligand "fragments" become attached to targeted aPPIs[14]. Subsequently a covalent bond will be formed between the weak affinity ligand fragments and different functional groups to establish high-affinity ligands against targets. The 2D-FAST method was used to synthesize OPs. The OP is an ideal scaffold for a fragment-based approach because the antagonistic activity of OPs against their biological targets were shown to significantly increase with the number of side chains (monopyridyl < dipyridyl < tripyridyl)[14,15]. Also, the backbone for OPs can be elongated from mono- to di- to tripyridyls using amide coupling. Overall, OP is an ideal scaffold for 2D-FAST studies; but no previous effort has been directed towards using OPs for 2D-FAST studies. There are several novel features of 2D-FAST over the earlier method for the generation of OPs, including, (1) It uses common precursors for the elongation of OP from mono- to di- to tripyridyl synthesis; (2) It uses a novel chromatography free amide coupling method for the elongation of the backbone chain; (3) It appends a high number and very chemically diverse library of side chains on OPs using an almost chromatography free synthetic method. It utilizes a much wider array of complex side chains than the earlier reported work, including primary hydroxyl, phenol, pyrazole, indole, which are equivalent to amino acid side chains as serine, tyrosine, histidine, tryptophan, respectively.

Stapled peptide (SK6) (Figure 1.1e) was used in this study as a potent antagonist for αS aggregation. Stapled peptides comprises of chains of peptides which induces a peptide structure into an α-helical structure[16]. In the past, peptide-based drugs were discovered but

they were not very useful as pharmacological compounds because they had low cell permeability[16]. Peptide stapling (Figure 1.1d) has become a promising technique for stabilizing peptides by cyclization of linear peptides. It involves the linkage between two side chains of the same peptide that can stabilize the helical structure of the chain. The flexibility of the molecule is reduced by the external brace, as a result, that reduces the entropic penalty of the binding and orientation of the peptides and improves the affinity and selectivity to the target[16].

C. elegans is a nematode which was among the worms first introduced by Sydney Brenner in 1974, as models for developmental and neurobiology studies[17]. After about four decades of research, *C. elegans* were manipulated for broader studies of different biological processes such as apoptosis, cell signaling, cell cycle, cell polarity, gene regulation, metabolism, aging and sex determination[18]. The Caldwell lab established two distinctive *C. elegans* models of PD in accordance with the two primary pathological features of PD: (1) Loss of DA neurons, and (2) αS aggregation[19]. Previous studies have shown that age- and dose-dependent neurodegeneration can be caused in these animals through the overexpression of WT human αS under the DA neuron-specific promoter (P_{dat-1}::α-syn)[20,21]. Another study related this phenotype findings to humans[22].

Another strain of *C.elegans* (NL5901) with overexpression of human αS fused with YFP under the unc-54 promoter (Punc-54:: α-syn::YFP); this resulted in the misfolding of αS in the body wall muscle cells of the nematode[19] and it served as another model of PD. The number and size of αS aggregates can be scored using fluorescent microscopy through the observation of YFP puncta indicated by αS aggregation[19]. This is important because it can provide data on how to identify therapeutic molecules/drugs for the inhibition of

amyloid aggregation. In this study, the NL5901 strain of *C. elegans* were used as PD models. Direct monitoring of gene expression levels in animals can be observed through transgenic YFP reporter strain of *C. elegans*[23]. This characteristic has been developed in the NL5901 strain expressing αS: YFP fusion proteins including the unc-54:: α-synuclein:YFP construct[24,25].

Also, in this study, we used a well-established PD model of *C. elegans* (UA196) that expresses the wild-type (WT) human αS and GFP in DA neurons. UA196 has six anterior DA neurons (two ADE (anterior deirid) and four CEP (cephalic))[5]. The chemosensory system in *C. elegans* presents a powerful tool for the animals to perceive chemicals in the environment including food, noxious elements, volatile compounds, gases, and mating signals[26]. Several behaviors of the animal are linked to chemo sensation including chemotaxis, avoidance, and motility. The behaviors are control by chemosensory neurons by signaling to downstream inter- or motor- neurons, and other tissues. Chemical (odorant) sensing in *C. elegans* is regulated by the AWA, AWB, and AWC olfactory neurons[26]. These neurons can mediate attractive or repulsive behavior depending on the properties of the chemical compound being sensed. ASE and ASI are other chemosensory neurons. Attraction towards water soluble chemicals such as Cl^-, Na^+, cAMP, and biotin is mediated by the ASE neurons. While chemotaxis and pheromone sensing are regulated by the ASI neurons. *C. elegans* was selected as a model for PD in this study because it has comprehensive characterized aging properties, and its transparency throughout its lifetime; when the animals grow older, these properties allow visualization of inclusions in their muscle cells and DA neurons.

Previous studies reported that patients (suffering from neurodegenerative diseases) have metal ions including Zn(II), Cu(II), Al(III), and Fe(III) accumulated in cerebral tissues[27]. It was also found using *in vitro* assays that fibrillation of amyloid proteins might be promoted by metal ions[28]. EGCG was found to decrease apoptosis, suppress the accumulation of reactive oxygen species and free extracellular calcium, change signaling pathways, lower nitric oxide levels and reduce oxidative stress in PD cells[29]. EGCG was used in this study for inhibition of αS aggregation by treatment of NL5901 and UA196 strains of *C. elegans* with the molecule. Several assays including paralysis assay were conducted in the absence and presence of the ligand to study the antagonistic effects of the molecule.

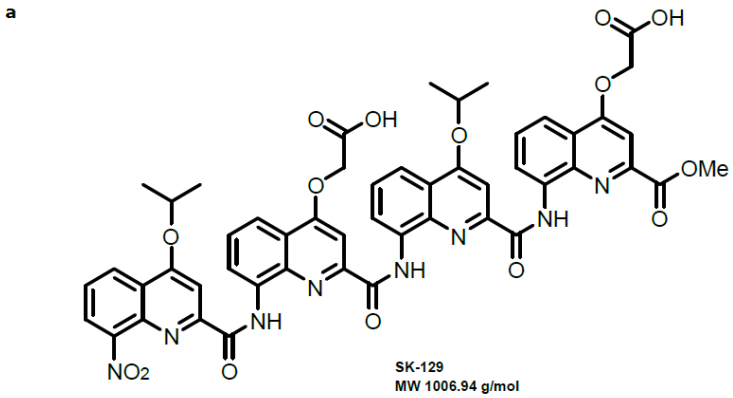

Figure 1.1 Chemical structures, and molecular weight (MW) of OQ and OPs and reaction mechanism for peptide stapling[2,30]. **a** SK-129. **b** NS132. **c** NS163. **d** Reaction mechanism for peptide stapling. **e** SK6.

1.2 Materials and Methods

1.2.1 Culture methods for *C. elegans* strains

The N2 (wild-type *C. elegans* Bristol strain), NL5901 (*C. elegans* model of PD, pkIs2386; unc-54p: α-syn:YFP + unc-119 (+)), and *Escherichia coli* OP50 (*E. coli*, uracil requiring mutant), strains were obtained from Caenorhabditis Genomics Center (Minneapolis, MN). Dopaminergic neuron-specific RNAi UA196 strain of *C. elegans* (bal11; Pdat-1:α-syn, Pdat-1:gfp) was generously donated by the laboratory of Dr. Guy Caldwell (Department of Biological Science, The University of Alabama, Tuscaloosa, AL, United States)[31]. The animals were maintained at standard conditions on nematode growth media (NGM) agar in 60 mm plates (CytoOne, Ocala, FL) using *E. coli* OP50 as the food source[2,32]. All strains were maintained using previous protocols[2,33]. NGM agar plates, M9 buffer (3 g KH_2PO_4, 6 g Na_2HPO_4, 5 g NaCl, 1 mL 1 M $MgSO_4$, milli-Q H_2O to 1 L), Chemotaxis (CTX) media plates (2% Agar, 5 mM KH_2PO_4, 1 mM $CaCl_2$, and 1 mM $MgSO_4$), CTX buffer (5 mM KH_2PO_4, 1 mM $CaCl_2$, and 1 mM $MgSO_4$) and OP50 solution at 0.5 OD_{600nm} were prepared using previous protocols[2,33–35].

1.2.2 Paralysis Assay for NL5901 strain treated with epigallocatechin gallate (EGCG) using 6-well plate

The paralysis assay was conducted based on a previously described protocol[2,36] with slight modifications. On day one, N2 and NL5901 strains were synchronized using the bleaching process, which involves egg lay[37] and incubation of the eggs (23 °C, 30 h) on a solution of NGM in 60 mm culture plates (CytoOne, Ocala, FL) with OP50 (350 µL, 0.5 OD_{600nm}) as a food source. On day two, the animals were transferred (using M9 buffer) from 60 mm NGM plates to 35 mm NGM plates (CellTreat Scientific, Pepperell, MA) containing 75 µM Fluorodeoxyuridine (FUDR; to prevent the worm reproduction and ensure that equal ages of animals were used for the experiment) with and without EGCG (65 µM in Dimethylsulfoxide, DMSO) and incubated at r.t. for 48 h. On day three, fresh stock of OP50 was prepared by diluting 1 µL of OP50 in 5 mL of LB Miller media (Neogen, Lansing, MI) and incubated in a shaking incubator (Eppendorf, Hamburg, Germany) at 37 ºC and ~200 rpm for ~24 h. The experiment was conducted using a sterile 6-well plate containing liquid media (1 mL/well). On day four, the liquid media was prepared with 67.28% (v/v) of M9 buffer, 0.018% (75 µM) of FUDR solution (v/v), 0.1% of 1 M magnesium sulfate (v/v), 0.1% of 1 M calcium chloride (v/v), 2.5% of 1 M potassium phosphate solution (pH 6, v/v), and 30% of 0.5 OD_{600nm} OP50 (v/v). EGCG (65 µM in DMSO) was reconstituted in the same liquid media for the NL5901 strain of *C. elegans* (for treatment). Three conditions of the animals were used including N2 strain (positive control), NL5901 strain (untreated negative control), and NL5901 strain (treated with 65 µM of EGCG). A total of 100 animals per well were transferred manually into a 6-well plate with a worm pick. Before conducting each paralysis assay, the 6-well plate was

mechanically tapped for about 30 sec to make the animals more active in the liquid media. The assay was started on day five where 20 activity scores per well were collected using the wMicroTracker Arena plate reader (Phylumtech, Santa Fe, Argentina) at 23 °C for 1 h per day over a 12-day period. Three biological replicates were performed and the average activity scores per well were reported with the error bars representing the standard error of the mean (s.e.m).

1.2.3 Paralysis Assay for NL5901 strain treated with SK-129 using 6-well plate

N2 and NL5901 strains of *C. elegans* were prepared for this experiment using previous protocols[2,36,37] in the absence and presence of ligand (SK-129, 15 μM) as described in section 1.2.2. Three conditions of the animals were used including N2 strain (positive control), NL5901 strain (untreated negative control), and NL5901 strain (treated with 15 μM of SK-129).

1.2.4 Paralysis Assay for NL5901 strain treated with SK-129 using 24-well plate

N2 and NL5901 strains (treated with and without different concentrations of SK-129; 50 μM, 65 μM, 90 μM and 120 μM in DMSO) were prepared as earlier described in section 1.2.2. Paralysis assay was conducted using previous protocols[2,36,37] with slight modifications. There were six worm conditions for this experiment including N2 strain (positive control), NL5901 strain (untreated negative control), and NL5901 strain treated with different concentrations of SK-129 as earlier described. And there were four technical replicates (four wells) for each worm condition. A total of 50 animals per well were transferred manually into a 24-well plate with a worm pick. Prior to each paralysis assay, the 24-well plate was mechanically tapped for about 30 sec to make the animals more active in the liquid media. The assay was started on day five where 20 activity scores per well

were collected using the wMicroTracker Arena plate reader at 23 °C for 1 h per day over a 12-day period. Two biological replicates were performed and the average activity scores per well were reported with the error bars representing the standard deviations.

1.2.5 Paralysis Assay for NL5901 strain treated with EGCG using 24-well plate

The animals were prepared based on previous protocols[2,36,37] with slight modifications as earlier described in section 1.2.2. There were five worm conditions for this experiment including N2 strain (positive control), NL5901 strain (untreated negative control), and NL5901 strain treated with three different concentrations of EGCG (65 μM, 100 μM, and 150 μM in DMSO).

1.2.6 Paralysis Assay for NL5901 strain treated with NS163 and NS132 using 24-well plate

NL5901 and N2 strains were prepared according to the protocol described in section 1.2.4. There were four worm conditions including N2 strain, NL5901 strain in the absence and presence of ligands (100 μM NS163 and 100 μM NS132 in DMSO).

1.2.7 Paralysis Assay for NL5901 strain treated with SK-6

NL5901 and N2 strains were prepared according to the protocol described in section 1.2.4. There were three worm conditions including N2 strain, NL5901 strain in the absence and presence of the ligand (100 μM SK-6 in DMSO).

1.2.8 Paralysis Assay for UA196 strain treated with NS163 and NS132

UA196 and N2 strains were prepared according to the protocol described in section 1.2.4. Four worm conditions were used for this experiment including N2 strain, UA196 strain in the absence and presence of ligands (100 μM NS163 and 100 μM NS132 in DMSO).

1.2.9 Dopamine dependent *C. elegans* (N2 and UA196) Assay

Paralysis assay was conducted for UA196 and N2 strains of *C. elegans* in the absence and presence of Dopamine (2 mM) and ligand (100 μM NS163) using previous protocols[2,33,36,37] as described in section 1.2.4. There were six worm conditions including (1,2) N2 in the absence (positive untreated control) and presence of Dopamine (2 mM), (3) UA196 (negative untreated control), (4) UA196 treated with 2 mM Dopamine, (5) UA196 treated with ligand (100 μM NS163), and (6) UA196 treated with both Dopamine (2 mM) and ligand (100 μM NS163). Animals were treated on days two and four and the paralysis assay was conducted as previously described.

1.2.10 Confocal microscopy of early stage treated *C. elegans* (NL5901 and UA196)

This experiment was performed based on a previously described protocol[2,38] with slight modifications. The animals in the absence and presence of ligands or PFFs were used for this experiment under conditions identical to the paralysis assay. At least 10 animals per condition were transferred with a worm pick to a cover slide containing an anesthetic (40 mM sodium azide) and mounted on glass microscope slides containing 2% agarose pads for imaging. The images of the animals were collected using an Olympus Fluoview FV3000 confocal/2-photon microscope (40 x Plan-Apo/1.3 NA objective with DIC capability) from day five through day ten (for NL5901 strain) and processed using the OlympusViewer in ImageJ software. The inclusions of amyloid protein aggregates (in the muscle cells) were manually counted (10 animals per condition for NL5901 strain) for the

six-day imaging period. For each condition, three biological replicates were performed, and the average number of aggregates was reported with the error bars representing the S.E.M.

1.2.11 Confocal microscopy of post-disease onset PD model of *C. elegans* (UA196)

The UA196 strain of *C. elegans* was synchronized and transferred into FUDR plates as previously described[2]. For this experiment, the animals were not treated with ligands until experimental day five. On day five, the animals were treated with ligands (NS132 and NS163, 100 μM) and incubated at r.t. Confocal imaging was conducted using Olympus Fluoview FV3000 confocal/2-photon microscope immediately prior to treatment with the ligand on day five, then again five- and ten-days following treatment.

1.2.12 Chemotaxis Assay for *C. elegans* (N2 and UA196)

The previous protocols[34,35] with slight modifications were used to perform this assay in CTX solid media 35 mm plates (CellTreat Scientific, Pepperell, MA). Earlier prepared UA196 strain (untreated) were studied for attraction towards ligands (NS132 and NS163, 100 μM) and repellant (EtOH) on day 0 of adulthood (L4 stage). Three CTX 35 mm plates (for UA196 in the presence of EtOH, and UA196 in the presence of ligands) were divided into four equal quadrants designated A and C (the left diagonal quadrant), B and D (the right diagonal quadrant). Solutions of ligands (10 μL, 100 μM) were placed at ~0.4 cm from the edge of quadrants B and D; and ethanol (10 μL, as a control) was placed at ~0.4 cm from the edge of quadrants A and C. The solutions in the quadrants were allowed to dry for about 1 h at r.t. to develop the gradient. CTX buffer (1 mL) was used to transfer

adult worms from the 35 mm plates to each of three sterile 1.7 mL microcentrifuge tubes (Eppendorf, Hamburg, Germany). The worm solution was centrifuged for 10 sec using a mini-Vortex mixer (VWR, China) to allow the worm pellets to settle at the bottom of the microcentrifuge tubes. The supernatant solution was aspirated and replaced with CTX buffer. This buffer exchange step was conducted three times to ensure that the animals were re-suspended in 100 µL of CTX buffer. After homogenizing the worm solution, 10 µL of the solution was transferred into a blank solid media 35 mm plate and the number of worms was counted under an Olympus microscope (SZ-6145, Waltham, MA) in triplicate. A worm suspension was then prepared with the CTX buffer containing 50 animals/10 µL. Approximately 50 animals were transferred to the center of the CTX plate, and the lids were covered with parafilm (Bemis Company, Inc., Neenah, WI). Subsequently, the worm activity was monitored using a wMicroTracker Arena plate reader (Phylumtech, Santa Fe, Argentina) at 23 °C for 2 h. The CTX reports were generated using MapPlot option on the Arena plate reader. Three biological replicates of this experiment were performed. A similar experiment was performed after treatment of UA196 with ligands (at L4 stage and day 7 of adulthood) and the chemotaxis assay was carried out for their attraction towards OP50 (food) and EtOH (repellant).

1.2.13 Measurement of intracellular Reactive Oxygen Species (ROS) of early stage treated *C. elegans* (UA196) under normal culture conditions

A fluorescent probe 2',7'-dichlorofluorescein diacetate (H_2DCF-DA) was used to measure the intracellular ROS based on previously established protocols[39,40] with slight modifications. In cells, H_2DCF-DA is retained after deacetylation by the intracellular

esterases but upon oxidation by ROS, non-fluorescent H_2DCF-DA is converted into highly fluorescent 2,7- dichlorofluorescein (DCF). The levels of intracellular ROS (in cells) correlate with the intensity of DCF fluorescence. The N2 and UA196 strains of *C. elegans* were synchronized and treated with ligands (NS163 and NS132, 100 μM) as previously described in section 1.2.2. On day seven, the animals were transferred into 1.7 mL microcentrifuge tubes using M9 buffer (1 mL). The samples were centrifuged for 2 min at 2,500 rpm and 20 °C. Subsequently, 0.8 mL of the supernatant was discarded. After, homogenizing the worm pellet in the remaining solution, 10 μL of the suspension was placed onto a glass slide for counting using an Olympus microscope (SZ-6145, Waltham, MA) in triplicate. The worm solution was then diluted with M9 buffer to approximately 50 animals/10 μL. Each desired well of a Costar 96-well black plate (Corning, Kennebunk, ME) contained M9 buffer (40 μL), worm solution (10 μL), and H_2DCFDA (50 μL, 50 μM in DMSO). For the vehicle, 50 μL of M9 buffer and 50 μL of H_2DCFDA reaction solution were placed in the desired wells. Subsequently, the Costar 96-well black plate was gently shaken for 30 sec at r.t. and the fluorescence intensity was quantified (λ_{ex} = 485 nm and λ_{em} = 530 nm) every h for 2 h using the Infinite M200 Pro Plate Reader. This experiment consisted of 3 biological replicates and 5 technical replicates. The normalized fluorescence intensity presented are the average values with the error bars representing the S.E.M. The statistical significance was determined by a one-way ANOVA with Tukey's post-hoc test. Immediately after running the ROS assay, worms were transferred into different 35 mm NGM plates, air-dried using the fume hood, and mounted on slides using 40 mM sodium azide and 2% agarose pad as earlier described.

1.2.14 Measurement of intracellular ROS of post disease onset PD model of *C. elegans* (UA196) under normal culture conditions

The previously described protocols[39,40] with slight modifications were used to conduct this assay. The N2 and UA196 strains of *C. elegans* were prepared as described earlier in section 1.2.12 in the absence of ligands. On day five, the ROS assay was conducted as previously described. Subsequently, the UA196 strain was treated with ligands (NS132 and NS163, 100 μM) and incubated at r.t. for 72 h. On day eight, the ROS assay was also conducted again. This experiment involved one biological replicate and four technical replicates. The normalized fluorescence intensities presented are the average values with the error bars representing the standard S.E.M. The statistical significance was determined by a one-way ANOVA with Tukey's post-hoc test.

1.2.15 Preparation and conjugation of αS preformed fibrils (PFFs) for prion studies

αS PFFs were formed using previous protocol[41] with slight modifications. Monomeric αS solution (70 μM) was incubated on a shaker at 1400 rpm for 48 h and Thioflavin T (ThT) Assay was conducted using previous protocol[42] to confirm the presence of the PFFs. Buffer exchange was conducted to resuspend the fibrils in 0.1 M sodium bicarbonate buffer (~pH 8.3). A centrifuge (ThermoFisher Scientific, Germany) was used for the buffer exchange at 22,000 g, and 4 ºC for 10 min. AF633 (10 mM in ultra-pure DMSO) was prepared. αS PFF (70 μM) was incubated with AF633 (700 μM) on a shaker at r.t for ~2 h. Buffer exchange was conducted with phosphate

buffered saline (PBS, ~pH 7.4); a suitable buffer for living organisms and cells. Subsequently, SDS-PAGE was conducted using previous protocol[43] to confirm that the fluorophore was conjugated to the fibrils.

1.2.16 Paralysis Assay for transfected NL5901 strain

NL5901 strain of *C. elegans* were transfected with αS PFF-AF633 using previous protocol[44,45] with slight modifications. Paralysis assay was conducted using previous protocols[2,36,37] as described earlier with slight modifications. On day one, the animals were prepared as described in section 1.2.2. On experimental day two, 20 μM of αS PFF–AF633 was prepared using Pulsin reagent and M9 buffer (containing the animals). Initially, αS PFF–AF633 was incubated with Pulsin reagent for 20 min. The animals were transferred from NGM plates (containing FUDR) into microcentrifuge tube using M9 buffer. Subsequently, the animals in M9 buffer were transferred into the 20 μM αS PFF–AF633 solution (containing Pulsin) and incubated on a shaker (Thermo Scientific, Waltham, MA) for 2 h at r.t. The animals were re-transferred into the NGM plate (containing FUDR) for further 48 h incubation at r.t. On experimental day four, the animals were re-transfected with the αS PFF-AF633 (as earlier described) to reconstitute the fibrils in the muscle cells. On day five, the animals were transferred into 6-well plates (for paralysis assay). There were three conditions of the animals including N2 strain (positive control), NL5901 strain (untreated negative control), and NL5901 strain transfected with 20 μM of αS PFF-AF633.

1.2.17 Sample preparation for Total Proteome Measurements

N2 and UA196 strains of *C. elegans* in the absence and presence of ligand (NS163, 100 μM in DMSO) were prepared as earlier described in section 1.2.4. The animals were treated and collected on day seven of adulthood by washing three times with M9 buffer,

flash frozen with liquid Nitrogen and stored in -80 ºC freezer. The Proteomics experiment described in this section 1.2.17, 1.2.17.1-3 was conducted at CU Anschutz Medical Campus, Mass Spectrometry Proteomics Core Facility. The animals (adult day 7) were lysed with chill 4% SDS in 100 mM Tris-HCl pH 7.5 lysis buffer[46]. Subsequently, the lysates were heat-treated for 5 min at 95 ºC to facilitate lysis and to inactivate endogenous proteases and phosphatases. The lysates were sonicated at 4 ºC (two 20 s-cycles of 1 s on and 1 s off at 80 % output power for tip-probe sonicator). Finally, the lysate was clarified by centrifugation for 20 min at 18,000 × g, 4°C and the soluble supernatant was recovered for further analysis. The samples were digested in the S-Trap micro spin column (Protifi, Huntington, NY) following the manufacturer's procedure. Samples were reduced with 10 mM DTT at 55 °C for 30 min, cooled to room temperature, and then alkylated with 25 mM iodoacetamide in the dark for 30 min. Next, a final concentration of 1.2% phosphoric acid and then six volumes of binding buffer (90% methanol; 100 mM triethylammonium bicarbonate, TEAB; pH 7.1) were added to each sample. After gentle mixing, the protein solution was loaded to a S-Trap micro spin column, spun at 1500 x g for 2 min, and the flow-through collected and reloaded onto the S-Trap micro spin column. This step was repeated three times, and then the S-Trap micro spin column was washed with 400 µL of binding buffer 3 times. Finally, 1 µg of sequencing-grade trypsin (Promega) and 125 µL of digestion buffer (50 mM TEAB) were added onto the filter and digested carried out at 37 °C for 6 h. To elute peptides, three stepwise buffers were applied, with 100 µL of each with one more repeat, including 50 mM TEAB, 0.2% formic acid in H_2O, and 50% acetonitrile and 0.2% formic acid in H_2O. The peptide solutions were pooled, lyophilized, and resuspended in 100 µL of 0.1 % FA.

1.2.17.1 Desalting

The digested peptides were desalted on a C18 stop-and-go-extraction tips (StageTips). StageTips were prepared by punching 3M Empore C18 material with a Hamilton 20-gauge needle and inserting the disk into P200 pipet tips. StageTips were conditioned with 200 µL of 80% acetonitrile in 0.1% formic acid, then centrifuged for 1 minute at 1,500x g. The StageTips were then washed with 200 µL 0.1% formic acid and transferred to clean microfuge tubes. Formic acid (0.1%) was then added to the concentrated sample to a final volume of 200 µL and vortexed for 15 – 20 minutes. The samples were then added to the equilibrated C18 columns and centrifuged for 1 minute at 1,500 x g. The flow-through was reapplied to the resin three additional times to maximize sample binding. The StageTips were washed twice with 200 µL of 0.1% formic acid and centrifuged at 1,500 x g for 1 minute. The StageTips were transferred to a clean micro-centrifuge tube and subjected to two rounds of elution with 100 µL of 0.1% formic acid in 80% acetonitrile followed by centrifugation at 1,500 x g. The eluent volume was reduced to near dryness via Speedvac, then resuspended with 20 µL of 0.1% formic acid for LC-MS analysis.

1.2.17.2 Mass spectrometry analysis

The samples (20 µL of each) were loaded onto individual Evotips for desalting and then washed with 20 µL 0.1% FA followed by the addition of 100 µL storage solvent (0.1% FA) to keep the Evotips wet until analysis. The Evosep One system (Evosep, Odense, Denmark) was used to separate peptides on a Pepsep column, (150 um inter diameter, 15 cm) packed with ReproSil C18 1.9 um, 120A resin. The system was coupled to the

timsTOF Pro mass spectrometer (Bruker Daltonics, Bremen, Germany) via the nano-electrospray ion source (Captive Spray, Bruker Daltonics).

The mass spectrometer was operated in PASEF mode. The ramp time was set to 100 ms and 10 PASEF MS/MS scans per topN acquisition cycle were acquired. MS and MS/MS spectra were recorded from m/z 100 to 1700. The ion mobility was scanned from 0.7 to 1.50 Vs/cm^2. Precursors for data-dependent acquisition were isolated within ± 1 Th and fragmented with an ion mobility-dependent collision energy, which was linearly increased from 20 to 59 eV in positive mode. Low-abundance precursor ions with an intensity above a threshold of 500 counts but below a target value of 20000 counts were repeatedly scheduled and otherwise dynamically excluded for 0.4 min.

1.2.17.3 Database Searching and Protein Identification

MS/MS spectra were extracted from raw data files and converted into .mgf files using MS Convert (ProteoWizard, Ver. 3.0). Peptide spectral matching was performed with Mascot (Ver. 2.5) against the Uniprot C.elegans database. Mass tolerances were +/- 15 ppm for parent ions, and +/- 0.4 Da for-fragment ions. Trypsin specificity was used, allowing for 1 missed cleavage. Met oxidation, protein N-terminal acetylation, peptide N-terminal pyroglutamic acid formation and Phospho (STY) were set as variable modifications with Cys carbamidomethylation set as a fixed modification. Scaffold (version 4.9, Proteome Software, Portland, OR, USA) was used to validate MS/MS based peptide and protein identifications. Peptide identifications were accepted if they could be established at greater than 95.0% probability as specified by the Peptide Prophet algorithm. Protein identifications were accepted if they could be established at greater than 99.0% probability and contained at least two identified unique peptides.

1.3 Results and discussions

1.3.1 Effects of ligands on αS aggregation mediated PD phenotypes in *in vivo C. elegans* models

Several ligands including SK-129 (Figure 1.1a), EGCG (Figure 2.1b), NS163 (Figure 1.1c), SK-6 (a stapled peptide, Figure 1.1e), and NS132 (Figure 1.1b) were tested *in vivo* in PD models NL5901 and UA196 strains of *C. elegans* for antagonistic activities. Paralysis assays (Figures 1.2a-d, 1.3a-d, 1.4a-b, 1.5a-b, 1.6a-b, 1.6g, and 1.14a-b). There are PD phenotypic readouts in NL5901 which includes a gradual increase in inclusions (αS-YFP) in the body wall muscle cells[2] and a gradual decline in locomotion during aging. And the PD phenotypic readouts in UA196 includes the aggregation of αS in DA neurons over time with aging resulting in death of neurons indicated by disappearance of GFP puncta which correlates with the disappearance of dead neurons. The potent ligands were initially tested for cell permeability through the parallel artificial membrane permeability assay (PAMPA) (Figure 1.4a) to ensure that the molecules can permeate the cell[2]. It was found that the ligands used in this study had good cell permeability. But the cell permeability of NS132 (Figure 1.4a) was found to be low in comparison to the PAMPA standards which may be due to the poor cell permeability of NS132 caused by the COOH functional group.

Previous studies had suggested that traditionally the carboxylic acid functional group is one of the most versatile and frequently identified substructures on small molecules because of its ability to establish interactions with a wide array of complementary functional groups using relatively strong electrostatic interactions,

hydrogen bonding, and participation in interactions with dipoles[47]. To enhance the cell permeability of NS132 without sacrificing the antagonistic activity of the ligand, we synthetically replaced the carboxylic acid functional group with hydroxamic acid (NS163, figure 1.1c) which is one of the most common and successful carboxylic acid isosteres and it has shown higher cell permeability compared to carboxylic acids[47]. The cell permeability of the hydroxamic acid analog of NS132 (NS163) was improved by ~2-fold and it was moderate in comparison to the PAMPA standards. Several *in vitro* assays were conducted to test the antagonistic effects of these molecules against the aggregation of αS including Thioflavin T (ThT) (Figure 1.4c) assay and TEM[2]. It was found that these molecules were potent antagonists for the aggregation of αS. Next, the small molecules were used to treat PD models of *C. elegans* (NL5901 and UA196 strains). Intially, the PD model NL5901 was treated with 15 μM SK-129 and the paralysis assay was studied and compared to the untreated negative control (NL5901) and positive control (N2) strains (in 6-well plate) using the wMicrotracker Arena plate reader. It was found that the locomotion of the animals improved in the presence of SK-129. The reason may be because SK-129 was able to bind to αS oligomers (implicated as a toxic species in αS aggregation and PD progression) and prevent them from aggregation. Another reason maybe that SK-129 might have bound to the monomeric αS in the muscle cells of the animals and prevented secondary nucleation and elongation of the fibrils. Another reason for conducting the paralysis assay with the novel arena plate reader was to report reproducible and consistent data and show that the instrument can be reliable for paralysis assay and chemotaxis assay.

In another paralysis experiment, different concentration of SK-129 (50 μM, 65 μM, 90 μM, and 120 μM) were used to treat NL5901 strain and the assay was conducted using

a 24-well plate in wMicrotracker Arena plate reader (figure 1.2c-d). It was found that the locomtion of the animals increased with increase in the concentration of the drug (SK-129). This data further suggested the potential of SK-129 at inhibiting αS aggregation. Also, using a 24-well plate to conduct the paralysis assay showed that the arena plate reader can be used to conduct high throughput paralysis assays. Another drug, EGCG, which was used in previous studies[48,49] as a potent antagonist for amyloid protein aggregation was used in this study to treat NL5901 strain (Figures 1.3a-d). In this study, it was also found that EGCG is a potent antagonist for αS aggregation after several experiments including paralysis assays and confocal imaging. And the main reason for using EGCG in this study is to suggest that the wMicrotracker Arena plate reader is a reliable instrument for high throughput paralysis assays. Also, confocal imaging of the NL5901 in the absence and presence of 150 μM EGCG at day 3 of adulthood showed significant disappearance of the αS-YFP aggregate (Figure 1.3e-f).

The number of inclusions (αS-YFP aggregate) were quantified by manually counting using confocal microscope in the animals with and without NS163 for various days of adulthood starting from day five to day ten (Figure 1.3g). We observed a gradual increase in the number of inclusions from day five (~7 inclusions/worm) to day nine (~34 inclusions/worm) in the untreated NL5901 strain. In contrast, there was significant decrease in the number of inclusions in the animals treated with EGCG from day five (~4 inclusion/worm) to day nine (~2 inclusion/worm) (Figure 1.3g). Although there was a slight decline (on day ten) for the number of inclusions found in the untreated NL5901 strain (~32 inclusions/worm), in general it may be concluded that the drug, EGCG, was

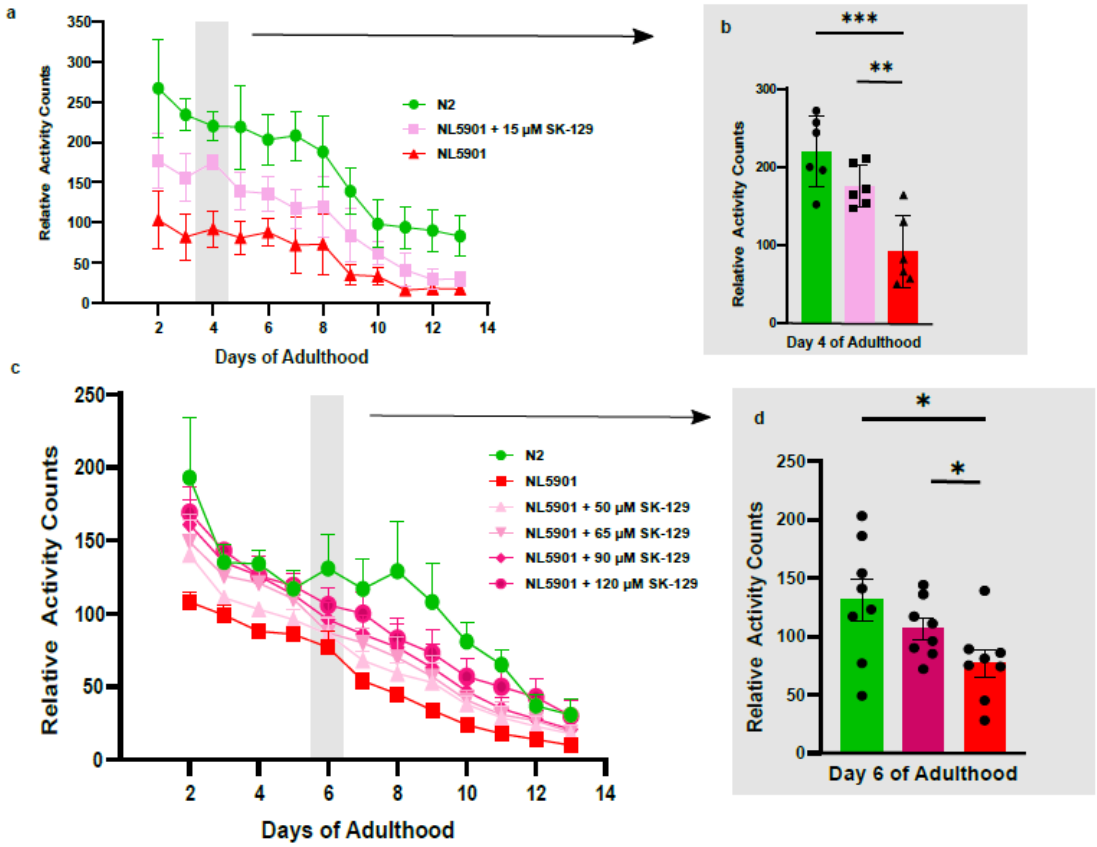

Figure 1.2 The intracellular inhibition of αS aggregation by SK-129 in NL5901 strain of *C. elegans*. **(a)** Paralysis assay (using 6-well plate) shows the relative activity counts for 12 days of adulthood of N2 and NL5901 strains in the absence and presence of 15 µM SK-129. **(b)** A graphical representation with statistical analysis of the relative activity counts of N2 and NL5901 strain in the absence and presence of 15 µM SK-129 for day 4 of adulthood. **(c)** Paralysis assay (using 24-well plate) shows the relative activity counts for 12 days of adulthood of N2 and NL5901 strains in the absence and presence of SK-129 (50 µM, 65 µM, 90 µM, and 120 µM). **(d)** A graphical representation with statistical analysis of the relative activity counts of N2 and NL5901 strains in the absence and presence of 120 µM SK-129 for day 6 of adulthood. The data shows the mean, and the error bars represents the s.e.m. (n=2 independent experiments and each n included four technical replicates. ANOVA with Tukey's multiple comparison test was used to perform statistical analysis. *p<0.05, **p < 0.01, ***p<0.001, ****p < 0.0001. Source data file was used to provide source data.

potent enough to inhibit αS aggregation in NL5901 strain. The confocal imaging data further supported the paralysis assay data earlier reported.

A small molecule, NS163, was synthesized in the Kumar lab as a potent antagonist for αS aggregation. After several *in vitro* assays including ThT, and TEM which suggested its antagonistic activity, NS163 (100 μM) was used to treat the the NL5901 strain in two doses/bursts on day two (L1) and day four (day 1 adults) followed by 24 h incubation at r.t. before assessing the effect of NS163 on the PD phenotypes (NL5901). Also, the number of inclusions was manually counted using confocal microscope in the animals with and without NS163 for various days of adulthood beginning from day five to ten (Figure 1.4c-e). In contrast to the high number of inclusions in the untreated NL5901 strain earlier reported, there was significant decline in the number of inclusions in the NS163-treated NL5901 strain from day five (~4 inclusions/worm) to day ten (~2 inclusions/worm) (Figure 1.4e).

The paralysis assay data showed that the motility rate of the NL5901 strain increased in the presence of the drug, NS163 compared to the untreated disease strain. The improved motility/locomotion of the animals was less than the WT N2 strain but more than the untreated disease strain which implies that the drug was able to inhibit the aggregation of αS-YFP and rescued the locomotion of the worm which was impaired in the disease strain. The wMicrotracker Arena plate reader was used to measure the locomotion/paralysis (overall activity counts) of the PD worms in the absence and presence of NS163 (hydroxamic acid analog of NS132) (Figure 1.4a-b) and NS132 (Figure 1.5a-b). There was significant decrease in the activities (including motion) of the PD animals compared to the diseased worms after treatment with the ligands. Also, the number of inclusion (in NL5901 treated with NS132) was counted using confocal microscope (Figure 1.5c-e); although there was decrease in the number of inclusions from day five (~5

inclusions/worm) to day ten (~2 inclusion/worm), the paralysis assay data showed significant increase in the locomotion of the animals treated with NS163 compared to NS132. The *C. elegans* based study suggests that NS163 permeates the body wall muscle cell membrane of the animals and effectively inhibits αS aggregation (Figure 1.4a-e). Overall, the study suggests that NS163 is a potent inhibitor of the aggregation of αS.

A staple peptide, SK6, was designed by the Kumar lab and used as a potent antagonist for αS aggregation in NL5901 PD models. The animals were treated with 100 of the molecule. The paralysis assay data (Figure 1.6a-b) and the confocal microscopy data (Figure 1.6c-e) showed a similar antagonistic activity earlier reported for the ligands (SK-129, EGCG, NS132 and NS163). Also, the data suggests that SK6 is a potent inhibitor for αS aggregation.

1.3.2 Effect of OPs on the degeneration of DA neurons in a *C elegans* PD model

NS163 and NS132 (100 μM) were also tested in another PD model (UA196 strain) for their inhibitory effects on αS aggregation in DA neurons. The paralysis assay data (Figure 1.4h-I, 1.5a-b) showed an increase in the locomotion of the UA196 strain in the presence of both ligands but the effect was significant in the animals treated with NS163. In healthy worms, there are 6 anterior DA neurons in the brain region including two ADE (anterior deirid) and four CEP (cephalic) neurons[5]; this can also be seen at the early ages of the UA196 (L1 – L4) with the help of the GFP fluorescence in the neurons. When the animals (UA196) grow older, αS aggregates in the DA neurons and result to
cell death observed by the disappearance of GFP. In the presence of ligands in UA196, the paralysis assay data (Figure 1.4h-I, 1.5a-b) showed significant improvement in the

locomotive activity compared to the diseased UA196 strain and the healthy N2 WT strain. It was also observed that NS163 had better antagonistic activity at inhibiting αS aggregation in DA neurons compared to the NS132. The number of anterior DA neurons was counted manually using the confocal microscope (Figure 1.4d-g) on days seven and twelve of adulthood for ten animals in each condition; within this aging period, the untreated UA196 had 1 out 10 animals (10%) with normal (6) anterior DA neurons, the UA196 treated with NS163 (100 μM) had 8 out of 10 animals (80%) with normal DA neurons, and the UA196 treated with NS132 (100 μM) had 3 out of 10 animals (30%) with normal DA neurons.

The aggregation of αS is associated with the neurodegeneration of DA neurons, which is a pathological hallmark of PD. We have also shown that NS163 rescues αS aggregation mediated PD phenotypes in the body wall muscle cells of C elegans worms. Next, we investigated the neuroprotective effect of NS-163 on αS aggregation mediated neurodegeneration of DA neurons in a well-established C elegans PD model (UA196). The UA196 worms express both human αS and GFP in DA neurons under the control of the dopamine promoter genotype (Pdat-1::GFP; Pdat-1::α-SYN). The expression and aggregation of αS in six DA neurons that are located within the anterior region of worms lead to progressive neurodegeneration characterstics during the aging of UA196 worms. This strain has been used to gain insights into the PD associated mechanisms and also tested to assess the neuroprotective effect of ligands against αS aggregation. The UA196 strain has six DA neurons in the anterior region, which degenerate from day 3 to day 15 represented by a gradual decline in the GFP fluorescence in DA neurons (Figure 1.7a-g). The number of DA neurons were decreased from 6 (day 3) to 1 (day 15) in UA196 worms

(Figure 1.7b-g). The degeneration and subsequent loss of DA neurons is a consequence of αS aggregation during the aging of worms (Figure 1.7d-f). In marked contrast, the % loss of six intact DA neurons loss in UA196 worms was 95%, 87%, and 78% on day 5, 10, and 15, respectively after treatment with 100 μM NS163 at L4 stage. The % decline in the total DA neurons in UA196 worms was 72%, 36%, and 23% after 5, 10, and 15 days, respectively. In contrast, in NS163 treated UA196 worms, the % loss of total number of DA neurons were less than 5% even after 15 days (Figure 1.7k). The data suggest a remarkable neuroprotective effect of NS163 as a significant number of DA neurons were intact upto day 15 (Figure 1.7h-k). Other reported ligands were not able to achieve such a remarkable neuroprotective effect against αS aggregation mediated degeneration of DA neurons in C elegans PD model even at 1 mM concentration[36]. Under matched conditions, NS132 also displayed a very good neuroprotective effect on the degeneration of DA neurons in UA196 worms[50]. The neuroprotective effect of NS163 was better than NS132, most likely due to former's better ability to permeate the cell membranes.

1.3.3 Effect of OPs on the motility rate of UA196 strain

The degeneration of DA neurons has been directly linked with the loss of motor functions, including the slow mortility rate. Therefore, we assessed the motility rate of UA196 in the absence and presence of NS163 using WMicroTracker ARENA plate reader (Figure 1.7o,p). There was a significant decline in the motility rate (overall activity counts) of the UA196 worms (Figure 1.7o,p, Blue) during the aging process in comparison to the positive control worms (Figure 1.7o,p, N2, green). In marked contrast, the motility rate of UA196 worms treated with NS163 (at L4 stage) was significantly improved dring the aging process. The improvement in the motility rate is likely due to the rescue of the degeneration

of DA neurons by NS163. Since, NS132 also displayed neuroprotective effect, we also assessed its effect on the motility rate of UA196 worms. At same conc. to NS163, we observed a noticeable rescue of motility rate of UA196 worms in the presence of NS132 during the aging process[50]. The effect of NS163 was better than NS132 on the motility rate of UA196 worms.

1.3.4 Effect of OPs on the dopamine level in UA196 strain of *C. elegans*

Dopamine is produced in the substantia nigra, ventral tegmental, and hypothalamus of the brain. It is a neurotransmitter that regulates movement in living systems[51]. We have shown that a decrease in the motility rate in UA196 worms is a consequence of the loss of DA neurons, which is potentially associated with a substantial decrease in the dopamine synthesis. Therefore, we hypothesized that the motility rate can be enhanced by administrating dopamine in UA196 worms. The 2 mM dopamine treated UA196 worms displayed a much higher motility rate during the aging process (Figure 1.9l). In marked contrast, we did not observe any significant difference in the motility rate for NS163 treated UA196 worms in the absence and presence of 2 mM dopamine (Figure 1.9m). We observed similar behaviour for the N2 worms in the presence of 2 mM dopamine (Figure 1.9k). The data suggest that the improvement in the motility rate of the dopamine treated UA196 worms is the compensation for the decrease in the dopamine synthesis due to the loss of DA neurons. However, we did not observe any change in the motility rate for N2 and NS163 treated UA196 worms because of the intact DA neurons and dopamine synthesis.

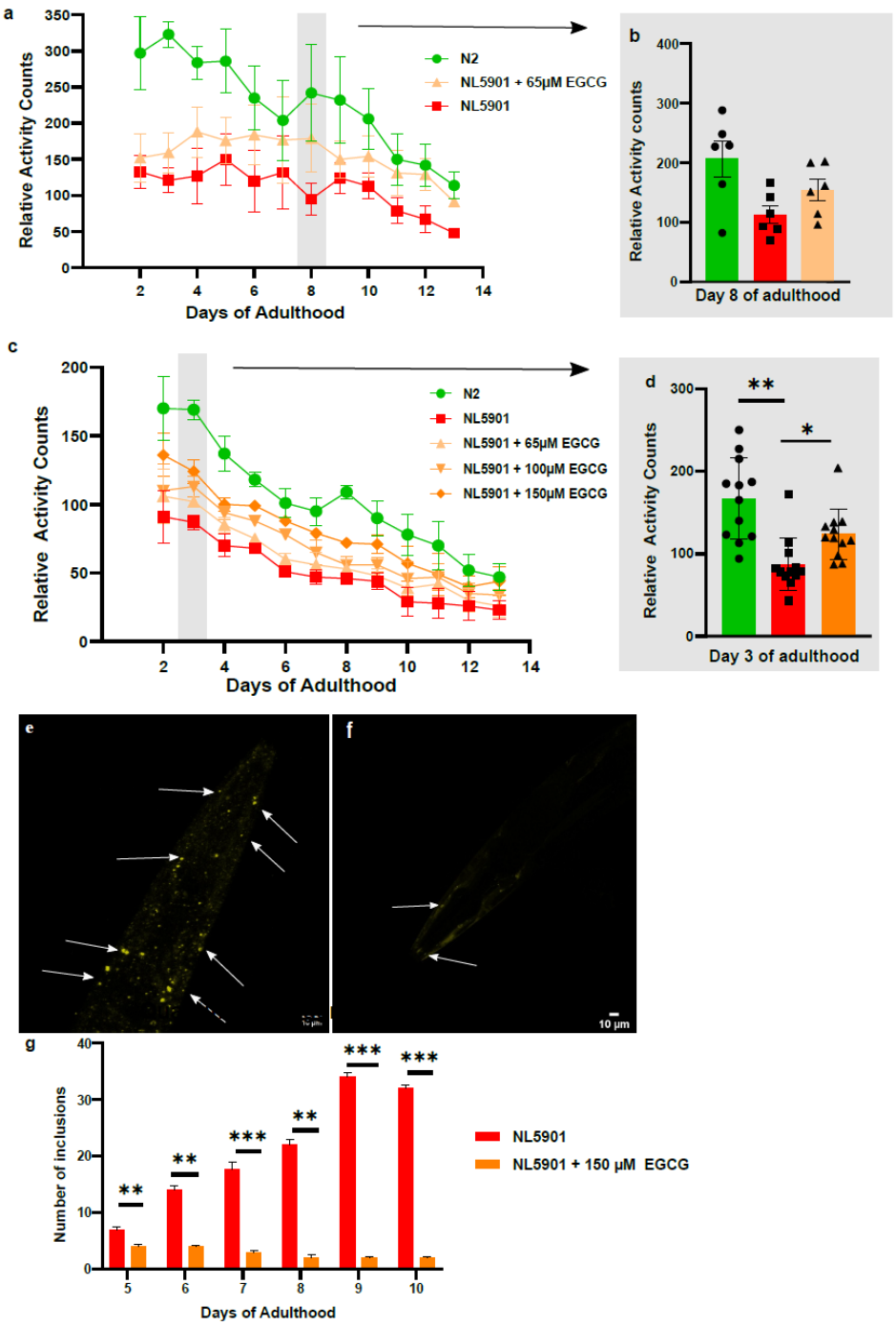

Figure 1.3 The intracellular inhibition of αS aggregation by EGCG in NL5901 strain of *C. elegans*. **a** Paralysis assay (using 6-well plate) shows the relative activity counts for 12 days of adulthood of N2 and NL5901 strains in the absence and presence of 65 µM EGCG. **b** A graphical representation with statistical analysis of the relative activity counts of N2 and NL5901 strain in the absence and presence of 65 µM EGCG for day 8 of adulthood. The data shows the mean, and the error bars expresses the s.e.m. (n = 3 independent experiments and each n included two technical replicates. **c** Paralysis assay (using 24-well

plate) shows the relative activity counts for 12 days of adulthood of N2 and NL5901 strains in the absence and presence of EGCG (65 μM, 100 μM, and 150 μM). **d** A graphical representation with statistical analysis of the relative activity counts of N2 and NL5901 strains in the absence and presence of 150 μM EGCG for day 3 of adulthood. The data shows the mean, and the error bars represents the s.e.m. (n = 3 independent experiments and each n included four technical replicates. Confocal images **(e, f)** of αS-YFP inclusions (white arrows) in muscle cells of NL5901 strain (days of adulthood = 3 days) in the absence **(e)** and **(f)** presence of 150 μM EGCG. **g** The number of inclusions for experiment **'e, f'** for NL5901 strain in the absence and presence of 150 μM EGCG (days 5 – 10 of adulthood). The data were expressed as mean and the error bars shows the s.e.m. (n = 3 independent experiments and each n included at least 10 technical replicates). ANOVA with Tukey's multiple comparison test was used to perform statistical analysis. *$p<0.05$, **$p < 0.01$, ***$p<0.001$, ****$p < 0.0001$. Source data file was used to provide source data.

1.3.5 Effect of OPs on Behavioral deficits in UA196 strain of *C. elegans*

Chemotaxis assay was conducted to investigate the chemosensory deficits caused by αS-induced toxicity in UA196 strain of *C. elegans* (1.8a-g, 1.9e-j). Chemotaxis Index (CI) was used as a measure to evaluate the attractive (positive value) and repulsive (negative value) responses[40]. This assay was first conducted on day 0 of adulthood (L4 stage) for untreated UA196 strain when the animals were in the early stage of growth and they had intact DA neurons. The assay was first performed in the presence of NS163 and NS132 (attractants) and EtOH was used as a repellant. The chemotaxis data (Figure 1.8a) showed that the animals were attracted to the ligands compared to the EtOH repellant. This suggests that when inhibitory drugs are adminstered to the diseased animals at early ages, they can become attracted to the drug and ingest the solution of the drug due to the proper functioning of their chemosensory DA neurons at the time prior to neurodegeneration. As a result, the drug can protect the neuronal cells against amyloid toxicity. Also, chemotaxis assay was conducted for N2 and UA196 in the absence and presence of NS163 and in the presence of OP50 and EtOH at L4 stage (Figure 1.9f) and day 7 of adulthood (Figure 1.9g).

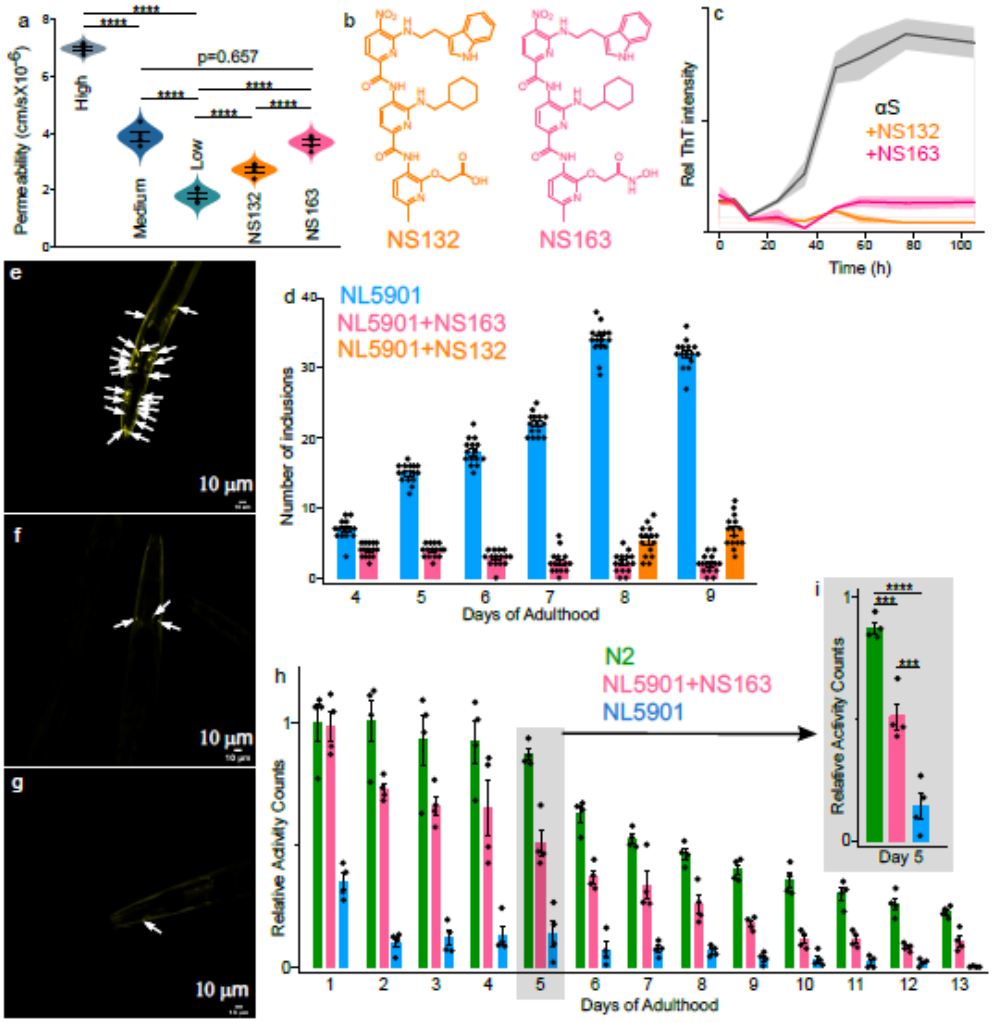

Figure 1.4 The intracellular inhibition of αS aggregation by OPs in an *in vivo* PD model. **a**, Assessment of cell permeability of the indicated ligands using the PAMPA. **b**, The chemical structures of NS132 and NS163. **c**, The ThT -based aggregation profile of 100 µM αS in the absence and presence of the indicated ligands at an equimolar ratio. **d**, The number of inclusions for experiment '**e-g**' in NL5901 in the absence and presence of NS132 and NS163 from day four to day nine of the adulthood. The representative confocal images of αS-YFP inclusions (white arrows) in the body wall muscle cells of NL5901 (Days of adulthood = 7 days) in the absence (**e**) and presence of 100 µM NS163 (**f**) and 100 µM NS132 (**g**). **h**, The locomotion for 13 days of adulthood of N2 and NL5901 and statistics (Day 5 of adulthood, **i**) in the absence and presence of 100 µM NS163. For each confocal imaging experiment (e-g), at least 10 worms were used, and the inclusions were counted manually, and each condition (each day of adulthood) consisted of at least four independent experiments. For locomotion experiment, a total of 50 worms were used in

duplicate for each experiment and each condition consisted of at least four independent experiments. The data were expressed as mean and the error bars report the s.e.m. (n = 3 independent experiments and each n consisted of three technical replicates). The statistical analysis was performed using ANOVA with Tukey's multiple comparison test. *p < 0.05, **p < 0.01, ***p < 0.001.

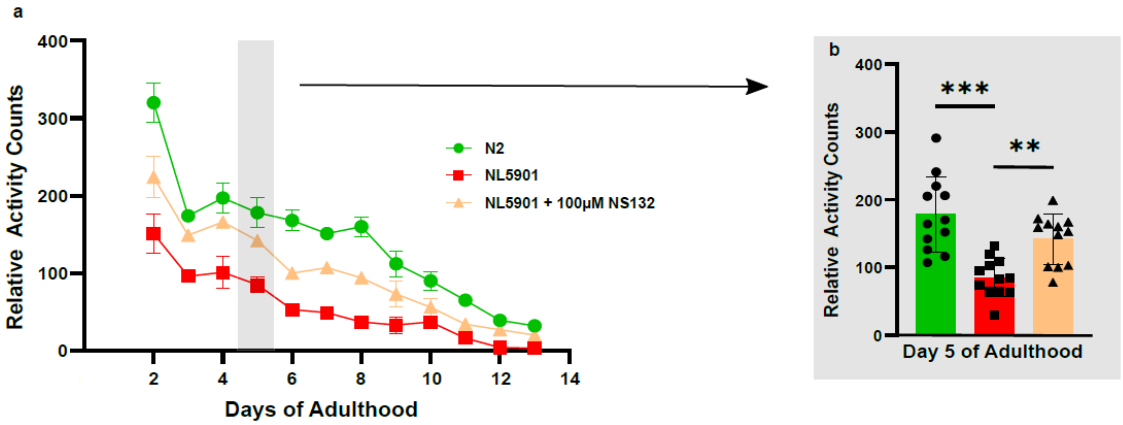

Figure 1.5 The intracellular inhibition of αS aggregation by NS132 in an *in vivo* PD model. **a** The locomotion for 12 days of adulthood of N2 and NL5901 and statistics (Day 5 of adulthood, **b**) in the absence and presence of 100 μM NS132. A total of 50 animals were used in four technical replicates for each condition and each condition consisted of at least three independent biological replicates. The reported values in each experiment represent the average of three data points and the reported error bars are the s.e.m's for at least three sets of experiments conducted on separate occasions. Statistical significance was analyzed using a one-way ANOVA followed by Tukey's multiple comparison test. *p<0.05, **p<0.01, ***p<0.001, ****p<0.0001.

At L4 stage, all the animals were attracted to OP50 and repelled from EtOH because all their DA neurons were functioning at normal levels. But on day 7, the chemotaxis data showed that the N2 WT strain and UA196 strain treated with NS163 maintained their behavior earlier observed at L4 stage but the untreated diseased UA196 strain moved randomly and could not differentiate between the OP50 food and the toxic repellant, ETOH; this maybe because some of the the neurons were dead in the older diseased animals and chemosensory abilities were lost**.**

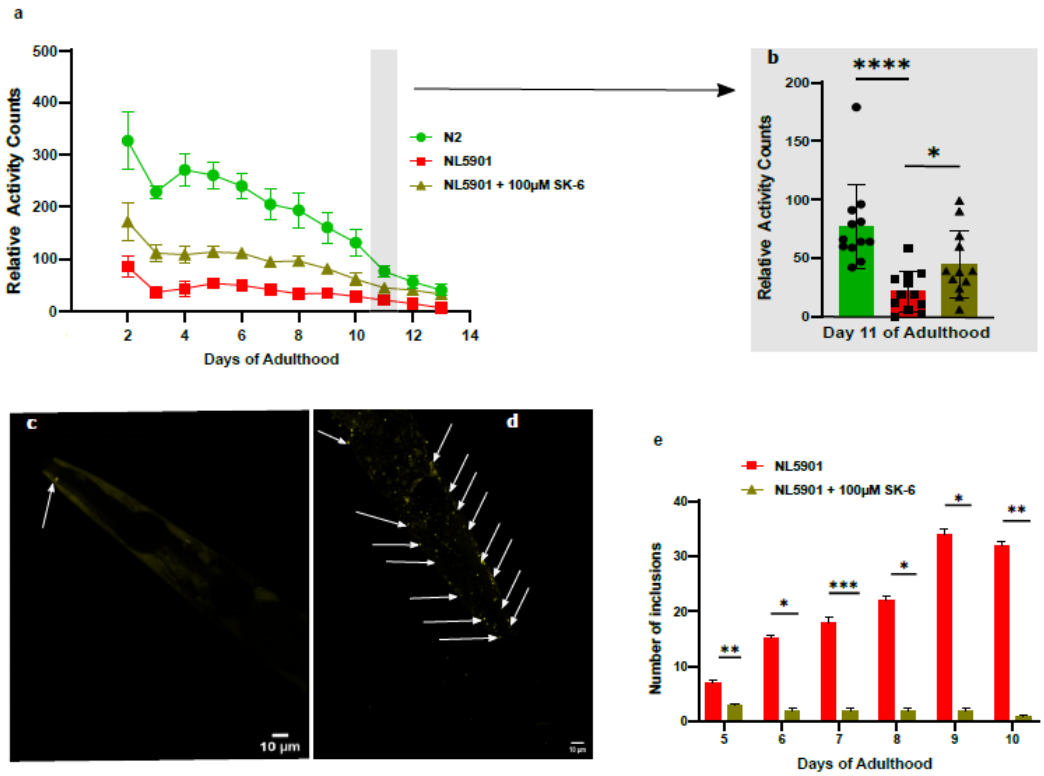

Figure 1.6 The intracellular inhibition of αS aggregation by stapled peptide (SK6) in an *in vivo* PD model. **a** The locomotion for 12 days of adulthood of N2 and NL5901 and statistics (Day 11 of adulthood, **b**) in the absence and presence of 100 µM SK6. A total of 50 animals were used in four technical replicates for each condition and each condition consisted of at least three independent biological replicates. Confocal images of αS-YFP inclusions (white arrows) in muscle cells of NL5901 in the presence **(c)** and absence **(d)** of 100 µM SK6 (days of adulthood = 11 days). The reported values in each experiment represent the average of atleast three data points and the reported error bars are the s.e.m's for at least three sets of experiments conducted on separate occasions. Statistical significance was analyzed using a one-way ANOVA followed by Tukey's multiple comparison test. *p<0.05, **p<0.01, ***p<0.001, ****p<0.0001.

It has been shown that the lack of dopamine synthesis in DA neurons in C elegans leads to the behavioural deficits including the food sensing behaviour. The DA neurons in UA196 worms degenerate overtime, which lead to a decrease in the amount of dopamine but NS163 can rescue the DA neuron degeneration. Therefore, we hypothesized that NS163

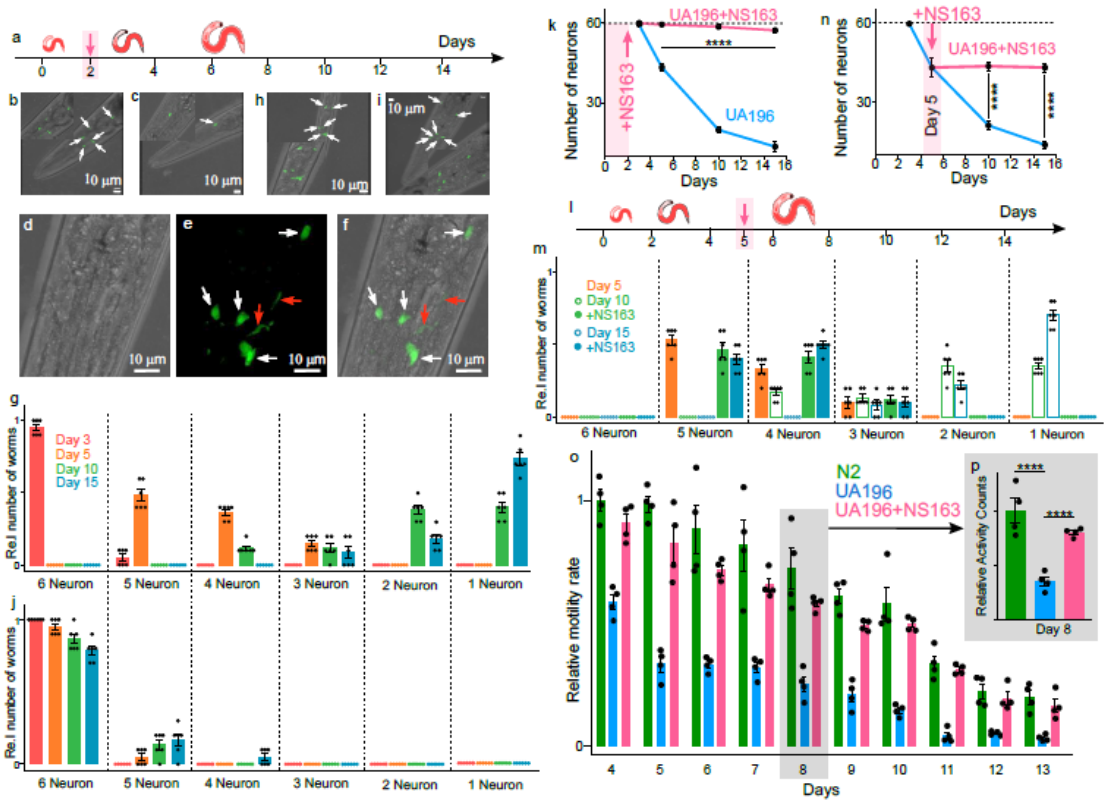

Figure 1.7 Neuroprotective effect of OPs on the degeneration of DA neurons. **a,** Schematic of the aging process of UA196 worms and their treatment with the ligands. Representative confocal images of UA196 worms in the absence (**b,c**) and presence (**h,i**) of NS163 on day 3 and day 12. **d,e**,**f**, The healthy (white arrow) and degenerated (red arrow) DA neurons in UA196 worms on day 5. **g,** The relative number of neurons in UA196 worms during the aging process in the absence (**g**) and presence of NS163 (**j**). **k**, Statistics for the total number of neurons in UA196 worms during the aging process in the absence and presence of NS163. **l**, Schematic of the aging process of UA196 worms and their treatment with the ligands at the mid-stage pathology (day 5). **m**, The relative number of neurons in UA196 worms during the aging process when treated on day 5 with NS163. **n**, Statistics for the total number of neurons in UA196 worms when treated on day 5 with NS163. **o**, The locomotion for 13 days of adulthood of N2 and UA196 and statistics (Day 8 of adulthood, **p**) in the absence and presence of 25 µM NS163. For each confocal imaging experiment (b-f, h-i), at least 10 worms were used, and the inclusions were counted manually, and each condition (day) consisted of six independent experiments. For locomotion experiment, a total of 50 worms were used in duplicate for each experiment and each condition consisted of at least four independent experiments. The data were expressed as mean and the error bars report the s.e.m. (n = 4 independent experiments and each n consisted of four technical replicates). The statistical analysis was performed using ANOVA with Tukey's multiple comparison test. *p < 0.05, **p < 0.01, ***p < 0.001, ****p < 0.0001.

will be able to rescue behavioural deficits of UA196 worms. We used a chemotaxis assay to assess the effect of NS163 on the behavioural deficits of UA196 worms. In this assay, a petri dish was divided into four quardants where two opposite quardants were treated with a toxic chemical for worms (ethanol, repellent) or food for worms (*E. coli*, attractant). For each experiment, 50 worms were placed at the center of the dish and ethanol (red dots) and *E. coli* (green) at the polar ends of the petri dish (Figure 1.9e). We used ARENA plate reader to measure the CI over time with values from -1.0 to +1.0. The kinetics of the CI index over time was generated based on the time spent by worms in ethanol or *E. coli* quardants. The kinetics of the CI over time was monitored on day 3 for 2 h for various worms, including N2, UA196, and UA196+NS163 (Figure 1.9f).

The kinetic data for the CI suggest that all the worms spent their time in the *E. coli* quardants with a value of ~1 during the course of 2h (Figure 1.9f). None of the worms displayed behavioural deficit on day 3 (Figure 1.96f). All the DA neurons in UA196 worms on day 3 were intact (Figure 1.9f); therefore, we anticipate similar behavioral response of UA196 (Figure 1.9f) and N2 (Figure 1.9f) worms. In marked contrast, on day 10 (day 7 of adulthood), the kinetics of the CI of UA196 did not display any preference for repellent or attractant for the whole time course of the experiment (Figure 1.9g,h). The lack of preference of UA196 worms is due to the behavioural deficits caused by the decrease in dopamine because of the degeneration of DA neurons. However, the UA196 worms treated with NS163 displayed a strong preference toward *E. coli* (Figure 1.9g,i), similar to the control worms (Figure 1.9g,j), indicated by the chemotaxis indices. Clearly, NS163 was able to rescue the behavioural deficits of UA196. Similarly, NS132 was also able to rescue behavioural deficits in UA196 worms under the matched conditions to NS163[50].

1.3.6 Effects of ligands (OPs) on the ROS level in *C. elegans* (N2 and UA196)

The antioxidant effects of ligands (NS163 and NS132, 100 μM) were evaluated *in vivo* by measuring the intracellular ROS level after treating the diseased animals (UA196) with the ligands. ROS molecules help with cell signaling for normal biological mechanisms in living organisms[52]. Normal physiology may be disrupted by the excessive generation of ROS which can induce damage to multiple cellular organelles and processes. It was observed that the fluorescence intensity for the UA196 treated with ligands was significantly low compared to the untreated diseased UA196 (Figure 1.9b-d). High amount of toxic intracellular ROS was observed in the untreated diseased UA196 (Figure 1.9a,c-d) because the aggregation of αS in DA neurons induces oxidative stress resulting to the increased intracellular ROS level[40].

In the presence of ligands, low amount of intracellular ROS was observed because the ligands might have inhibited αS aggregation and resulted to no cellular oxidative stress and less amount of ROS level in cells. One of the causal agents associated with the etiology of PD is the generation of the ROS, which oxidizes various lipids, proteins, and DNA. The neurodegeneration in UA196 worms due to αS aggregation leads to the production of intraworm ROS. The ROS level was determined using a fluorescent probe (H_2DCFDA), which reacts with intraworm ROS and produces green fluorescent signal, whose intensity increases up to 2 h (Figures 1.9a-b, 1.10a-j). In marked contrast, NS163 treated UA196 worms displayed a significant decrease in the intracellular ROS level (Figures 1.9b-d, 1.10h-j). The data suggests that the decrease in the ROS level in UA196 worms in the presence of NS163 is a consequence of the rescue of neurodegeneration of DA neurons. In comparison with NS163, NS132 was able to decrease ROS level in UA196 worms almost

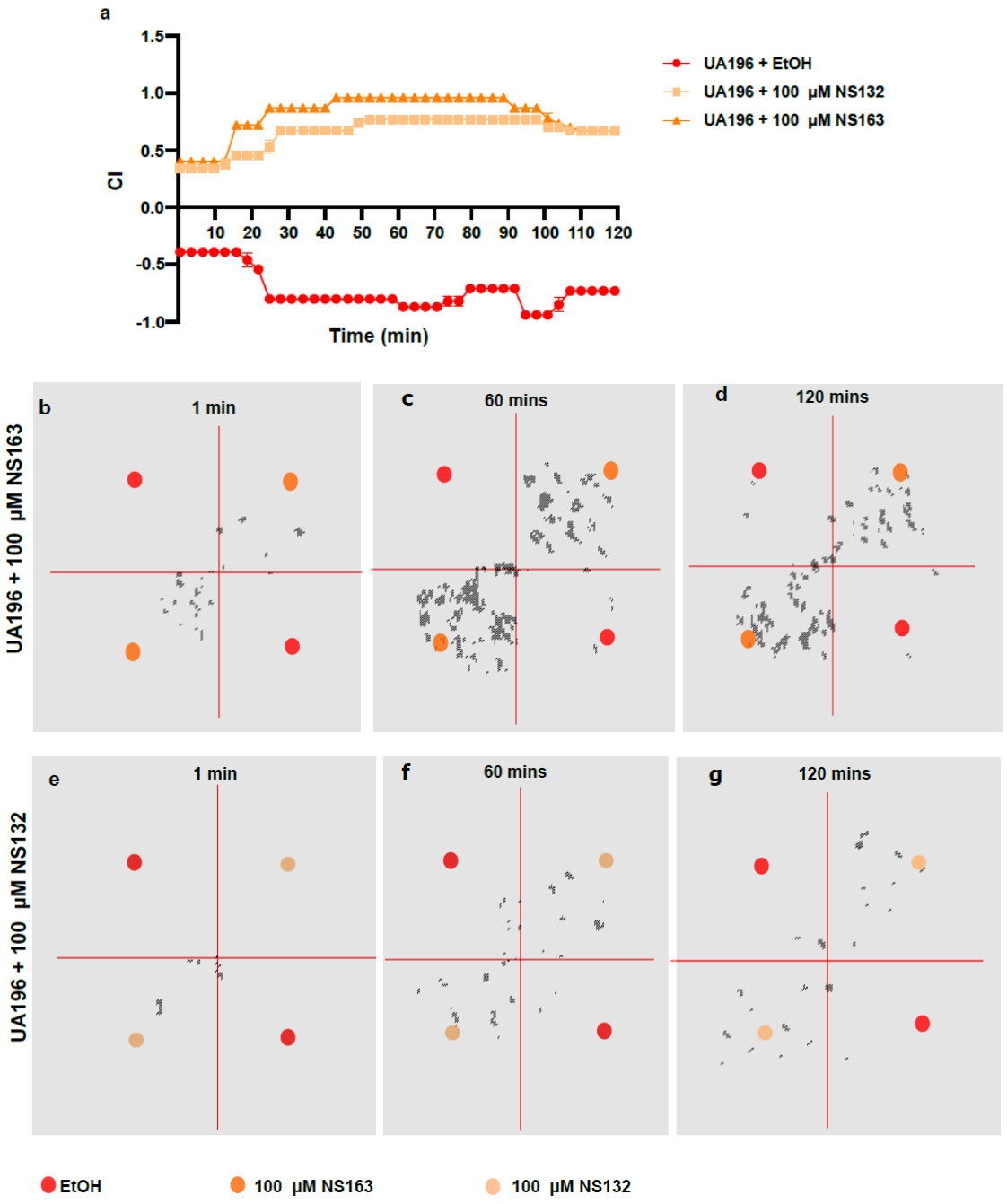

Figure 1.8 Chemotaxis assay for the behavior of UA196 in the absence and presence of ligands on day 0 of adulthood (L4 stage). **a** The chemotaxis behavior assay for UA196 strain in the presence of ligands (100 µM NS163, orange color, and 100 µM NS132, light orange color) and repellant (EtOH, red color). The Chemotaxis images at 1 min (b), 60 min (c) and 120 min (d) of UA196 in the presence of 100 µM NS163 (orange spots) and EtOH (red spots). The chemotaxis images at 1 min (e), 60 min (f), 120 min (g) of UA196 in the presence of 100 µM NS132 (light orange spots) and (red spots). A total of 50 animals were used in two technical replicates for each condition and each condition consisted of at least

two independent biological replicates. The reported values in each experiment represent the average of atleast two data points and the reported error bars are the s.e.m's for at least two sets of experiments conducted on separate occasions. Statistical significance was analyzed using a one-way ANOVA followed by Tukey's multiple comparison test. *p<0.05, **p<0.01, ***p<0.001, ****p<0.0001.

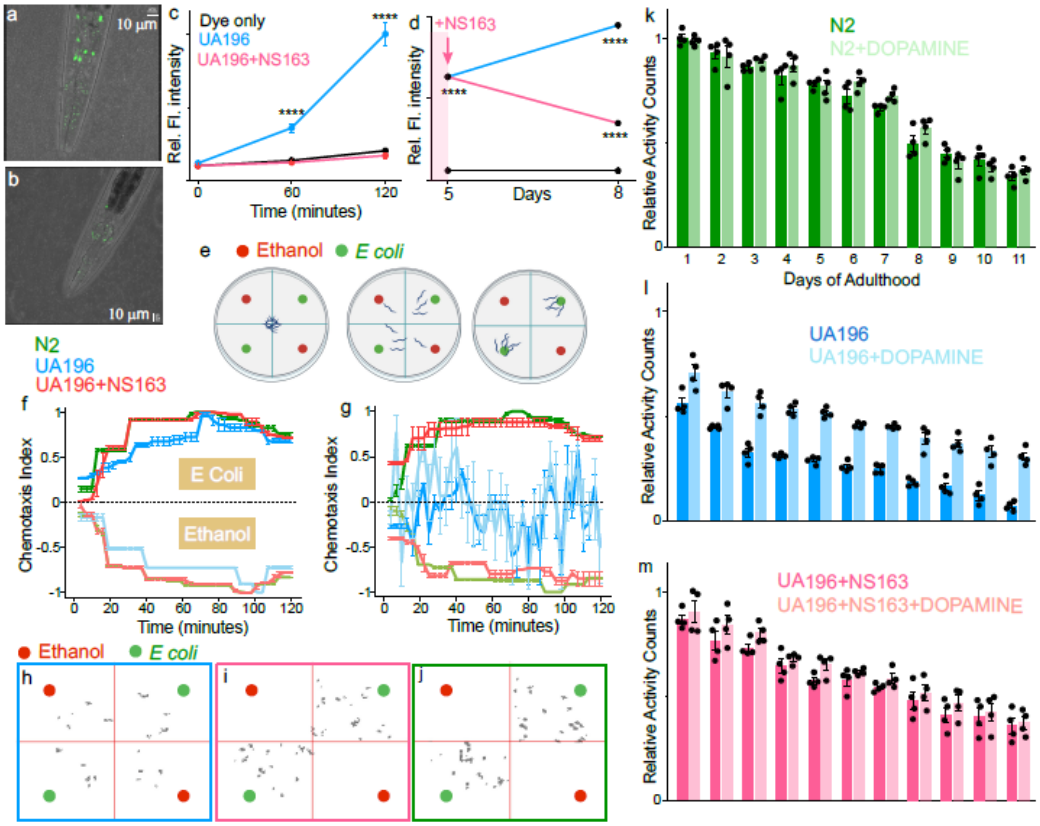

Figure 1.9 Effect of OPs on the PD phenotypes in UA196 strain. Representative confocal images of UA196 worms (day 8) treated with CM-H_2DCFDA dye to quantify ROS level (green) in the abence (**a**) and presence of NS163 (**b**, day 2 treatment). **c**,**d**, Statistical analysis of the the production of ROS level for experiment **a-b**. The locomotion for 13 days of adulthood of N2 (**k**), UA196 worms (**l**) and UA196 worms treated with NS163 (**m**) in the absence and presence of 2 mM dopamine. Chemotaxis index (CI) graph for attraction towards OP50 and repulsion towards EtOH at L4 stage **(f)** and day 7 of adulthood **(g)** for N2 and UA196 in the absence and presence of NS163. **e** Schematic to assess the behavioral deficits in UA196 worms in a petri dish in the presence of ethanol and *E. coli* as a function of time. Snapshots at 60 min. of the animated videos collected for the CI for UA196 (**h**), UA196+NS163 (**i**), and N2 (**j**) under the indicated conditions. For ROS level quantification, at least 50 worms were used, and each condition consisted of three independent experiments. For locomotion experiment, a total of 50 worms were used in duplicate for each experiment and each condition consisted of four independent experiments. For chemotaxis assays, a total of 50 worms were used for each experiment

and each condition consisted of three independent experiments. The data were expressed as mean and the error bars report the s.e.m. (n = 3 or 4 independent experiments and each n consisted of a minimum of two technical replicates). The statistical analysis was performed using ANOVA with Tukey's multiple comparison test. *p < 0.05, **p < 0.01, ***p < 0.001, ****p < 0.0001.

at the same level (Figure 1.10a). The effect of NS163 (and NS132) on the intraworm ROS level was also tested when these ligands were added to the pre-existing PD *C. elegans* model. The ROS level of UA196 worms was measured on day 5, followed by the addition of ligands and subsequently, the ROS level was assessed on day 8 in the absence and presence of ligands. In the diseased UA196, the ROS level increased from day 5 to day 8 due to the increase in the degeneration of DA neurons mediated by αS aggregation (Figure 1.9d). However, the ROS level was significantly decreased in UA196 worms treated with NS163 (Figure 1.9d, 1.14a-b) and NS132 (Figure 1.14a-b). Clearly both ligands are potent ligands in rescuing degeneration of DA neurons (and ROS level) when added to pre-existing PD *C. elegans* model.

1.3.7 Extensive Proteome analysis during aging of *C. elegans*

Proteome changes were studied in N2 and UA196 strains of *C. elegans* in the absence and presence of ligand (NS163, 100 μM) at day seven of adulthood. 2071 different proteins were identified and quantified. One of the major reasons for this sutdy is to identify proteins that might have been upregulated or downregulated due to sequestration or recruitment by lewy bodies. Lewy bodies are massive protein deposits including αS aggregates and other mitochondrial and cytoplasmic proteins. Several proteins of interest including HSP/HSR (Figure 1.11a-b), Proteasome (Figure 1.11c-d), and Ubiquitin (Figure 1.11e-f). In the untreated diseased UA196 strain, several HSP/HSR protein profiles were

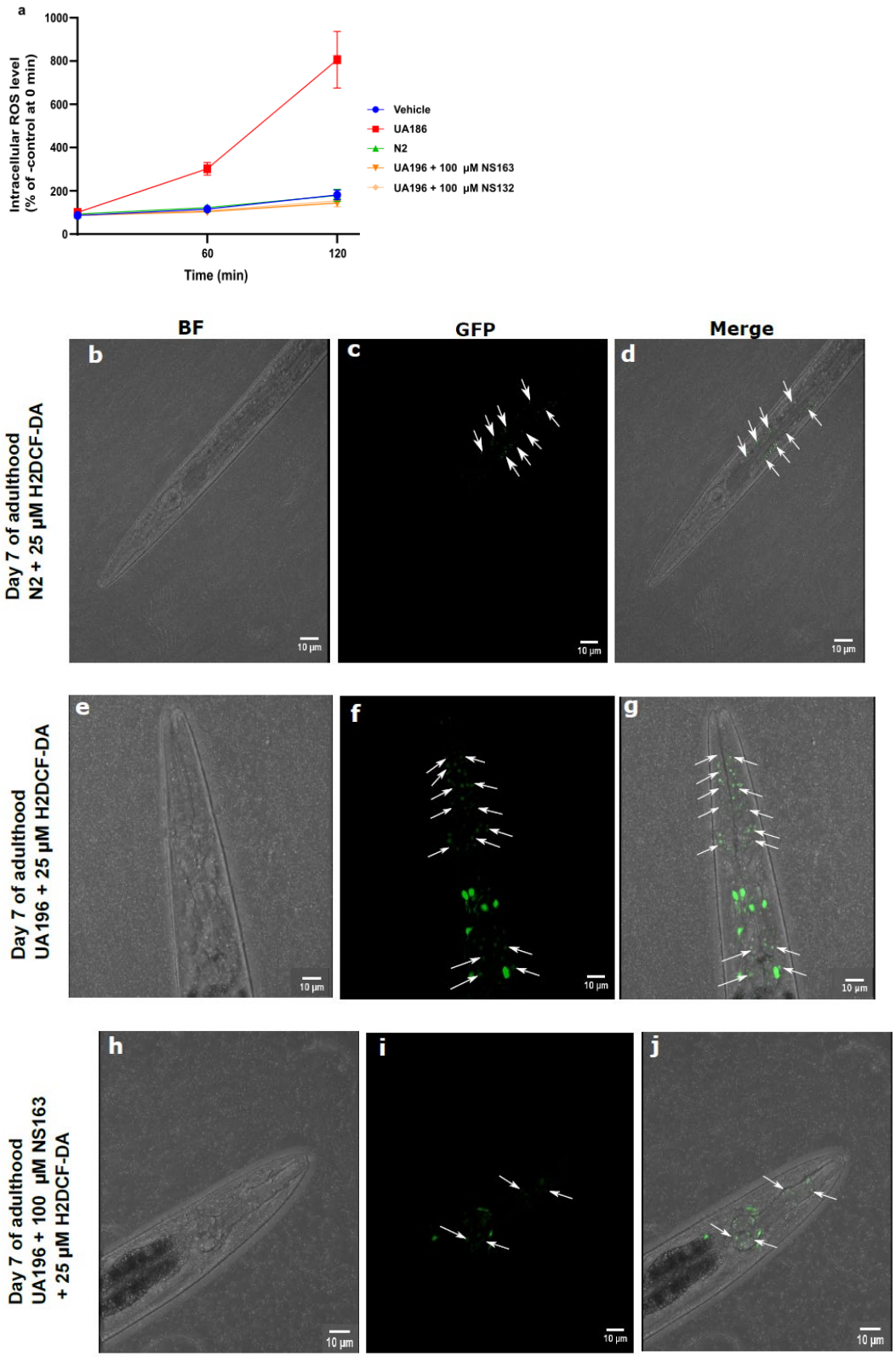
a
Intracellular ROS level (% of -control at 0 min)
1000
800
600
400
200
0
60
120
Time (min)
Vehicle
UA186
N2
UA196 + 100 µM NS163
UA196 + 100 µM NS132
BF
GFP
Merge
Day 7 of adulthood N2 + 25 µM H2DCF-DA
Day 7 of adulthood UA196 + 25 µM H2DCF-DA
Day 7 of adulthood UA196 + 100 µM NS163 + 25 µM H2DCF-DA
b
c
d
e
f
g
h
i
j
10 µm

Figure 1.10 The effect of ligands on the ROS level in UA196 strain. **a** The comparison of the ROS level in UA196 worms in the absence and presence of 100 μM NS132 at the indicated time points. The UA196 worms were treated with NS132 on day 2 and day 4. The ROS level was measured on day 10. For ROS level quantification, at least 50 animals were used, and each condition consisted of three independent experiments. The data were expressed as mean and the error bars reported the s.e.m. (n = 3 independent experiments and each n consisted of three technical replicates). **c-d** DCF fluorescence images of N2 (positive control) in the presence of 25 μM H_2DCF-DA. **e-g** DCF fluorescence images of untreated UA196 (negative control) in the presence of 25 μM H_2DCF-DA. **h-j** DCF fluorescence images of UA196 treated with 100 μM NS163 in the presence of 25 μM H_2DCF-DA. The statistical analysis was performed using ANOVA with Tukey's multiple comparison test. *$p < 0.05$, **$p < 0.01$, ***$p < 0.001$, ****$p < 0.0001$.

found to change by almost 2-folds (Figure 1.11a). Statistical analysis was conducted for hsp 16.1 (Figure 1.11b) showing downregulation of the protein in the diseased UA196 strain by almost 2-folds and upregulation of the protein in the presence of NS163 comparable to the WT N2 strain. In the untreated diseased UA196 strain, several proteasome protein profiles changed by almost 5-folds (Figure 1.11c). Statistical analysis was conducted for rpt-2 (Figure 1.11d) showing downregulation of the protein in the untreated diseased UA196 strain by about one-fold but in the presence of NS163, there was upregulation of the protein comparable to the WT N2 strain. Also, in the untreated diseased UA196 strain, ubiquitin protein profile changed by about two-fold. Statistical analysis was conducted for rnp-13 (Figure 1.11f) showing downregulation of the protein in the untreated diseased UA196 strain by about 0.25-fold and upregulation of the protein in the presence of NS163 comparable to the WT N2 strain.

1.3.8 Effects of OPs on the neurodegeneration in a post-disease onset PD model

PD model UA196 strain of *C. elegans* used in this study were not treated at an early stage or at the onset of the disease until when the animals became adults with high level of αS inclusions resulting to some DA neuronal death. The reason for this study was to test

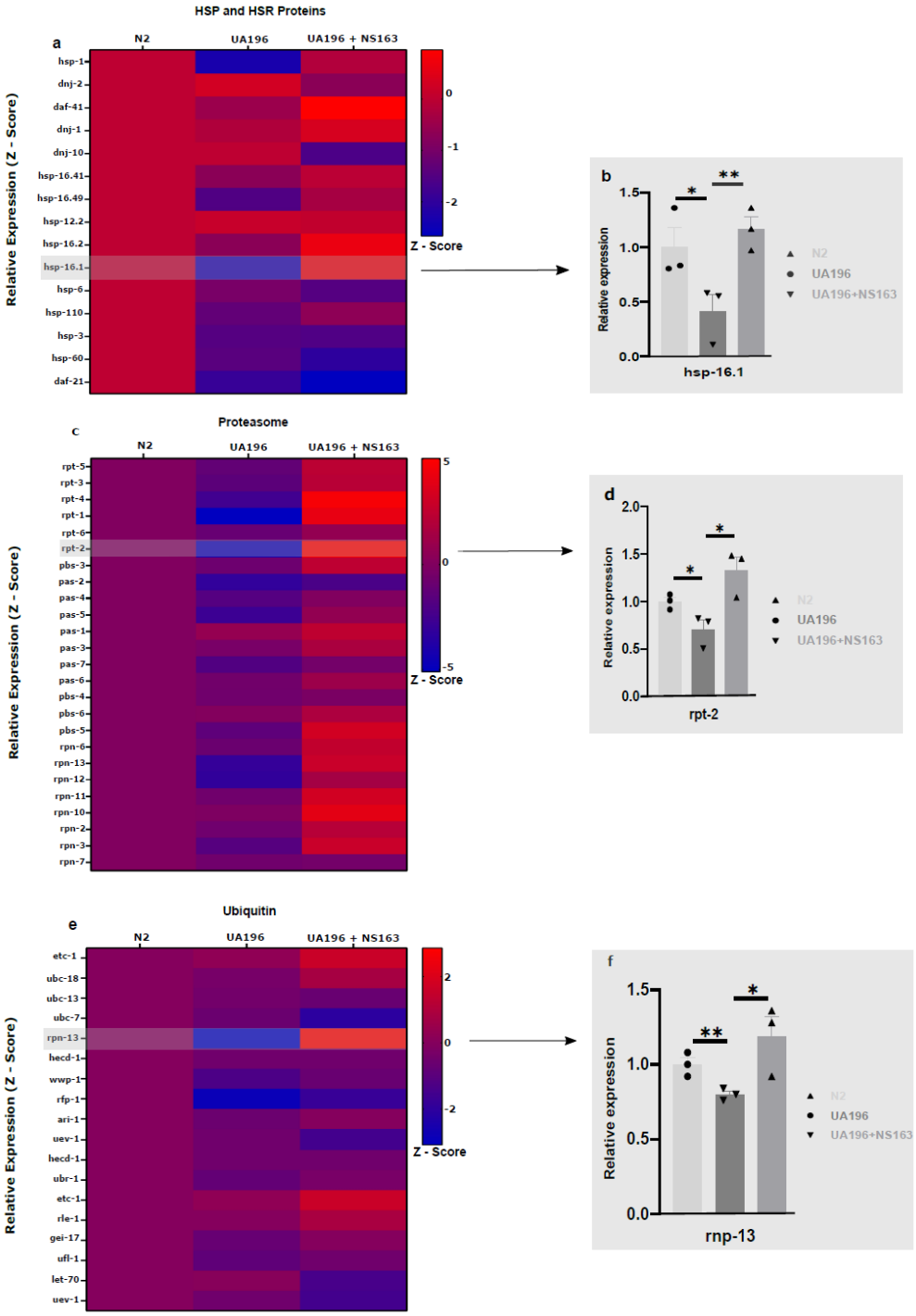

Figure 1.11 Total proteomics analysis of *C. elegans* in the absence and presence of ligands at day seven of adulthood. **a** hsp and hsr protein profiles changing by one- or two-folds in the absence and presence of NS163 (100 µM in DMSO). The red shadings indicate increased abundance/upregulation of proteins and the blue shadings indicate decreased abundance/downregulation of proteins. Each protein group (one per line) is shown along the y-axis and the different worm conditions are shown on the x-axis. **b** Statistical analysis

of hsp 16.1 showing downregulation of the protein in the diseased UA196 by about two-fold and upregulation of the protein in UA196 in the presence of NS163 comparable to the WT N2 strain. The results are expressed as normalized mRNA expression relative to the control N2 worms. **c** Proteasome profiles changing by five-folds in the absence and presence of NS163 (100 μM in DMSO). The red shadings indicate increased abundance/upregulation of proteins and the blue shadings indicate decreased abundance/downregulation of proteins. Each protein group (one per line) is shown along the y-axis and the different worm conditions are shown on the x-axis. **d** Statistical analysis of rpt-2 showing downregulation of the protein in the diseased UA196 by about one-fold and upregulation of the protein in UA196 in the presence of NS163 comparable to the WT N2 strain. The results are expressed as normalized mRNA expression relative to the control N2 worms. **e** Ubiquitin protein profiles changing by two-folds in the absence and presence of NS163 (100 μM in DMSO). The red shadings indicate increased abundance/upregulation of proteins and the blue shadings indicate decreased abundance/downregulation of proteins. Each protein group (one per line) is shown along the y-axis and the different worm conditions are shown on the x-axis. **f** Statistical analysis of rnp-13 showing downregulation of the protein in the diseased UA196 by about 0.25 fold and upregulation of the protein in UA196 in the presence of NS163 comparable to the WT N2 strain. The results are expressed as normalized mRNA expression relative to the control N2 worms. The reported values in each experiment represent the average of atleast three data points and the reported error bars are the s.e.m for at least three sets of experiments conducted on separate occasions. Statistical significance was analyzed using two-way ANOVA followed by Tukey's multiple comparison test. *$p<0.05$, **$p<0.01$, ***$p<0.001$, ****$p<0.0001$.

the antagonistic activity of the ligands (NS163 and NS132) at inhibiting αS aggregation in the presence of high concentration of aPPIs. In this experiment, the animals were not treated until at day two of adulthood when they were treated (separately) with the ligands (NS163 and NS132, 100 μM). Confocal images collected at day two of adulthood (before treatment) (Figure 1.12a-c, 1.13a-c) showed that some of the diseased worms (~40%) had 5 anterior DA neurons. After treatment with the ligands, on day seven of adulthood, confocal imaging was conducted and the DA neurons were manually counted; it was found that ~40% animals treated with NS163 (100 μM) had 5 anterior DA neurons intact with no complete (6) DA neurons intact (Figure 1.12d-f, j) while 40% animals treated with NS132 (100 μM) had 4 anterior DA neurons intact with no complete (6) or 5 DA neurons intact

(Figure 1.13d-f, j). Also, on day seven of adulthood, confocal imaging (Figure 1.12g-i, 1.13g-i) showed the untreated diseased UA196 strain had only 1 anterior DA neuron intact. Based on the results, it can be concluded that NS163 was able to rescue 100% of the 5 DA neurons (from the day of treatment, day two of adulthood) without causing further loss of the neurons during the aging of the animals while NS132 was not able to rescue all the 5 DA neurons, but it was able to rescue only 4 out of the 5 DA neurons.

These results further suggested the potent antagonistic effects of NS163 against the aggregation of αS. Also, the antioxidant effects of ligands (NS163 and NS132, 100 μM) were evaluated *in vivo* by measuring the intracellular ROS level after mid stage/delayed treatment of the diseased animals (UA196) with the ligands (Figure 1.14a-b). Two ROS assays were conducted pre- and post-treatment with the ligands. On day two of adulthood, the ROS assay was conducted pre-treatment of the animals (WT N2 and UA196 strains); high concentration of toxic intracellular ROS was found in the UA196 at almost 2-folds compared to the ROS concentration found in the WT N2 strain and based on the fluorescent intensity of the assay samples (Figure 1.14a).

Also, on day two of adulthood, two separate populations (~300) of the diseased UA196 strain were treated (separately) with the NS163 (100 μM) and NS132 (100 μM) ligands. And on day four of adulthood, the animals were re-treated with the ligands to re-constitute the drug in the organisms. On day five of adulthood, a time course ROS fluorescence assay was conducted for all the untreated and treated animals (Figure 1.14b). It was observed that the fluorescence intensity for the UA196 treated with ligands (NS163 and NS132) was significantly low compared to the untreated diseased UA196. High amount of toxic intracellular ROS was observed in the untreated diseased UA196 because

the aggregation of αS in DA neurons induces oxidative stress resulting to the increased intracellular ROS level[40]. In the presence of ligands, low amount of intracellular ROS was observed because the ligands might have inhibited αS aggregation and resulted to no cellular oxidative stress and less amount of ROS level in cells. These results showed that the ligands are effecctive at inhibiting the aggregation of αS at onset and at mid stage of the disease progression.

1.3.9 Study of the prion-like spread of αS in *C. elegans* model

Prion proteins are referred to as infectious agents involving the conformationally changed protein PrPSc which recruits and infects its normal counterpart PrPc and subsequently generating self-propagating misfolded species, which can spread from cell-to-cell[53]. Previous studies have demonstrated that amyloid forming proteins may have prion-like spreading mechanism including αS, β-amyloid, tau, and Huntingtin[54,55]. The transfer of misfolded protein species from an affected cell to neighboring cells caused by propagation (seeding of protein aggregates) can induce templated conversion of native proteins[56–59]. This process is referred to as the prion-like spread of amyloid proteins. αS aggregation in grafted fetal mesencephalic progenitor neurons several years after transplantation was the initial suggestion that supported prion-like propagation of αS[53].

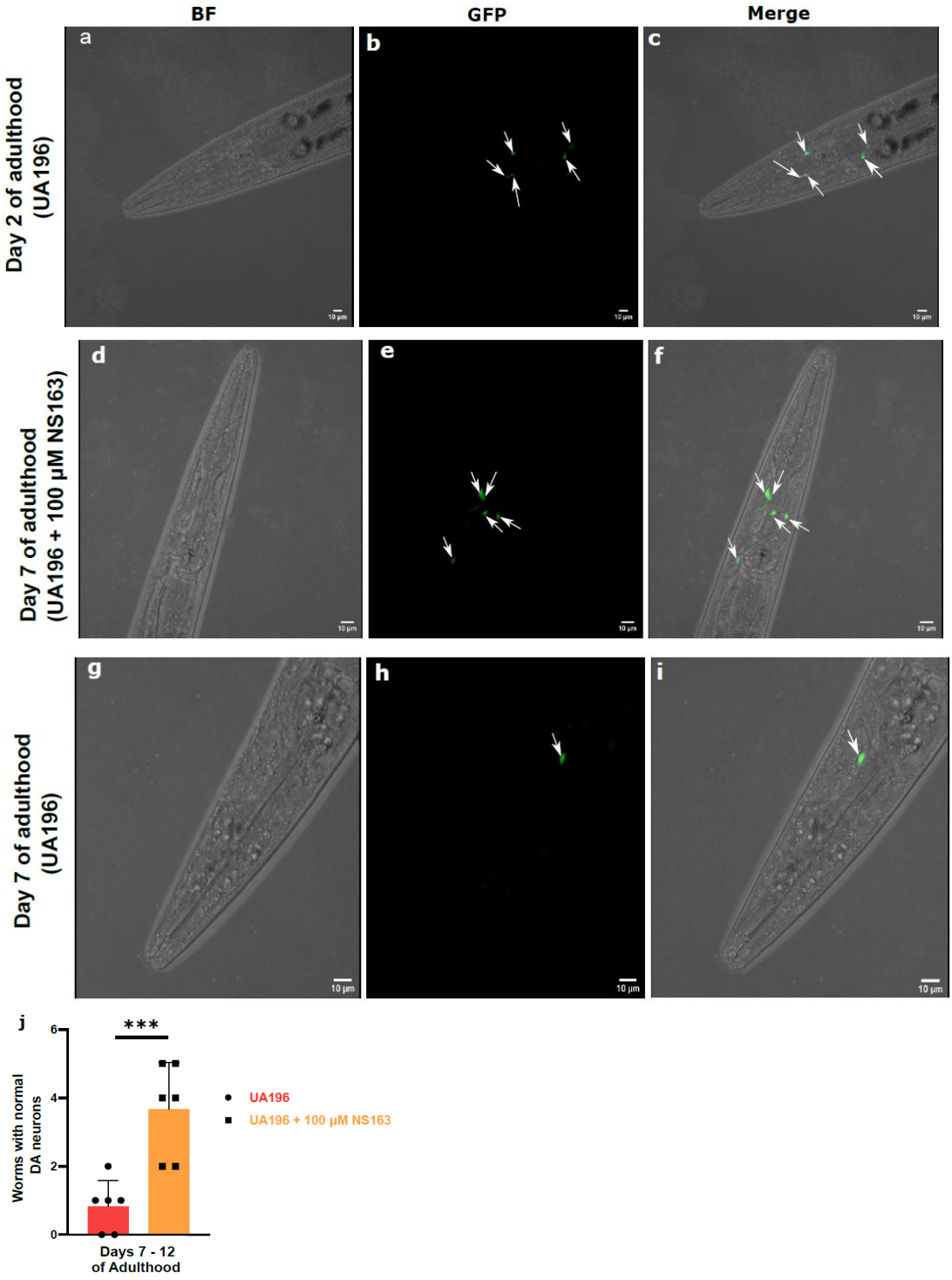

Figure 1.12 The post disease onset intracellular inhibition of αS aggregation in DA neurons by ligands in an *in vivo* PD model. Confocal images at day 2 of adulthood of UA196 strain of *C. elegans* showing the BF **(a)**, GFP in DA neurons **(b)**, and merged panel **(c)**. Confocal images at day 7 of adulthood of UA196 strain in the presence of 100 µM NS163 showing the BF **(d)**, GFP in DA neurons **(e)**, and merged panel **(f)**. Confocal images at day 7 of

adulthood of UA196 strain in the absence of 100 µM NS163 showing the BF **(g)**, GFP in DA neurons **(h)**, and merged panel **(i)**. **j** Quantified DA neurons (4) in UA196 strain in the absence and presence of 100 µM NS163 (days 7 and 12 of adulthood). The reported values in each experiment represent the average of atleast three data points and the reported error bars are the s.e.m's for at least three sets of experiments conducted on separate occasions. Statistical significance was analyzed using a one-way ANOVA followed by Tukey's multiple comparison test. *p<0.05, **p<0.01, ***p<0.001, ****p<0.0001.

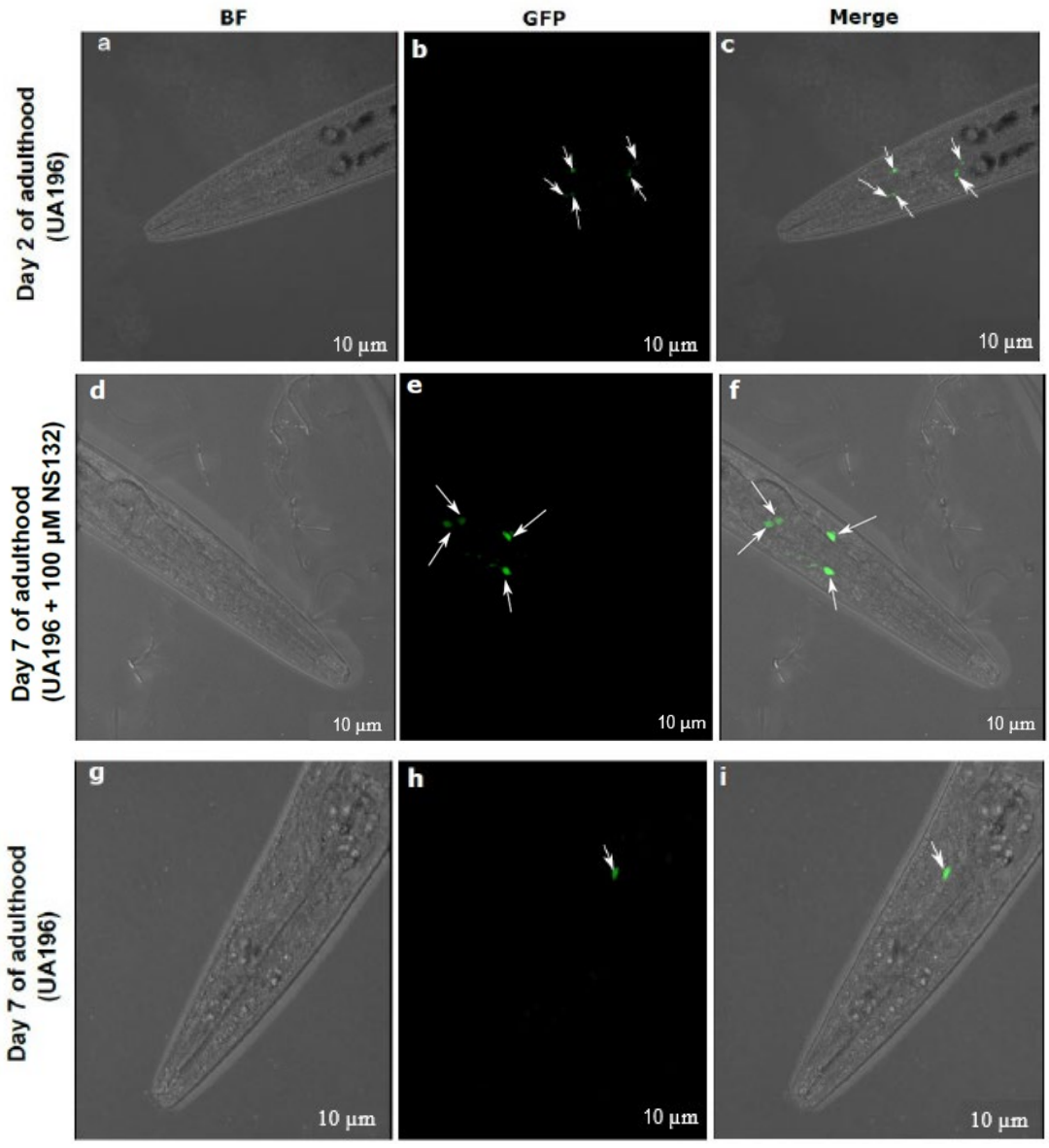

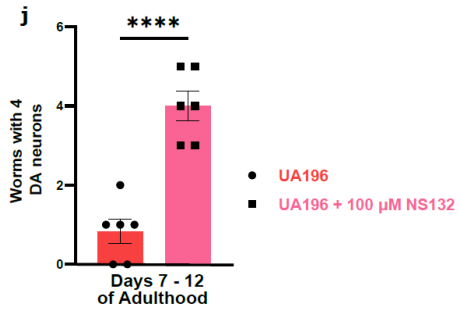

Figure 1.13 The post disease onset intracellular inhibition of αS aggregation in DA neurons by ligands in an *in vivo* PD model. Confocal images at day 2 of adulthood of UA196 strain *of C. elegans* showing the BF **(a)**, GFP in DA neurons **(b)**, and merged panel **(c)**. Confocal images at day 7 of adulthood in the presence of 100 µM NS132 showing the BF **(d)**, GFP in DA neurons **(e)**, and merged panel **(f)**. Confocal images at day 7 of adulthood in the absence of 100 µM NS132 showing the BF **(g)**, GFP in DA neurons **(h)**, and merged panel **(i)**. **j** Quantified DA neurons (4) in UA196 strain in the absence and presence of 100 µM NS132 (days 7 and 12 of adulthood). The reported values in each experiment represent the average of atleast three data points and the reported error bars are the s.e.m's for at least three sets of experiments conducted on separate occasions. Statistical significance was analyzed using a one-way ANOVA followed by Tukey's multiple comparison test. *p<0.05, **p<0.01, ***p<0.001, ****p<0.0001.µ

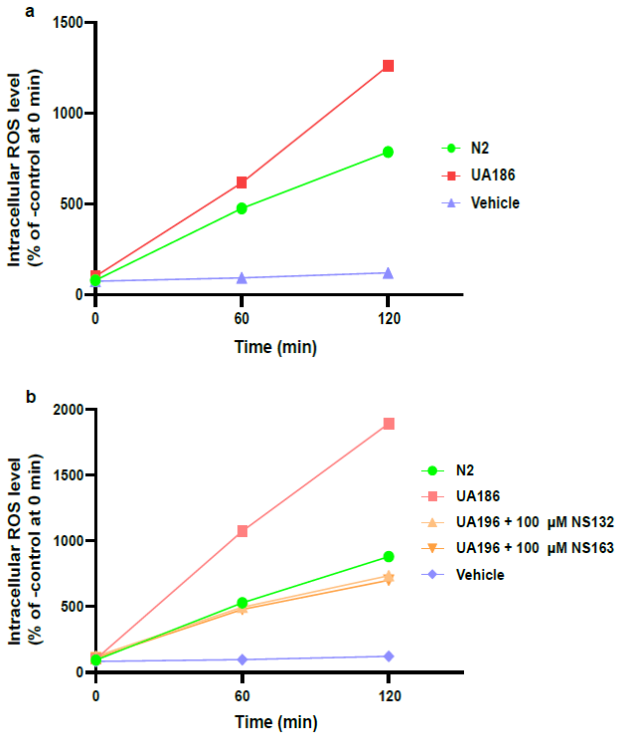

Figure 1.14 The effect of ligands on the ROS level for post disease onset UA196 strain of *C. elegans.* **a** The conparism of the ROS of N2 and UA196 on day 2 of adulthood pre-treatment with ligands. **b** The comparison of the ROS level in N2 and UA196 worms in the absence and presence of ligands (NS132 and NS163, 100 μM) at the indicated time points. The UA196 worms were treated with ligands on day 2 of adulthood. The ROS level was measured on day 5 of adulthood. For ROS level quantification, at least 50 animals were used, and each condition consisted of three independent experiments. The data were expressed as mean and the error bars reported the s.e.m. (n = 3 independent experiments and each n consisted of three technical replicates).

In this study, WT αS was made into preformed fibril (PFF) and labeled using a fluorescent marker (Alexa Fluor 633, AF633). The labeled αS-AF633 was confirmed through SDS PAGE (Figure 1.15f). Subsequently, αS-AF633 was used to transfect the cells of NL5901 strain of *C. elegans* which are transgenic animals that overexpress αS-YFP in their muscle cells. Paralysis assay was conducted for WT N2 and NL5901 strain in the absence and presence of αS-AF633 (Figure 1.15a-b). It was observed that the locomotion of the NL5901 (in the presence of αS-AF633) was significantly impaired and we suggest that may be due to the secondary nucleation of αS and the cell-to-cell prion-like spread of the protein aggregates. Confocal imaging was also conducted over time and the image on day seven of adulthood was reported (Figure 1.15c-d). It was observed that the transfected αS-AF633 co-localized with the αS-YFP in the muscle cells of the animal and there were high amount of inclusions compared to the animals without transfection (Figure 1.4c). This might have caused secondary nucleation of the amyloid protein, elongation of the fibrils and cell-to-cell propagation.

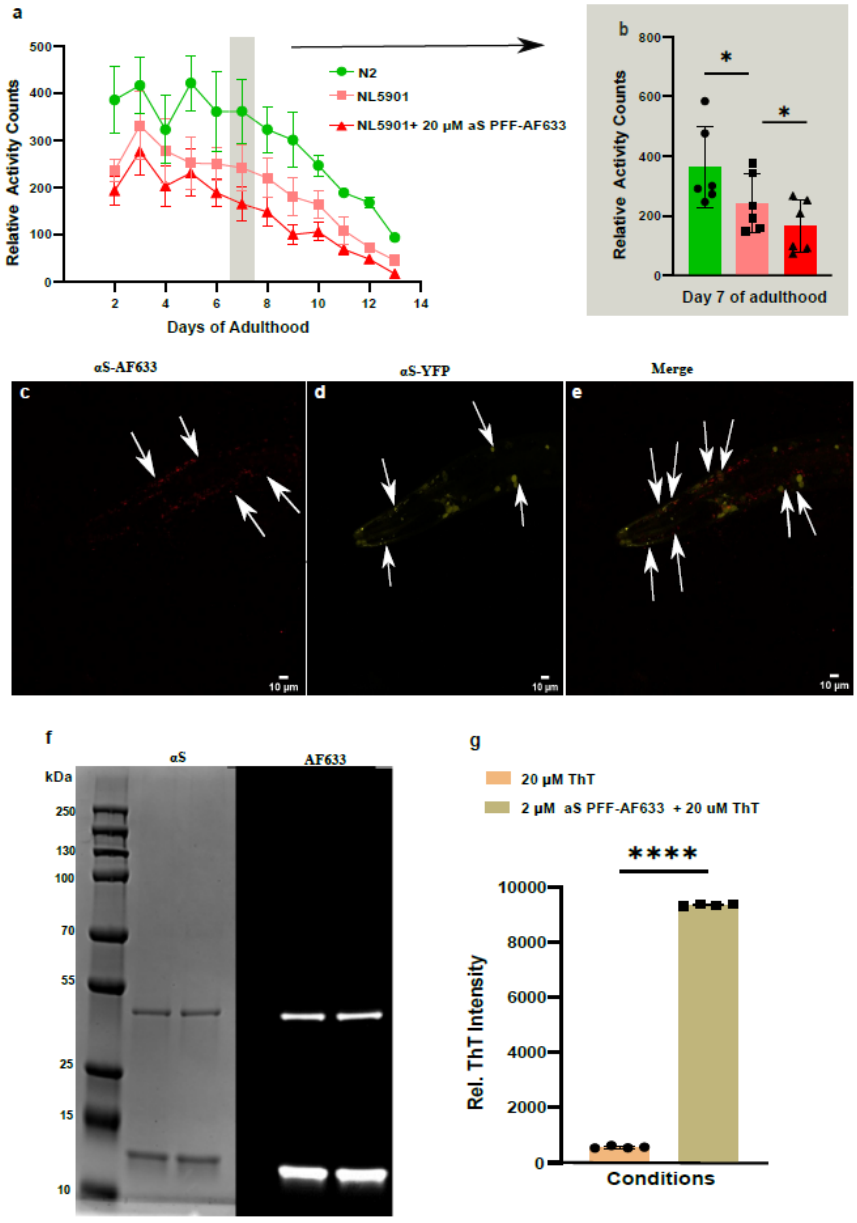

Figure 1.15 Prion-like spread of αS in NL5901 strain of *C. elegans*. **a** Paralysis assay (using 6-well plate) shows the relative activity counts for 12 days of adulthood of N2 and NL5901 strains in the absence and presence of 20 µM αSyn PFF-AF633. **b** A graphical representation with statistical analysis of the relative activity counts of N2 and NL5901 strain in the absence and presence of 20 µM αSyn PFF-AF633 for day 7 of adulthood. The data shows the mean, and the error bars expresses the s.e.m. (n = 3 independent experiments and each n included two technical replicates. Confocal images of αSyn PFF-AF633 **(c)** αS-YFP **(d)** and both **(e)** inclusions (white arrows) in muscle cells of NL5901 strain (days of adulthood = 9 days) in the presence of 20 µM αSyn PFF-AF633. **f** SDS PAGE gel analysis of 70 µM αSyn PFF-AF633 to confirm the conjugation of the fibrils to the fluorophore. The SDS-PAGE gel shows the Coomassie-stained αSyn PFF-AF633 and the fluorescence

images. The reference of the masses (in kDa) is shown on the left side of the gel. **g** ThT fluorescent intensity in the absence and presence of 2 μM αSyn PFF-AF633. The data were expressed as mean and the error bars represent the s.e.m. (n = 1 ThT fluorescence assay and n included four technical replicates). ANOVA with Tukey's multiple comparison test was used to perform statistical analysis. *p<0.05, **p < 0.01, ***p<0.001, ****p < 0.0001. Source data file was used to provide source data.

1.4 Conclusions and future work

Libraries of OPs (NS132, NS163 etc.) and OQs including SK-129 with potent antagonistic effects for αS aggregation were synthesized in the Kumar lab and several *in vitro* and *in vivo* assays have been conducted to test the efficacies of the molecules. Other proposed experiments are Western blot (WB) analysis on protein lysates from *C. elegans* PD models (NL5901 and UA196 strains) in the absence and presence of ligands to identify the presence or absence of protein aggregates and further validate the efficacy of a potent inhibitory ligand/molecule.

Further *in vivo* studies are required for the secondary nucleation of αS. Several populations of transfected PD model NL5901 strain may be treated with ligand(s) and experiments such as paralysis assay, confocal microscopy, ROS assay, and WB analysis maybe conducted to investigate the efficacy of the ligands as potent antagonists for αS aggregation at the secondary nucleation phase.

Also, Proteomics experiments maybe considered for PD model NL5901 strain in the absence and presence of ligands to investigate protein upregulation and downregulation and further re-validate the antagonistic activities of the ligands.

2. Investigation of small molecule inhibitors of amyloid-β (Aβ) aggregation using *C. elegans* models

2.1 Introduction

The accumulation of β-amyloid (Aβ) due to misfolding and formation of β-sheet rich amyloid fibrils or aggregates in cells has been linked to AD[38,48]. Previous studies found that the prefibrillar soluble oligomers of Aβ, and not the fibrils, are implicated in neurotoxicity in AD patients[60]. Aβ is part of the transmembrane portion of amyloid precursor protein (APP). There are several isoforms that result from the cleavage of APP in aPPIs including Aβ40 and Aβ42. Aβ42 was found to be the major constituent of amyloid plaques and it is more neurotoxic compared to Aβ40[61]. In aqueous solutions, Aβ40 and Aβ42 are random coils and they can have secondary structures under certain conditions[11]. Both peptides were found to adopt α-helical conformations at residues 15-24 and 29-35 in the presence of SDS micelles and 1,1,1,3,3,3-hexafluoro-2-propanol (HFIP)[11]. In this case, residues 16, 20, 22, and 23 become exposed to solvent interactions[11].

Inhibition of AD was also studied by treatment of the GMC101 (AD) strain of *C.elegans* with several small molecules including Bexarotene, EGCG and RD242. Paralysis assay and confocal microscopy were used to investigate the effects of the molecules in GMC101 strain. A small molecule, EGCG, was found in green tea with anti-

amyloidogenic properties that prevents the misfolding of disease proteins and prions[48]. EGCG was shown to inhibit β-sheet formation, (an onset event in the amyloid fibril formation process) by binding directly to unfolded polypeptide chains[48]. This molecule was used to treat GMC101 strain to re-validate the effectiveness of the molecule and show that wMicrotracker is a high throughput instrument for screening molecules.

Bexarotene is an anticancer drug approved by U.S Food and Drug Administration; this molecule was found to specifically target the primary nucleation step in Aβ42 aggregation and it was found to delay the formation of toxic species in neuroblastoma cells[38]. In GMC101 strain of *C. elegans*, Bexarotene was found to effectively suppress Aβ42 accumulation, toxicity and reduce the risk of AD[38]. This molecule was used to treat GMC101 strain to re-emphasize the effectiveness of the molecule and to re-validate wMicroTracker as an instrument that can produce consistent and reliable data.

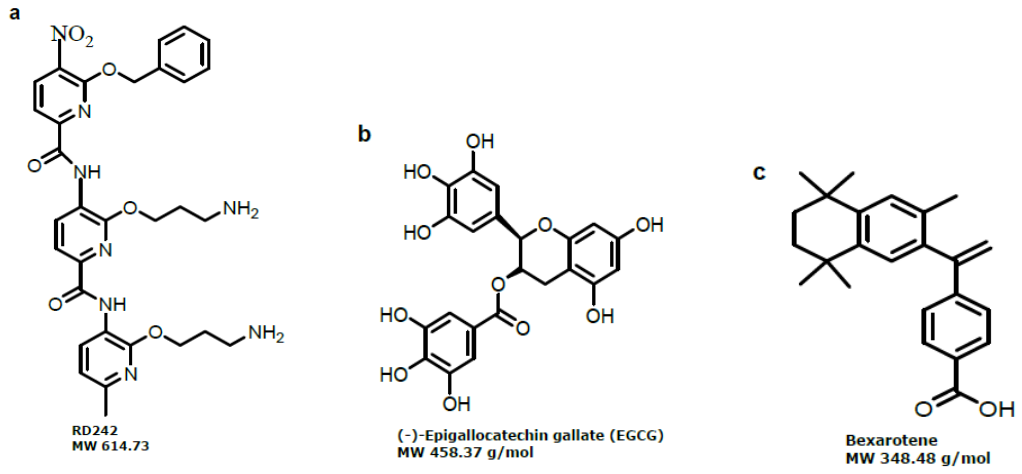

Figure 2.1 Chemical structures and MW of small molecule potent antagonists of Aβ aggregation including RD242 **(a),** EGCG **(b),** and Bexarotene **(c).**

RD242 is a novel small molecule synthesized in the Kumar lab. RD242 is a tripyridylamide-based α-helix mimetic that was found as inhibitor of the self-assembly of

Aβ peptide[11–13] and islet amyloid polypeptide (IAPP) associated with AD and type II diabetes (T2D)[13]. α-helix mimetics can imitate the topography of so many protein secondary structures and hence, they can be potent antagonists of aberrant PPIs[13]. Considering the side chain residues of α-helix mimetics which can be manipulated or changed; these small molecules have been found to target aberrant PPIs[13]. Several *in vitro* assays including ThT assay have shown that RD242 is a potent antagonist for the inhibition of Aβ42 aggregation. This molecule was also used to treat GMC101 strain, and several assays including paralysis assay, confocal imaging and ROS assay were conducted to show the effectiveness of the molecule.

EGCG, Bexarotene, and RD242 were used in this study to treat GMC101 strain and show that wMicroTracker Arena plate reader, is a reliable new instrument for high throughput assays including paralysis assays. wMicroTracker has been in use in different research works[37,62] and it has provided reliable and consistent data.

2.2 Materials and Methods

2.2.1 Culture methods for *C. elegans* strains

The N2 (wild-type *C. elegans* Bristol strain), GMC101 (*C. elegans* model of Alzheimer's Disease, AD), and *Escherichia coli* OP50 *(E. coli*, uracil requiring mutant), strains were obtained from Caenorhabditis Genomics Center (Minneapolis, MN). The animals were maintained at standard conditions on nematode growth media (NGM) agar in 60 mm plates (CytoOne, Ocala, FL) using *E. coli* OP50 as the food source[2,32]. All strains were maintained using previous protocols[2,33]. NGM agar plates, M9 buffer (3 g KH_2PO_4,

6 g Na_2HPO_4, 5 g NaCl, 1 mL 1 M $MgSO_4$, milli-Q H_2O to 1 L), and OP50 solution at 0.5 OD600nm were prepared using previous protocols[2,33–35].

2.2.2 Paralysis Assay for GMC101 strain treated with EGCG using 6-well plate

The previously described protocols[2,36,37] were used to prepare GMC101 and N2 strains of *C. elegans* as described in section 1.2.2. Three conditions of the animals were used including N2 strain (positive control), GMC101 strain (untreated negative control), and GMC101 strain (treated with 65 μM of EGCG).

2.2.3 Paralysis Assay for GMC101 strain treated with Bexarotene using 6-well plate

GMC101 and N2 strains of *C. elegans* were prepared using previous protocols[2,36,37] as earlier described in section 1.2.2. Three conditions of the animals were used including N2 strain (positive control), GMC101 strain (untreated negative control), and GMC101 strain (treated with 75 μM of Bexarotene).

2.2.4 Paralysis Assay for GMC101 strain treated with EGCG using 24-well plate

This experiment involved six worm conditions including N2 strain (positive control), GMC101 strain (untreated negative control), and GMC101 strain treated with four different concentrations of EGCG (50 μM, 65 μM, 90 μM, and 120 μM in DMSO). The animals were prepared using the protocol described in section 1.2.4.

2.2.5 Paralysis Assay for GMC101 strain treated with Bexarotene using 24-well plate

There were six worm conditions for this experiment including N2 strain (positive control), GMC101 strain (untreated negative control), and GMC101 strain treated with four different concentrations of Bexarotene (50 μM, 65 μM, 90 μM, and 120 μM in DMSO). GMC101 and N2 strains of *C. elegans* were prepared as described in section 1.2.4.

2.2.6 Paralysis Assay for GMC101 strain treated with RD242

GMC101 and N2 strains of *C. elegans* were prepared as described in section 1.2.4. There were four conditions for this experiment including N2, GMC101 in the absence and presence of 30 μM RD242 and 30 μM Bexarotene.

2.2.7 Staining of GMC101 with NIAD-4 dye

Living GMC101 strain of *C. elegans* were treated with 5 μM NIAD-4 dye on days seven and ten after initial synchronization according to previously described protocol[38]. The animals were transferred using a worm pick into NIAD-4 solution (5 μM in M9 buffer) and incubated at room temperature for 4 h at 150 rpm on a shaker (Thermo Scientific, Waltham, MA). This incubation ensured that the animals were thoroughly stained. Subsequently, they were transferred into NGM plates containing FUDR and incubated again at r.t for 24 h to allow the animals to recover through metabolism.

2.2.8 Confocal microscopy of GMC101 strain of *C. elegans*

This experiment was performed based on a previously described protocol[2,38] with slight modifications as described on section 1.2.10. For GMC101 strain, images were collected on days seven and ten. For each condition, three biological replicates were performed, and the average number of aggregates was reported with the error bars representing the S.E.M.

2.2.9 Measurement of intracellular Reactive Oxygen Species (ROS) of *C. elegans* (GMC101 and N2 strains) under normal culture conditions

The intracellular ROS was measured using previous protocols[39,40] with slight modifications as described in section 1.2.12. The worm conditions included N2 strain and GMC101 strains in the absence and presence of RD242 (10 μM and 30 μM in DMSO).

2.3 Results and discussions

2.3.1 High throughput assay for screening inhibitory molecules of Aβ42 aggregation

Small molecules that have shown *in vitro* antagonistic effects for the inhibition of Aβ42 aggregation were used to treat GMC101 strain of *C. elegans* through *in vivo* assays including paralysis assay, confocal microscopy, and ROS assay. GMC101 strain is a transgenic disease model of AD which shows the formation of toxic Aβ42-mediated dysfunction[38]. One of the small molecules tested was EGCG; this molecule at 65 μM in M9 buffer (Figure 2.2a-b) was used to treat GMC101 strain and paralysis assay was conducted initially using a 6-well plate in a wMicrotracker arena plate reader. It was found that the locomotion of the diseased GMC101 improved after treatment with the drug. EGCG might have bound to unfolded polypeptide chains and inhibited β-sheet formation during the primary nucleation phase of Aβ42. Another situation is that EGCG might have disassembled preformed, β-sheet-rich structures and intermediate oligomers during Aβ42 fibrilization process.

A high throughput paralysis assay was conducted by treating GMC101 strain at different concentration of EGCG (50 μM, 65 μM, 90 μM, and 120 μM, Figure 2.2 c-d). This assay showed that with the increased concentration of EGCG used for treatment of GMC101 strain, there was relative increase in the locomotion of the animals which further validates EGCG as a potent antagonist for Aβ42 aggregation. And the data also authenticates the wMicrotracker plate reader as an efficient instrument for high through put paralysis assays. Confocal images of GMC101 stained with 5 μM NIAD-4 dye in the absence (Figure 2.2e) and presence of 120 μM EGCG (Figure 2.2f) shows the disappearance of toxic Aβ42

aggregates (red) after treatment with the molecule (day 7 of adulthood). This data is consistent with the paralysis assay data earlier shown. Another small molecule used for treatment of GMC101 was Bexarotene. This molecule (at 75 μM in M9 buffer, Figure 2.3a-b) was first used to treat the animals and paralysis assay was conducted using a 6-well plate in wMicrotracker arena plate reader. Subsequently, the assay was conducted using 24-well plate to show that increased concentration of Bexarotene (50 μM, 65 μM, 90 μM, and 120 μM,) (Figure 2.3c-d) rescued the locomotion of the animals and further suggested that the wMicrotracker is a high throughput and efficient instrument. Confocal images of GMC101 stained with 5 μM NIAD-4 dye in the absence (Figure 2.3e) and presence of 120 μM Bexarotene (Figure 2.3f) shows the disappearance of toxic Aβ42 aggregates (red) after treatment with the molecule (day 7 of adulthood). The earlier reported paralysis assay data is consistent with the results shown through the confocal images. RD242 (at 10 μM, and 30 μM in M9 buffer) and Bexarotene (at 10 μM, and 30 μM in M9 buffer) were used for treatment of GMC101 strain. The results from the paralysis assay (Figure 2.4a-c) showed improvement in the locomotion of the animals with increase in the concentration of RD242 used for the treatment compared to Bexarotene. Confocal images of GMC101 stained with 5 μM NIAD-4 dye in the absence (Figure 2.5a) and presence of 30 μM RD242 (Figure 2.5b) and 30 μM Bexarotene (Figure 2.5c) shows the disappearance of toxic Aβ42 aggregates (red) after treatment with the molecule (on day 7 of adulthood).

Also, after quantifying the Aβ fibril inclusions in the animals (Figure 2.5d), it was found that there were less fibril inclusions in the animals treated with RD242 compared to Bexarotene but both molecules showed significant antagonistic effect to Aβ42

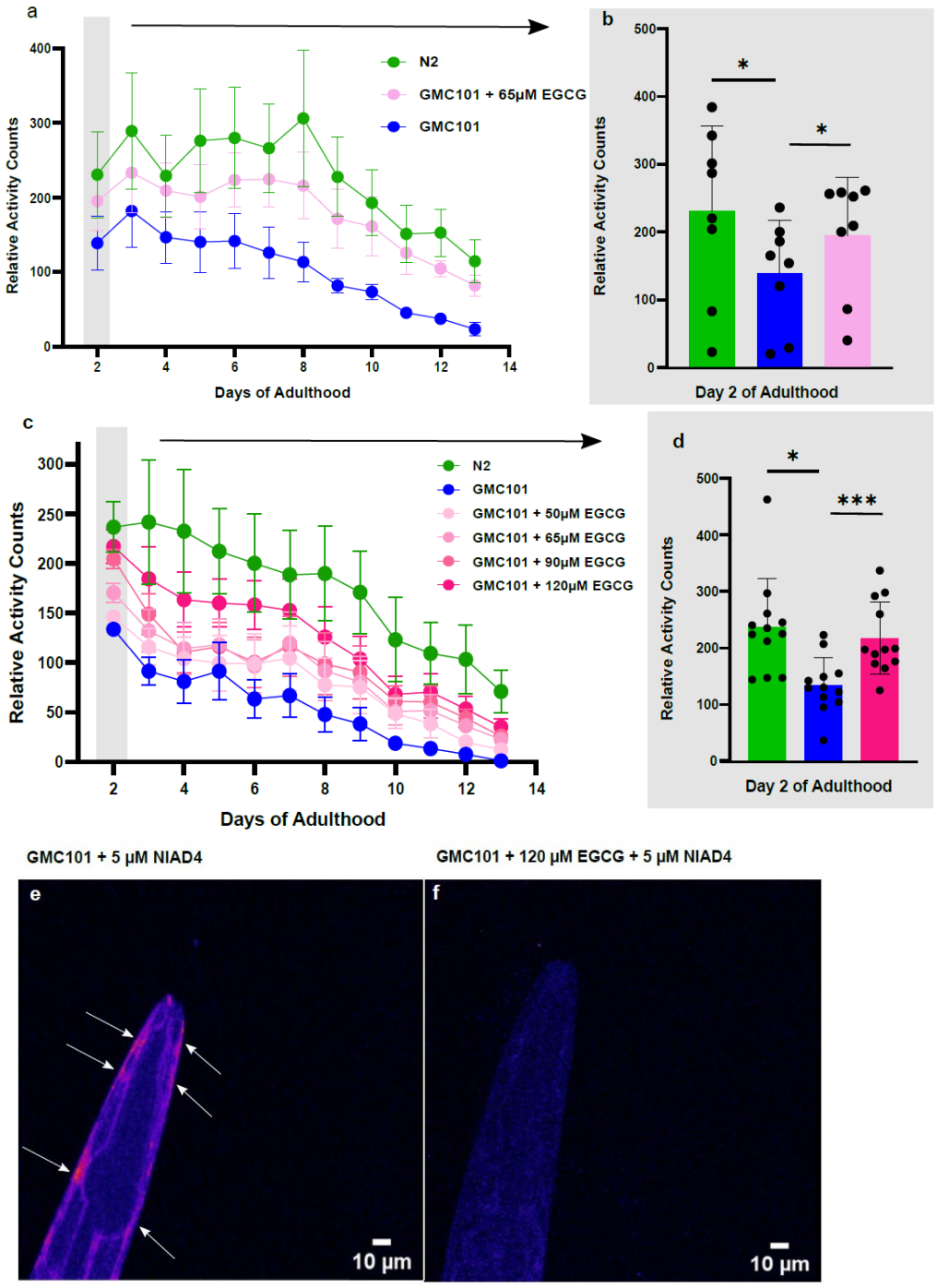

Figure 2.2 The intracellular inhibition of Aβ42 aggregation by EGCG in GMC101 strain of *C. elegans*. **a** Paralysis assay (using 6-well plate) shows the relative activity counts for 12 days of adulthood of N2 and GMC101 strains in the absence and presence of 65 μM EGCG. **b** A graphical representation with statistical analysis of the relative activity counts of N2 and GMC101 strains in the absence and presence of 65 μM EGCG for day 2 of adulthood. The data shows the mean, and the error bars expresses the s.e.m. (n = 3 independent experiments and each n included two technical replicates. **c** Paralysis assay

(using 24-well plate) showing the relative activity counts for 12 days of adulthood of N2 and GMC101 strains in the absence and presence of EGCG (50 μM, 65 μM, 90 μM, and 120 μM). **d** A graphical representation with statistical analysis of the relative activity counts of N2 and GMC101 strains in the absence and presence of 120 μM EGCG for day 2 of adulthood. The data shows the mean, and the error bars represents the s.e.m. (n = 3 independent experiments and each n included four technical replicates. *In vivo*/Confocal images **(e, f)** of Aβ42 inclusions (white arrows) in muscle cells of GMC101 strain (days of adulthood = 2 days) stained with 5 μM NIAD-4 amyloid-specific dye in the absence **(e)** and **(f)** presence of 120 μM EGCG. ANOVA with Tukey's multiple comparison test was used to perform statistical analysis. *$p<0.05$, **$p < 0.01$, ***$p<0.001$, ****$p < 0.0001$. Source data file was used to provide source data.

aggregation and neurotoxicity (from day 0 - 10 of adulthood). The earlier reported paralysis assay data is consistent with the results shown through the confocal images. ROS assay was also conducted (on day 7 of adulthood). This assay quantifies the amount of reactive oxygen species in the cells which accumulate due to oxidative stress that might be caused by amyloid aggregation.

The results from the ROS assay (Figure 2.5e) showed significant decrease in the reactive oxygen species in GMC101 strain after treatment with RD242 (10 μM and 30 μM in M9 buffer). The higher concentration (30 μM) of RD242 used to treat the diseased animals showed a smaller number of oxidative species compared to the treatment at lower concentration (10 μM). Also, these results validated the fact that RD242 is a potent antagonist for the inhibition of Aβ42.

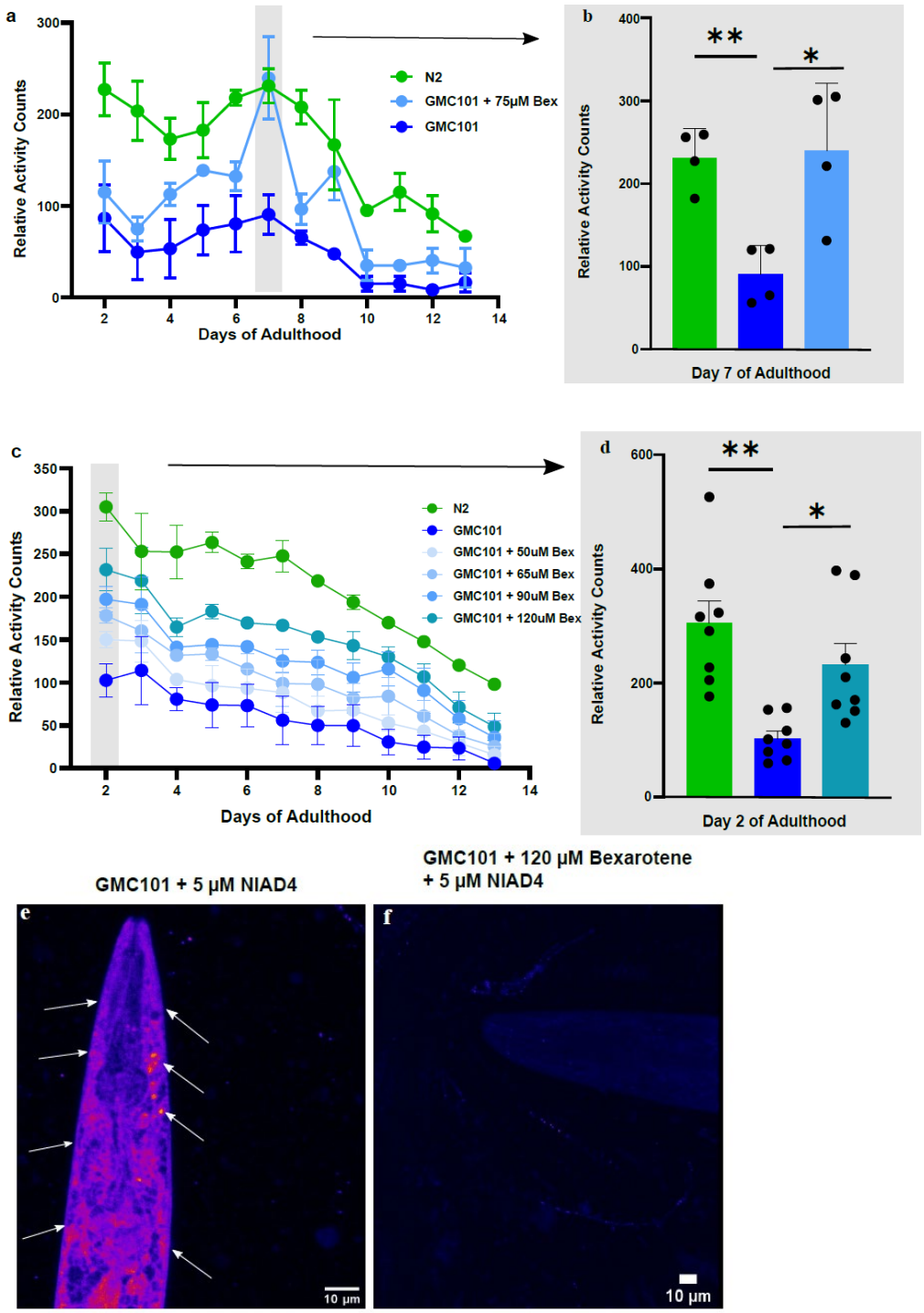

Figure 2.3 The intracellular inhibition of Aβ42 aggregation by Bexarotene in GMC101 strain of *C. elegans*. **a** Paralysis assay (using 6-well plate) shows the relative activity counts for 12 days of adulthood of N2 and GMC101 strains in the absence and presence of 75 μM Bexarotene. **b** A graphical representation with statistical analysis of the relative activity counts of N2 and GMC101 strains in the absence and presence of 75 μM Bexarotene for

day 7 of adulthood. The data shows the mean, and the error bars expresses the s.e.m. (n = 2 independent experiments and each n included two technical replicates. **c** Paralysis assay (using 24-well plate) shows the relative activity counts for 12 days of adulthood of N2 and GMC101 strains in the absence and presence of Bexarotene (50 µM, 65 µM, 90 µM, and 120 µM). **d** A graphical representation with statistical analysis of the relative activity counts of N2 and GMC101 strains in the absence and presence of 120 µM Bexarotene for day 2 of adulthood. The data shows the mean, and the error bars represents the s.e.m. (n = 2 independent experiments and each n included four technical replicates. *In vivo*/Confocal images **(e, f)** of Aβ42 inclusions (white arrows) in muscle cells of GMC101 strain (days of adulthood = 7 days) stained with 5 µM NIAD-4 amyloid-specific dye in the absence **(e)** and **(f)** presence of 120 µM Bexarotene. ANOVA with Tukey's multiple comparison test was used to perform statistical analysis. *p<0.05, **p < 0.01, ***p<0.001, ****p < 0.0001. Source data file was used to provide source data.

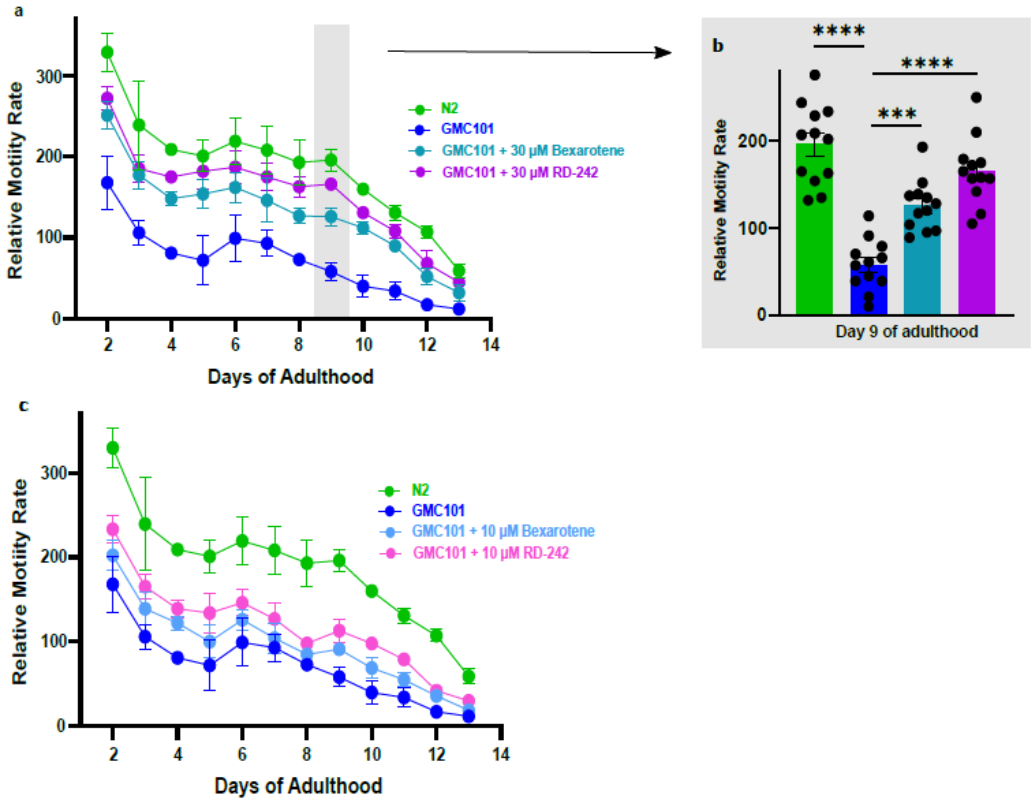

Figure 2.4 The intracellular inhibition of Aβ42 aggregation by Bexarotene and RD242 in GMC101 strain of *C. elegans*. **a** Paralysis assay shows the relative activity counts for 12 days of adulthood of N2 and GMC101 strains in the absence and presence of 30 µM Bexarotene and 30 µM RD242. **b** A graphical representation with statistical analysis of the relative activity counts of N2 and GMC101 strains in the absence and presence of 30 µM Bexarotene and 30 µM RD242 for day 7 of adulthood. The data shows the mean, and the error bars and expresses the s.e.m. (n = 3 independent experiments and each n included

four technical replicates. **c** Paralysis assay shows the relative activity counts for 12 days of adulthood of N2 and GMC101 strains in the absence and presence of 10 µM Bexarotene and 10 µM RD242. The data shows the mean, and the error bars represents the s.e.m. (n = 3 independent experiments and each n included four technical replicates. ANOVA with Tukey's multiple comparison test was used to perform statistical analysis. *p<0.05, **p < 0.01, ***p<0.001, ****p < 0.0001. Source data file was used to provide source data.

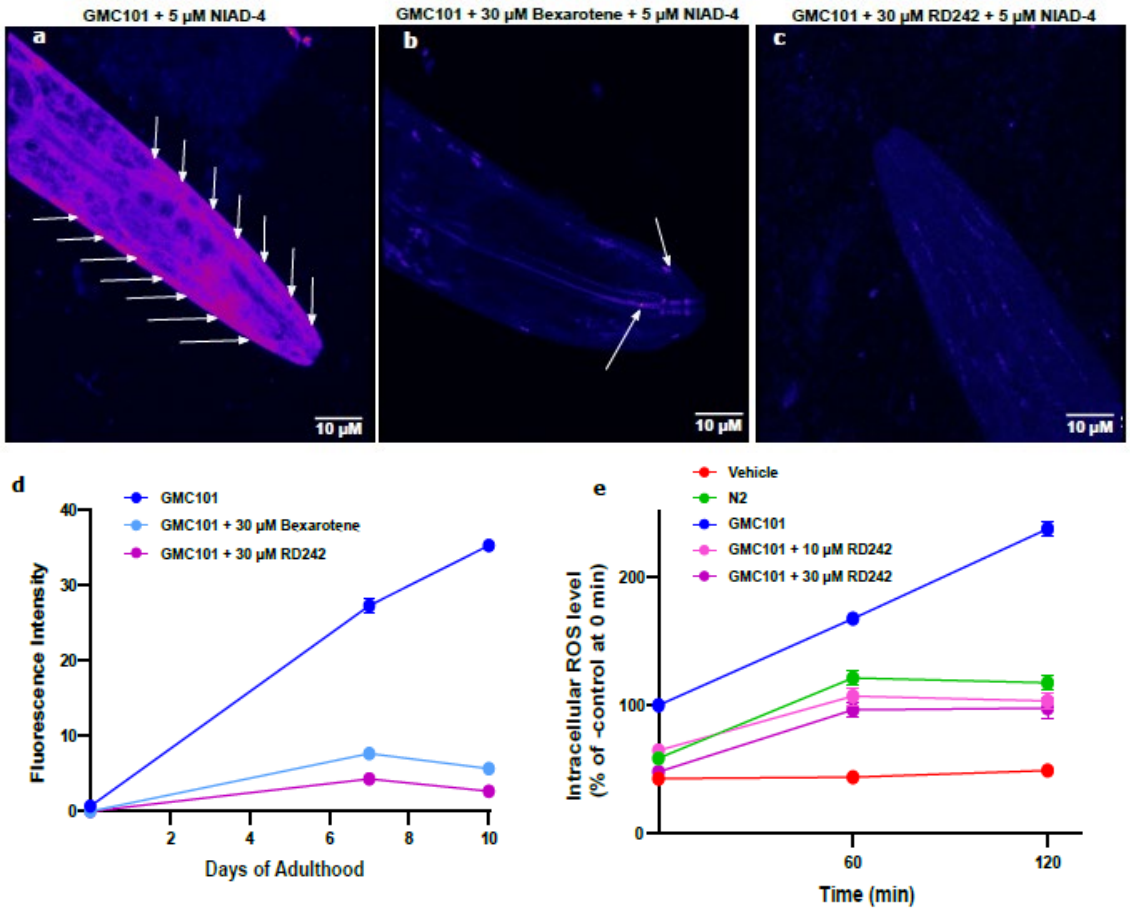

Figure 2.5 RD242 is a potent antagonist for the inhibition of Aβ42 aggregation in *C. elegans* models of Aβ42-mediated toxicity. *In vivo* confocal images of Aβ42 aggregates (white arrows) in GMC101 strain of *C. elegans* stained with 5 µM of amyloid-specific dye NIAD-4 in the absence **(a)** and presence of 30 µM Bexarotene **(b)** and 30 µM RD242 **(c).** Images were shown for day 7 of adulthood. **d** Time course confocal microscopy assay for Aβ42 aggregation in GMC101 strain in the absence and presence of 30 µM Bexarotene and 30 µM RD242. Fluorescent intensity was quantified using ImageJ software (n = 3 confocal microscopy assays and n included two technical replicates). **e** The time course of the increase in DCF fluorescence detected using a microplate reader ((λ_{ex} = 485 nm and λ_{em} = 530 nm). The data were expressed as percentage of fluorescence (intracellular ROS level) relative to the untreated control (- control) at t = 0, set as 100% with mean and error bars representing the s.e.m. (n = 3 ROS assays and n included two technical replicates).

2.4 Conclusions and future work

An OP (RD242) was synthesized in the Kumar lab and several *in vitro* and *in vivo* assays were conducted to test the efficacies of the molecule as a potent inhibitor for Aβ42 aggregation. Other proposed experiments are WB analysis on protein lysates from *C. elegans* AD model (GMC101) in the absence and presence of ligands to identify the presence or absence of protein aggregates and further validate the efficacy of a potent inhibitory ligand/molecule.

Further *in vivo* studies are required for the secondary nucleation of Aβ42. Several populations of transfected AD model GMC101 strain may be treated with ligand(s) and experiments such as paralysis assay, confocal microscopy, ROS assay, and WB analysis maybe conducted to investigate the efficacy of the ligands as potent antagonists for Aβ42 aggregation at the secondary nucleation phase.

Also, Proteomics experiments maybe considered for AD model GMC101 strain in the absence and presence of ligands to investigate protein upregulation and downregulation and further re-validate the antagonistic activities of the ligands.

3. Investigation of the prion-like spread of cancer-associated mutant p53 and its inhibition using MIA PaCa-2 mutant cells

3.1 Introduction

Another amyloidosis studied is the aggregation of p53 implicated in cancer. During cellular stresses such as DNA damage, oncogene activation, oxidative stress or hypoxia, p53, a tumor suppressor protein, will be activated[63]. E3 ubiquitin ligase, MDM2 (murine double minute 2), a negative regulator, controls the level of p53 in the cells by targeting unwanted p53 peptides for proteasome-mediated degradation[63]. This involves ubiquitinating unwanted p53 peptides for degradation/clearance from the cells. Cellular stresses (earlier mentioned) can disrupt p53-MDM2 interaction through phosphorylation of those two proteins and triggers p53 acetylation resulting to its activation[13]. The activated p53 can repair DNA damage, cause cell cycle arrest, senescence, apoptosis or autophagy; all these actions are aimed at suppression of neoplastic transformation and inhibition of tumor progression[63]. It was found that p53 functions as a sequence-specific transcriptional activator because it can bind to many DNA sequences[64]. p53 is considered to be the most mutated protein in cancer because the missense mutations are found in more than half of all human cancers[64]. Hence, p53 is very important in the study and development of cancer therapeutic drugs/molecules.

p53 exists as a homotetramer (Figure 3.1a) under physiological conditions, and each monomer has globular DNA-binding domain (DBD) (Figure 3.1b) and tetramerization domain, connected by a flexible linker and flanked by intrinsically disordered regions (a transactivation domain followed by a proline-rich region at the N-terminus and a C-terminal regulatory domain)[65].

In the p53 sequence (Figure 3.1a), there is a central immunoglobulin-like β-sandwich that serves as a scaffold for the DBD surface, consisting of a loop-sheet-helix motif and two large loops that are stabilized by the tetrahedral coordination of a single zinc ion[66]. p53 mutation such as R248W (Figure 3.1c), possess the characteristics of both DNA interactions (contact mutants) and proper folding (structural mutants)[13]. Previous studies have shown that various p53 DBD

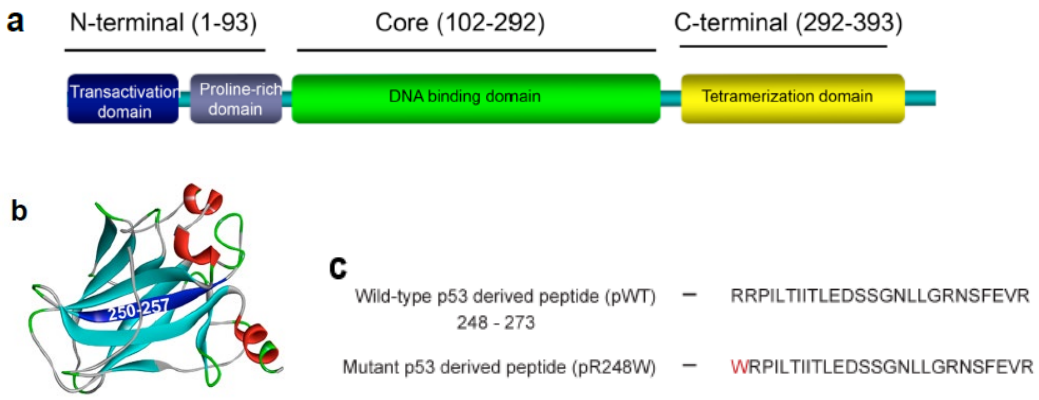

Figure 3.1 Domain organization of p53 tumor suppressor protein.[67] **a** Schematic representation of the different functional domains within p53. **b** 3D structure of the DNA binding domain with the amyloidogenic region (250-257) colored blue (PDB entry 20CJ). **c** Primary sequences of the studied WT and mutant R248W p53 DBD-derived peptides represented by pWT and pR248W, respectively, including residues 248-273.

mutants along with fragments of these proteins, form amyloid-like aggregates in solution, cancer cell lines and tumors[68]. Characteristics of p53 DBD includes low thermodynamic

and kinetic stability[66] and mutations in the domain can further decrease its stability and cause it to unfold leading to exposure of its hydrophobic core[69]. The commonly known DBD mutations including R248W/Q, R273C/H and R175H[70] involves the replacement of the cationic arginine, called "gate-keeper" amino acid that prevents protein aggregation using the repulsive effect of its charge, with residues (tryptophan, cysteine, histidine or glutamine) that have high aggregation/amyloidogenic propensity[71]. Hence, these DBD mutations also enhance p53 aggregation tendencies in addition to exposing its hydrophobic core domain. Therefore, mutant p53 is triggered to self-aggregate into amyloid-like aggregates within inactive cellular inclusions that combine the wild type (WT) isoforms, resulting to the prevention of p53's tumor suppressor functions[72].

There are many suggestions that implicate aggregation of mutant p53 (e.g. R248Q, R248W, and R175H) in the associated oncogenic gain-of-function (GoF), i.e. promotion of tumor growth, metastasis and chemoresistance through the acquisition of activities[68]. Example, co-sequestration of mutant and WT p53 into inactive cellular inclusions may result in overexpression of antiapoptotic and pro-proliferative genes previously suppressed by p53[64]. It was also found that misfolding of the p53 paralogs (p63 and p73) can occur due to aggregation of mutant p53; these paralogs are then incorporated into the inclusions, facilitated by interactions of the aggregation-prone core of p53 DBD with almost identical segments present in the p63 and p73 DBDs[72]. It was found that aggregation of mutant p53 can trigger overexpression of heat-shock proteins, in particular, Hsp70[72]; this action promotes tumor cell proliferation and inhibit apoptosis[73]. Hence, p53 loss of tumor suppressor function and its oncogenic GoF may be linked to the amyloid-like aggregation of mutant p53.

MDM2 and MDMX proteins were shown to be the main negative regulators of p53; these proteins function in normal cells to suppress p53 activity[74]. But if there is cellular stress, those proteins (MDM2 and MDMX) should be inhibited so that p53 can respond to the stress[74]. It was found that MDM2 and MDMX bind together and play important role in regulating p53 protein activity. The MDM2 complex can bind to p53 to inhibit the later from transcriptional activities, favor nuclear export, and stimulates its degradation[75]. Upregulation of MDM2 in various tumors inhibits p53, hence favoring uncontrolled cell proliferation. E3 ubiquitin protein ligase MDM2 regulates p53 transcriptional factor[76].

Recent studies found that many amyloid associated disorders are infectious[77,78] and amyloid fibrils where found to spread from cell-to-cell in a prion-like manner. Prions are regarded as 'proteinaceous particles' that are infectious agents involving misfolded prion protein (PrP) molecules[77]. An induced chain-reaction of PrP misfolding and aggregation is caused by the act of prions as corrupt templates (seeds)[77]. The growth, fragmentation and propagation of prions can change the function of the nervous system and consequently lead to cell death. It was hypothesized that p53, an amyloid protein, might have prion-like properties[68] because the full-length (pWT) p53 aggregates (PFFs) can be internalized in cells and propagate rapidly[79]. But comprehensive studies on prion-like spread of amyloids has not been done. In this study, three unique properties of p53 amyloids were shown including, (1) internalization of pWT PFFs in cells, (ii) templating of aggregates of endogenous p53, and (iii) cell-to-cell transmission of p53 amyloids.

It was found that the replacement of a hydrophobic amino acid in the aggregation-prone core of p53 DBD with the "gate-keeper" arginine residue (I254R) prevents coaggregation of mutant p53 with the WT protein and its paralogs, p63 and p73 and also prevents

overexpression of Hsp70[72]. Specifically, an aggregation-suppressing I254R mutation (known as ReACp53, (Rg)RPILTRITLE) harbored by a p53 DBD-derived peptide was shown to prevent mutant p53 aggregation by masking the aggregation-prone core, hence restoring the mutant protein to a WT p53-like functionality and significantly reduced cancer cell proliferation *in vitro* and stopped tumor progression *in vivo*[80]. This study can be regarded as a feasible and effective cancer therapeutic strategy that targets mutant p53 aggregation.

Oligopyridylamide-based α-helix mimetics were previously reported as potent modulators of the self-assembly of amyloid-β peptide (Aβ)[11,12] and islet amyloid polypeptide (IAPP)[8]. α-helix mimetics are also regarded as influential antagonists of aberrant protein-protein interactions (aPPIs) at the interaction interface[81,82]. These types of protein mimetics are crucial in this study because they can target specific disease-related aPPIs due to the fact that their side-chain residues can be manipulated[81,82]. In this study, we tried to find out whether protein mimetic-based strategy can be used to disrupt mutant p53 self-assembly.

Hence, the following questions were presented; (i) Can oligopyridylamide-based α-helix mimetics potently prevent the process by which intrinsically disordered mutant p53 and other amyloid proteins (Aβ and αS) aggregate via an amyloid pathway? (ii) Is it possible to rescue p53 and other amyloid protein's function and inhibition of cancer cell proliferation *in vitro* using oligopyridylamide-mediated abrogation? and (iii) Is it possible to reverse tumor growth *in vivo* without adversely affecting healthy tissues using oligopyridylamide-based strategy? To answer these questions, functionalized amyloid inhibitors were used in this study as amyloid aggregation-targeted therapeutics. A library

of OPs including RD148 (Figure 3.2a) was synthesized by Ryan Dohoney in Kumar Lab at University of Denver and ADH40 (Figure 3.2b) was synthesized in Hamilton Lab at New York University. ADH40, a tripyridylamide was previously reported[13] as a potent antagonist for p53 aggregation and it was also tested in this study and its antagonistic effects were compared with a library of dipyridylamides including RD148.

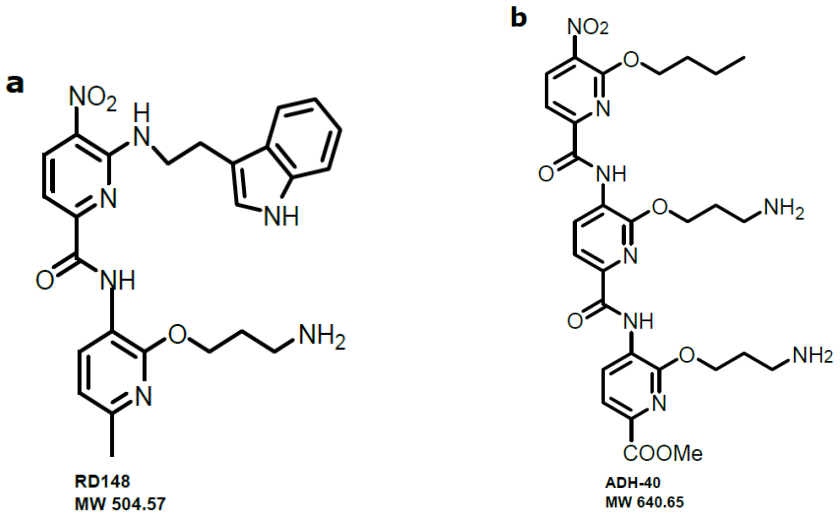

Figure 3.2 Chemical structures and MW of Ops. **a** RD148. **b** ADH-40.

3.2 Materials and Methods

3.2.1 Cell Culture

Previous protocol was used for cell culture and maintenatance[13]. The human pancreatic cancer, MIA PaCa-2 (ATCC no. CRL-1420) and human breast cancer MCF-7 (ATCC no. HTB-22) cell lines used in this study were purchased from American Type Culture Collection (ATCC). These cell lines were cultured in Dulbecco's Modified Eagle Medium (DMEM) (Sigma) augmented with 10% fetal bovine serum (FBS; Cytiva 29361669, HyClone, GE Healthcare Life Sciences, Canada), 4 mM L-glutamine, 1 mM sodium pyruvate and 1% penicillin/streptomycin (pen/strep) (all were purchased from Fisher Scientific). All the cells were cultured in an incubator with 5% CO_2 supply at 37ºC and the cell viabilities were checked regularly using trypan blue exclusion test on a cell counting hemocytometer using a countess 3 automated cell counter (Thermo Fisher Scientific, Waltham, MA). When the cells are ~95% confluent, they were passaged (using detachin for trypsinization) and ~70% of the cells will be discarded or used for an experiment.

3.2.2 Preparation of wild type p53 preformed fibrils (pWT PFF) and labeling

pWT PFF was prepared according to previous protocol[83] with slight modifications. pWT (4 mg) was obtained and dissolved in PBS for a final concentration of 600 μM. The solution was placed on a shaker and incubated at 37ºC, 1400 rpm for seven days. On day one, 10 μM of the PFF was obtained and dissolved in PBS for a final concentration of 20 μM of pWT PFF and the solution contained 40 μM of ThT in PBS. A vehicle was also

prepared with only 40 μM of ThT in PBS. There were three technical replicates for each condition in a black 96-well plate with flat bottom (Corning Inc., NY). The ThT fluorescence intensity was measured using a microplate reader (Tecan, Männedorf, Switzerland) at ($\lambda_{ex/em}$ = 440/490 nm). On day seven, ThT assay was performed again using the same concentrations of pWT PFF and ThT earlier report for day one. The fibrils were labeled with Fluorescein isothiocyanate (FITC) using the protocol earlier described on section 1.2.15.

3.2.3 Thioflavin T (ThT)-based aggregation assay

This aggregation assay was performed in accordance with previous protocol[13] with slight modifications. Peptide (pR248W) amyloid formation kinetics in black 96-well plates with flat bottom (Corning Inc., NY) were measured in quadruplicates using a microplate reader. Initially, the aggregation began with the dilution of the peptide from a freshly prepared stock solution (1 mM in DMSO) to PBS containing ThT, with or without the OPs. An equal amount of DMSO was added to the wells with peptide only reactions to maintain identical conditions. The final concentrations of the samples in the wells were 10 μM pR248W, 10 μM oligopyridylamide and 100 μM ThT. Shaking and measuring of the ThT fluorescence (λex/em = 440/490 nm) at 5-min intervals at 37 °C was used to monitor the progression of the peptide aggregation. The sample data was processed by setting the maximum value to one through subtraction of the blank and renormalizing the fluorescence intensity.

3.2.4 Immunofluorescence assay (IFA)

This assay was carried out based on a previously described protocol[13] with slight modifications. The MIA PaCA-2 cells (200,000 cells/mL) were plated in μ-slide 8 well plate (Ibidi, Gräfelfing, Germany) (200 μL/well), incubated at 37 ºC and 5% CO_2 supply, and the cells adhered to the plate for 24 h in media (DMEM, 10% FBS, 1% pen/strep). After 24 h, the media was aspirated from the wells and 200 μL of OptiMEM containing 1μM pWT PFF in lipofectamine were used to replace the cells media (in duplicates) in wells 3 – 8 respectively. The plate was incubated for 48 h after internalizing the fibrils. For the cells treated with the Oligopyridylamide-based α-helix mimetic molecules including 20 μM ADH-40, 20 μM RD-149 and 20 μM of RD148, these cells were incubated at 37ºC for only 6 h. Afterwards, PBS was used to wash the cells and 4% paraformaldehyde (PF) was used to fix the cells for 30 min. The cells were washed three times with PBS.

Subsequently, the cells were permeabilized and blocked with a solution of 0.5% Triton X-100 and 5% Bovine serum albumin (BSA) for 1 h. The cells were washed three times and mouse anti-p53 antibody DO-7 (1:1000; Novus Bio) was used to incubate the cells overnight at 4 ºC. Subsequently, the cells were washed three times with PBS and Alexa flour 647 secondary mouse antibody was used to incubate the cells for 1 h at 37 ºC. And then the cells were washed three times with PBS and re-suspended in PBS for confocal imaging. An Olympus Fluoview FV3000 confocal/2-photon microscope, using a 20×Plan-Apo/1.3 NA objective with DIC capability was used to image the cells. The images were processed using the OlympusViewer in Fiji/ImageJ processing software.

3.2.5 Cell fractionation and western blot analysis

This experiments were done according to previous protocols[84,85] with slight modifications. Cells were seeded at a density of 10^6 cells/mL of complete DMEM media and incubated in an incubator with 5% CO_2 supply at 37ºC for 24 h. The cells were treated with 5 μM RD148 and 1 μM pWT PFF for 24 h. Subsequently, the cells were washed with PBS, trypsinized with detachin and lysed by using 100 μL RadioImmunoPrecipitation Assay (RIPA) buffer. The cell lysates were centrifuged at 14,000xg for 10 min at 4 ºC and the supernatant (soluble) fraction and pellet (insoluble) fractions were separated. The bicinchonimic acid (BCA) protein assay was used to determine the protein concentration and normalized accordingly[86].

The protein samples were prepared in loading buffer with 2-mercaptoethanol and heated at 95ºC for 5 minutes. And then 10 μL of the protein samples were loaded in each gel lane for electrophoresis on a 6-12% SDS-PAGE in a Mini-PROTEAN Tetra cell (Bio-Rad, Hercules, CA). Subsequently, the gel was transferred to a polyvinylidene fluoride (PVDF) membrane (Bio-Rad, Hercules, CA) for 30 min. After, the blocking buffer (Bio-Rad, Hercules, CA) was used to block the protein samples on the membrane for 5 min at r.t. on a shaker (Thermo Fisher Scientific, Waltham, MA). And then the membrane was incubated with mouse anti-p53 antibody DO-7 (1:20,000; Novus Bio) for 15 min and washed five times with 10x Tris-buffered saline and 0.1% Tween 20 (TBST) for 5 min at r.t. on a shaker.

After incubating the proteins on the membrane with Goat anti-mouse IgG (H+L)-HRP conjugate secondary antibody (1:20,000; Bio-Rad, Hercules, CA) for 15 min, the membrane was washed five times with TBST for 5 min at r.t. on a shaker. Subsequently, the proteins on the membrane were incubated with Clarity Western ECL substrate (Bio-Rad, Hercules, CA) for 5 min at r.t. on a shaker and visualized using the ChemiDoc MP Imaging System (Bio-rad, Hercules, CA). β-actin served as the control in this experiment: the cell lysate containing the mixed protein fractions (soluble and insoluble fractions) were transferred to the membrane after the gel electrophoresis and the membrane was blocked with the blocking buffer for 5 min at r.t. on a shaker. Subsequently, the membrane was incubated with HRP-conjugated β-actin Mouse McAb (Proteintech) for 15 min on a shaker (120 rpm) at r.t. and washed five times with TBST for 5 min at r.t. on a shaker. And then, the samples on the membrane were incubated with Clarity Western ECL substrate for 5 min at r.t. on a shaker and visualized using the ChemiDoc MP Imaging System.

3.2.6 The 3-(4,5-dimethylthiazol-2-yl)-2,5-diphenyltetrazolium bromide (MTT)-Based Cytotoxicity Assay (MIA PaCa-2 cells)

MTT assay was performed in accordance with a previously described protocol[87] with slight modifications. This assay was performed to probe the effects of Oligopyridylamide-based α-helix mimetics including ADH-40, and RD-148 on the cytotoxicity mediated by p53 aggregation in MIA PaCa-2 cells and MCF-7 cells. Phenol red free DMEM with 10% FBS and 1% pen/strep were used to culture the cells at 37 ºC and 5% $CO_{2(g)}$ supply. A clear, flat bottom 96-well black plate was used to plate the cells

at a density of 10,000 cells per well and the cell viability was greater than 90%. After 24 h incubation of the cells, the media was aspirated, and 100 µL of fresh OptiMEM (Fisher Scientific, Pittsburgh, PA) containing the Oligopyridylamide-based α-helix mimetics was added at various stoichiometric ratios and incubated for 24 h at 37 ºC and 5% $CO_{2(g)}$ supply. MTT dye solution (10 µL prepared in PBS buffer, 5 mg/ml) was added into each well that contained the cells and the OPs. Thin foil was used to cover the plate(s) and it was incubated for 3 h in an incubator at 37 ºC and 5% $CO_{2(g)}$ supply. Formation of formazan crystal was observed under the microscope and the solution in each well was carefully aspirated without disrupting the formazan crystals and it was replaced with 100 µL of DMSO to dissolve the formazan crystals. And then, the plate was shaken in a plate reader for 5 min before measuring the absorbance at 570 nm. A scale of 100% was used to report the cell viability and cytotoxicity of the OPs. The control wells with regular media were used as 100% cell viability and the wells that contained 10% DMSO (v/v) served as 0% viability. The vehicle used in this experiment contained 1% DMSO considering that the OPs were prepared using DMSO as a solvent.

3.2.7 Thioflavin S (ThS) assay

ThS assay was carried out based on a previously described protocol[13] with slight modifications. This assay was performed to probe the p53 fibril aggregation in the mutant MIA PaCa-2 cells in the absence and presence of PFFs and the cells in the absence and presence of Oligopyridylamide-based α-helix mimetics including ADH-40, and RD148. Phenol red free DMEM with 10% FBS and 1% pen/strep were used to culture the cells at

37 ºC and 5% $CO_{2(g)}$ supply. A black, flat bottom 96-well cell culture plate was used to plate the cells at a density of 10,000 cells per well and the cell viability was greater than 90%. After 24 h incubation of the cells, the media was aspirated, and 100 µL of fresh OptiMEM (Fisher Scientific, Pittsburgh, PA) containing the pWT PFFs with Lipofectamine and/or Oligopyridylamide-based α-helix mimetics were added at various stoichiometric ratios and incubated for 24 h at 37 ºC and 5% $CO_{2(g)}$ supply. The cell media was replaced with 100 µL of 125 µM ThS solution (prepared in PBS) and incubated for 30 min in an incubator at 37 ºC and 5% $CO_{2(g)}$ supply. The cells were washed at least 2 times with PBS and the fluorescence intensity was measured on the plate reader at λex/em = 391/428 nm.

3.2.8 Preparation of peptide with Lipofectamine solution for transfection

The Lipofectamine solution was made fresh for each transfection to avoid denaturation of reagents in a stored stock solution. For each transfection protocol, the total volume of lipofectamine solution required is equivalent to 30% of the total volume of αS/lipofectamine solution needed. The solution was made by mixing OptiMEM media, Lipofectamine, and P3000 reagents (Invitrogen, Carlsbad, CA) at a ratio of 50:1:1 (v/v/v), homogenized, and incubated at r.t. for 20 min. To prepare a 5 µM αS/Lipofectamine solution, 250 µL of an aggregated solution of αS (100 µM) was diluted with OptiMEM to a final volume of 3.5 mL and sonicated for 10 min. Subsequently, the Lipofectamine solution (1.5mL) was combined with the αS protein solution for a total volume of 5 mL. The resulting solution (5 µM) was homogenized and further incubated for 10 min.

Subsequently, the media in the plated cell wells was aspirated and replaced with the transfection pWT PFF solution.

3.3 Results and discussion

3.3.1 RD148 is a potent antagonist for of amyloid formation of the aggregation-nucleating sequence of p53 DBD in an *in vitro* ThT assay

A previous study used aggregation prediction algorithms developed from biophysical studies of amyloids to identify an aggregation-nucleating subdomain (p53 residues 251-258) in the hydrophobic core of the p53 DBD that is crucial for inducing p53 aggregation[13,72,80] (Figure 3.1a-b). This subdomain forms a β-strand within the hydrophobic core of the DBD. But many mutations in the p53 DBD destabilize its intrinsically unstable tertiary structure further[88] and enhances exposure of the aggregation-nucleating subdomain resulting to the increase in aggregation of the protein. Hence, our study was focused on $p53_{251\text{-}258}$ but we expanded the sequence to include two of the most common mutation hotspots, R248 and R273 (IARC TP53 database)[89]. Two peptides were synthesized in previous study[13], one corresponds to residues 248-273 of WT p53 DBD (pWT), and the other was composed of the same sequence but harboring the R248W mutation (pR248W) (Figure 3.1c).

R248W mutation involves the replacement of the cationic arginine, an aggregation "gate keeper" residue[71] with the hydrophobic tryptophan, an aromatic residue with the highest amyloidogenic potential of all the 20 naturally occurring amino acids[90]. R248W (compared to pWT) was found to exhibit higher aggregation propensity, as shown by its

shorter lag/nucleation phase, more rapid elongation phase and higher final ThT fluorescence intensity. In a wide range of malignancies including pancreatic cancer, R248W is one of the most common p53 DBD mutations[70,89]. Pancreatic cancer was found as an intractable malignancy that can be undetected during early diagnosis and resist treatment, and it is associated with a very poor prognosis: it is the seventh most common cause of death from cancer worldwide, with a five-year survival rate of <5%[91,92].

Considering the fact that OPs have carboxylic acid and hydrophobic side chains that can specifically target sequences that have high amount of positive charges and hydrophobic side chain residues, they have been regarded as modulators for the self-assembly of amyloid proteins[10]. Hence, various OPs with carboxylic acid and hydrophobic side chains were utilized in this study. RD148 (Figure 3.3c) and several other OPs including ADH40 (Figure 3.3b) were screened through an *in vitro* ThT-based amyloid kinetic assay (Figure 3.3a) on the aggregation of pR248W[13] as part of our studies for the inhibition of the primary nucleation of p53. The distinct chemical fingerprints and the ability to modulate amyloid assemblies are some of the reasons for selecting the OPs. A sigmoidal ThT curve was formed by the p53 DBD-derived peptides alone with t50 (time to reach 50% fluorescence) of ~38.1±1.8 h; this is a suggestion of nucleation-dependent process typical for amyloids[93].

The structure of ThT shows that it has a hydrophobic end with a dimethylamino group bound to a phenyl group and connected to a more polar benzothiazole group containing the polar N and S. In aqueous solution, the ThT molecule can form micelles due

to the interaction of the polar and hydrophobic regions of the molecule with the hydrophobic interiors and the positively charged N group pointing towards the solvent[94,95]. Previous studies suggested that the hydroxyl groups of amyloid protein fibrils form hydrogen bond with the thiazole nitrogen group of the dye resulting to specific binding on amyloid fibrils[94]. This interaction might have led to the high fluorescence intensity observed through the assays. And ThS molecule has a similar mechanism of interaction with amyloid fibrils compared to ThT molecule.

The OPs had different antagonistic activities against pR248W aggregation. Based on the ThT assay, we observed that ADH40 had about 75% inhibitory effect on pR248W aggregation while RD148 had about 90% efficacy. The determinants of efficacy of the OPs appears to be the number and positioning of cationic sidechains (Figure 3.2a). This suggests that the inhibition of pR248W aggregation occurs through specific interactions involving the compounds' cationic sidechains. It can be proposed that the OP-pR248W binding is stabilized by cation-π interactions of the cationic sidechain of the protein mimetic and the aromatic tryptophan residue of the mutant peptide and this provides a base for strong binding and confers a degree of specificity to the interaction. Although the binding affinity of RD148 to pR248W was not established but based on the binding affinity of ADH40 (ADH-6; K_d = 366$\pm$13 nM for pR248W), it may be proposed that RD148 has higher binding affinity for hotspots on pR248W.

The hotspots are sidechains on proteins for aPPIs. Data obtained from this experiment showed that RD148 is potent antagonist of p53 mutant (R248W) aggregation

at equimolar and sub-stoichiometric ratios. A reductionist approach commonly used in the amyloid field of research, was implemented in this study to target a short aggregation-prone segment within the protein of interest (p53)[96]. Aggregation can be nucleated in a structure-specific mechanism in amyloid systems through a small stretch of residues with robust independent capacity for self-assembly[96].

3.3.2 RD148 causes selective cytotoxicity in cancer cells bearing mutant p53

Due to RD148's potent antagonism of the self-assembly of aggregation prone segment of mutant p53 DBD (Figure 3.3a), and its multiple interaction sites on the DBD (Figure 3.3b), we investigated the cytotoxicity of the OP on the viability of intracellular mutant R248W p53 cancer cell (MIA PaCa-2) and WT p53 bearing breast cancer MCF-7 cells using MTT assay (Figure 3.3d-e, 3.4a-g, 3.5a-c). Several OPs were screened in this experiment including RD148 and ADH40. MCF-7 cells were also used in this study because we wanted to find out if the OPs are also toxic in non-p53 aggregation cells. The cells were separately treated in the absence and presence of 5 μM of OPs. RD148 was the most potent antagonist of pR248W amyloid formation, and it was also the most toxic ligand in MIA PaCa-3 cells and not MCF-7 cells based on the MTT assay (Figure 3.3d-e).

And Thioflavin S (ThS) assay was conducted to quantify the pR248W inclusions in MIA PaCa-2cells (Figure 3.5a). ThS molecule can bind to fibrils *in vivo* and this was observed through the ThS assay with the increase in fluorescence intensity over time. The increase in fluorescence intensity is observed for both ThT and ThS assays because the molecules form micelles in PBS buffer; and these micelles bind to the fibrils and cause

enhancement of fluorescence[94]. For the ThS assay, MIA PaCa-2 cells were treated in the absence and presence of 5 µM of the OPs. The cells treated with RD148 showed the lowest fluorescence intensity and this may be due to low concentration of pR248W fibrils in the cells. RD148 presented better antagonistic activity compared to ADH40.

Immunofluorescence assay (IFA) was performed to show the endogenous inclusions of pR248W in MIA PaCa-2 cells treated in the absence and presence of OPs (Figure 3.4a-g). After treating the cells with the OPs for 24 h, the cells were fixed with paraformaldehyde and permeabilized as described in section 3.2.4. Subsequently, the cells were stained with PAb 240-AF647. PAb 240 is an antibody specific for partially unfolded p52 because it identifies an epitope (residues 213-217) that is buried in folded p53. Considering that p53 aggregation involves partial unfolding of the protein, PAb 240 is often used as a marker for aggregated p53[13,80]. After treatment of the cells with the OPs and imaging them using a confocal microscope, the pR248W inclusions were manually counted using the confocal microscope. It was observed that the cells treated with RD148

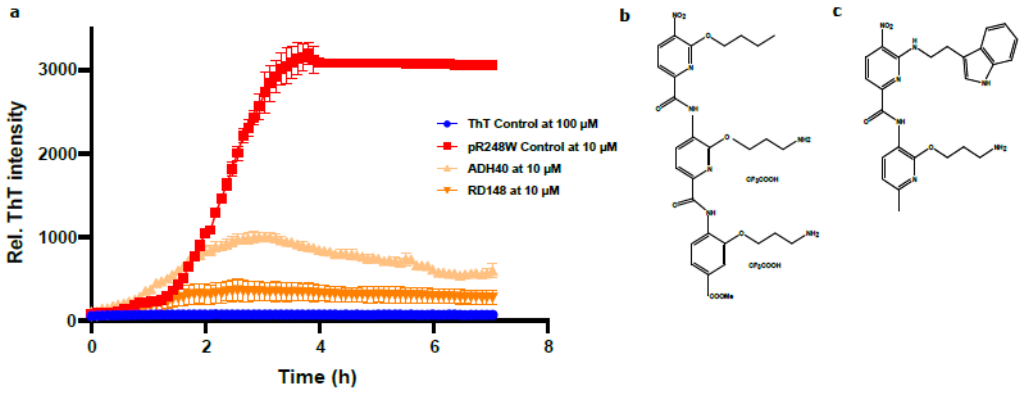

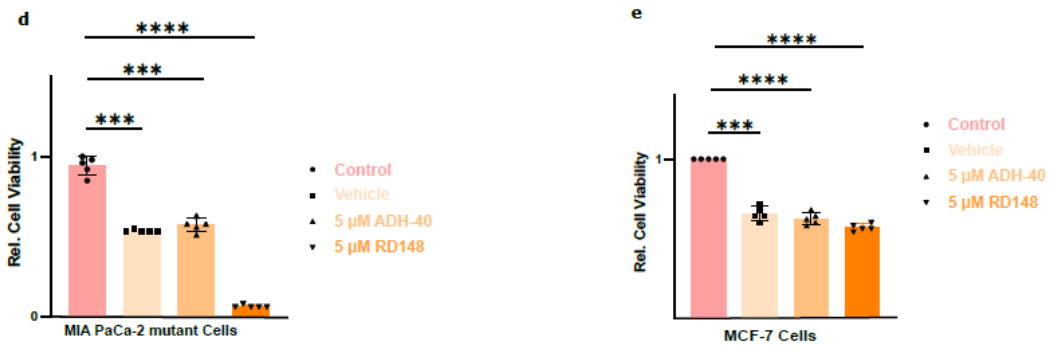

Figure 3.3 RD148 inhibits amyloid fibril formation of aggregation-prone region of p53 DBD. **a** effects of the OPs on pR248W amyloid fibril formation. Chemical structures of the OPs including ADH-40 **(b)** and RD148 **(c).** Effects of ADH-40 and RD148 on viability of cancer cells with mutant p53 inclusion (MIA PaCa-2 cells, **d**) and WT p53 (MCF-7, **e**). The data shows the mean, and the error bars represents the s.e.m. (n=2 independent experiments and each n included five technical replicates. ANOVA with Tukey's multiple comparison test was used to perform statistical analysis. *p<0.05, **p < 0.01, ***p<0.001, ****p < 0.0001. Source data file was used to provide source data.

showed significant disappearance of pR248W inclusions (~60%) (Figure 3.4a-c, g) compared to the cells treated with ADH40 (~30% of inclusions disappeared) (Figure 3.4d-f, g) and the cells without treatment (Figure 3.6c-e). The significant disappearance of the pR248W inclusions in the MIA PaCa-2 cells treated with RD148 further re-validates the potent antagonism of the OP for p53 amyloid fibril formation.

In concurrence with the previous assays conducted for the toxicity of RD148 in MIA PaCa-2 cells, western blot analysis revealed significant decrease in the concentration of pR248W fibrils in the cells treated with RD148 by almost three folds compared to the cells transfected with and without pWT PFF (Figure 3.5c-d). The supernatant fraction of

the cells treated with RD148 showed high concentration of non-aggregated form of the protein while the pellet fraction showed low concentration of the aggregated form of the protein.

3.3.3 Prion-like behavior of p53 amyloid aggregates

Intracellular or extracellular aggregation of proteins are commonly linked to cancer[68,97]. The core domain of p53 has higher propensity to form aggregates than the globular domain of the prion protein (PrP)[68]. The formation of mutant p53 aggregates have been linked (in recent studies) to loss-of-function (LoF), dominant-negative (DN), and gain-of-function (GoF) effects[68]. DN regulatory effects may be exerted by mutant p53 on WT p53 resulting to the conversion of the later to aggregated species and complete loss of its tumor suppressor function. p53 may be transformed by mutations into malignant oncogene with GoF phenotypes including invasion, migration, angiogenesis, proliferation, tissue remodeling, and chemoresistance with several different mechanisms proposed to explain these new functions[76].

Formation of pWT PFF was confirmed through *in vitro* (ThT Assay, Figure 3.6a). ThT molecule can bind to pWT fibrils *in vitro* but not *in vivo* and this is detected through the increase in ThT intensity over time during the preparation of the pWT PFFs in the absence and presence of FITC. The PFFs were transfected in MIA PaCa-2 mutant cells using lipofectamine to induce secondary nucleation, elongation, and templating of fibrils.

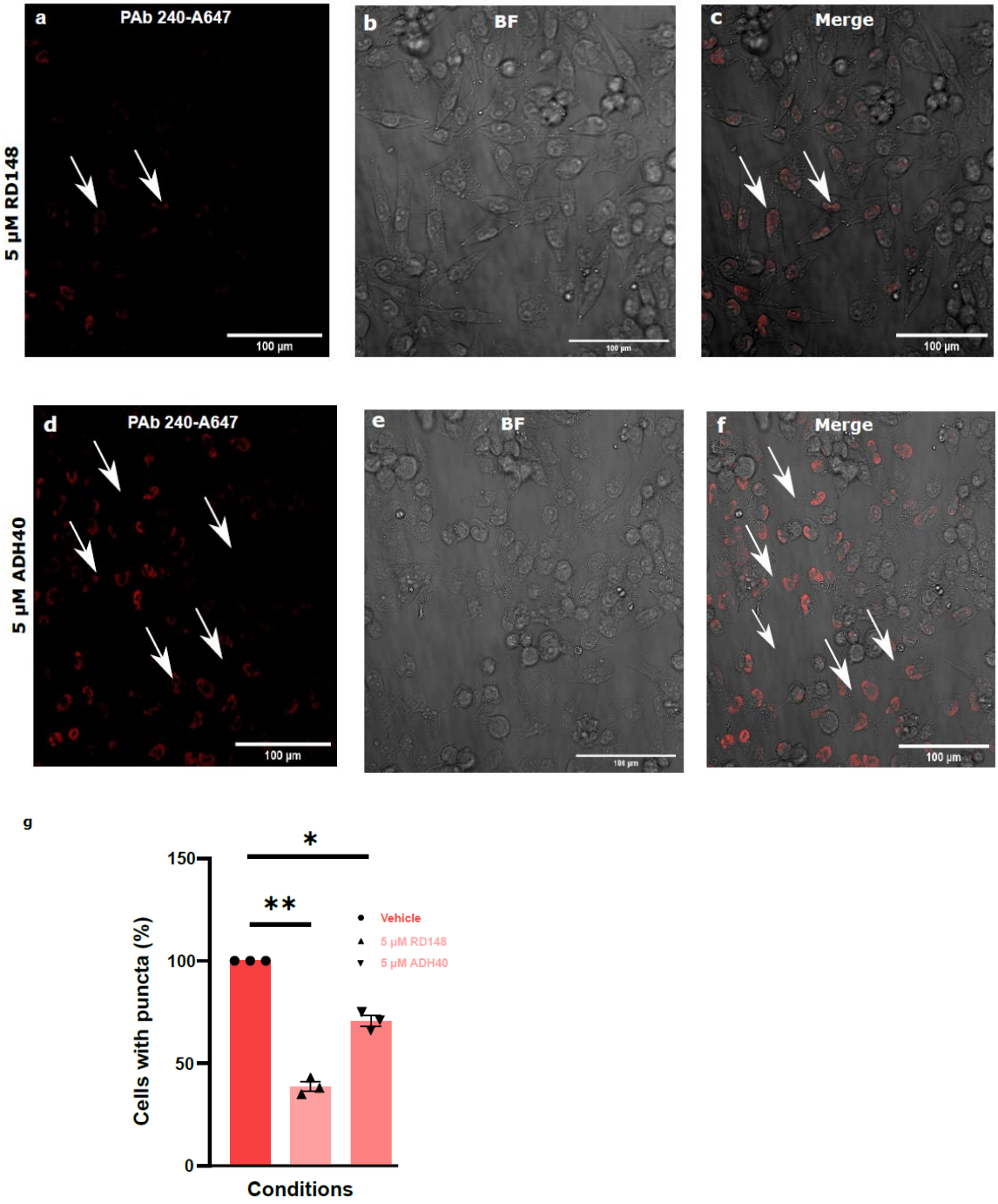

Figure 3.4 Confocal fluorescence microscopy images of MIA PaCa-2 cells stained with PAb 240-A647 in the presence of 5 µM RD148 **(a-c)** and 5 µM ADH-40 **(d-f). g** Quantification of p53 fibril inclusions in MIA PaCa-2 mutant cells treated with OPs for 24

h and stained with PAb 240-A647. The data shows the mean, and the error bars represents the s.e.m. (n= 3 independent experiments. ANOVA with Tukey's multiple comparison test was used to perform statistical analysis. *p<0.05, **p < 0.01, ***p<0.001, ****p < 0.0001. Source data file was used to provide source data.

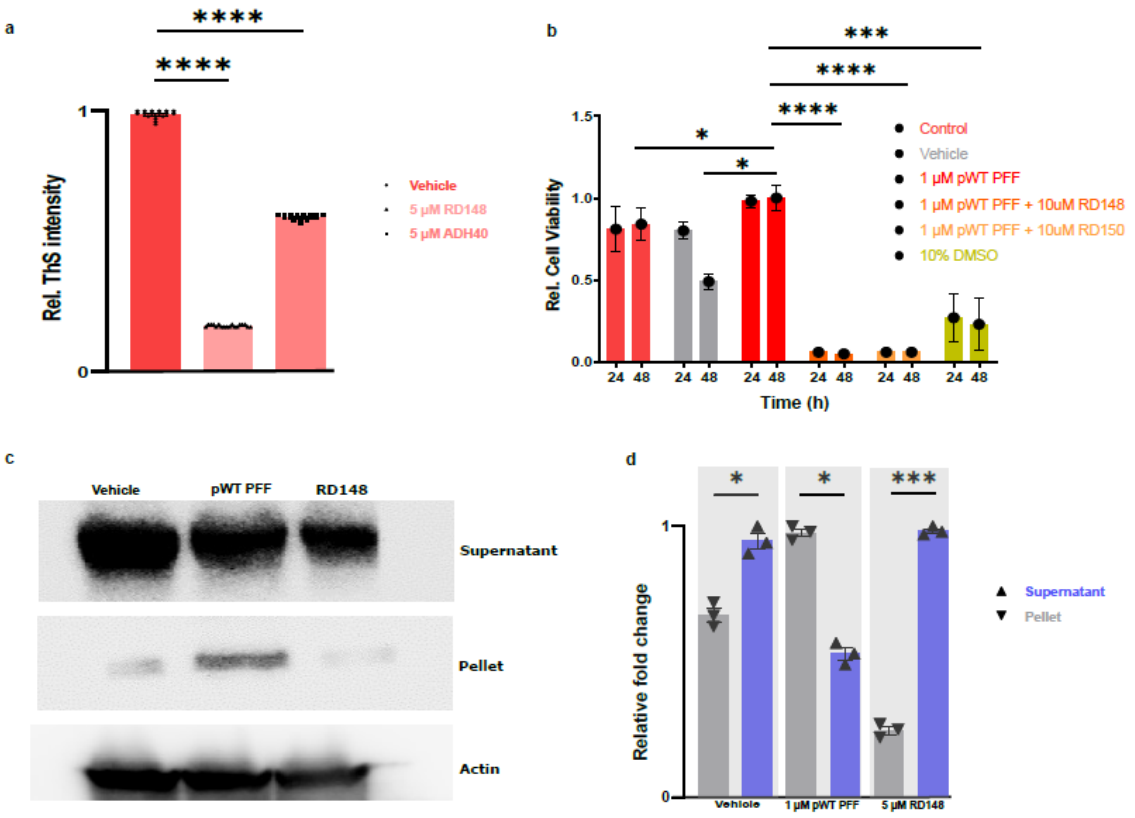

Figure 3.5 ThS assay, Cell viability assay, and Western blot analysis for p53 inclusions in MIA PaCa-2 cells in the absence and presence of OPs. **a** Relative ThS intensity of mutant p53 inclusions in MIA PaCa-2 cells. **b** Effects of RD148 and ADH40 on viability of cancer cells with mutant p53 inclusions (MIA PaCa-2 cells), and pWT PFFs. **c** Western blot analysis of the effects of RD148 on mutant p53 aggregation in MIA PaCa-2 cells. Immunoblots of mutant p53 in the soluble (supernatant) and insoluble (pellet) fractions of MIA PaCa-2 cells treated with vehicle or 1 µM pWT PFF or 5 µM RD148 for 24 h and detected with PAb 240. **d** Densitometric quantification of the immunoblot bands of mutant p53 in the soluble and insoluble fractions (n = 1). *p<0.05, **p < 0.01, ***p<0.001, ****p < 0.0001. Source data file was used to provide source data.

In vivo immunofluorescence assay was performed (Fig 3.6b-l) after staining the cells with pAb-240-AF647. The cells transfected with pWT PFF in the absence of FITC showed high cell confluency compared to the cells without PFFs (Figure 3.6f-h). This showed that the PFFs might have induced secondary nucleation, elongation of the fibrils, and templating. To help understand the interaction of the PFFs with the fibrils (in the cells), we imaged the cells transfected with pWT PFF-FITC and we observed colocalization of the pWT PFF-FITC (green) with the fibrils for in the cells (green) (Figure 3.6i-l). This result further suggested that p53 is implicated in the amyloid protein aggregation in MIA PaCa-2 cells and it shows the prion-like progression of cancer.

Also, the effects of OPs (RD148 and RD150) on MIA PaCa-2 mutant cells transfected with pWT PFF (Figure 3.5b) were assessed using the cell viability assay. It was found that the OPs were toxic to the cells. We suggest that the OPs were able to inhibit the primary nucleation, secondary nucleation, and elongation of p53 inclusions. Also, we suggest that the OPs rescued the apoptotic process in the cells and resulted to tumor suppression.

3.4 Conclusions and future work

Dipyridylamides including RD148, RD150, and RD152 were synthesized in the Kumar lab and several *in vitro* and *in vivo* assays were conducted to test the efficacies of the molecules as potent inhibitors of the primary nucleation, secondary nucleation, and elongation of p53 *in vitro* and *in vivo*. Other proposed experiment is Tryptophan fluorescence quenching assay to determine the binding interaction between OPs and mutant

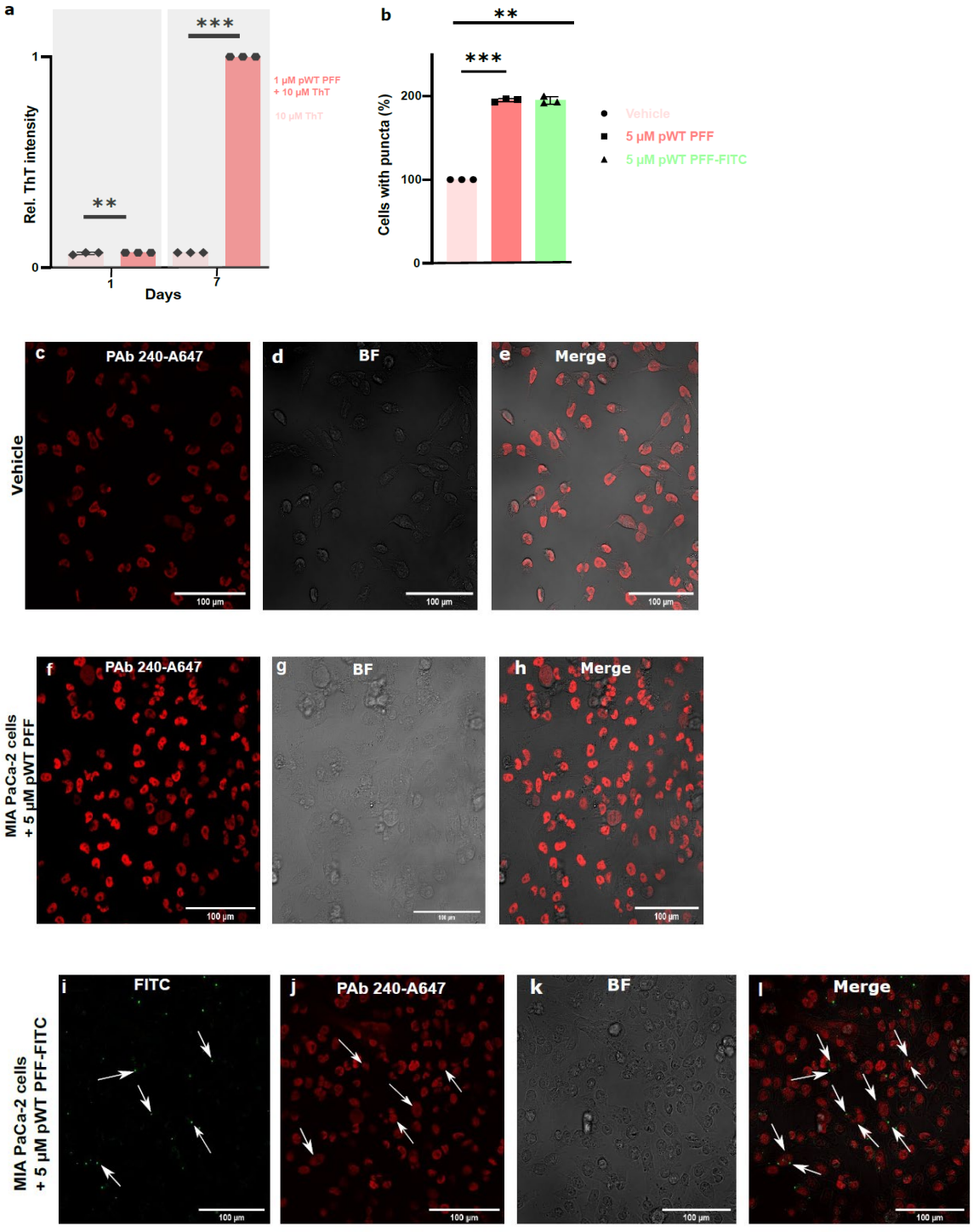
a
Rel. ThT intensity
Days
1 µM pWT PFF
+ 10 µM ThT
10 µM ThT
b
Cells with puncta (%)
Vehicle
5 µM pWT PFF
5 µM pWT PFF-FITC
c PAb 240-A647
d BF
e Merge
Vehicle
f PAb 240-A647
g BF
h Merge
MIA PaCa-2 cells
+ 5 µM pWT PFF
i FITC
j PAb 240-A647
k BF
l Merge
MIA PaCa-2 cells
+ 5 µM pWT PFF-FITC
100 µm

Figure 3.6 Prion-like spread of p53 in MIA PaCa-2 mutant cells. **a** Relative ThT fluorescence intensity for 1 μM pWT (day 1 and day 7). **b** Quantification of p53 fibril inclusions in MIA PaCa-2 mutant cells transfected with 5 μM pWT PFF and 5 μM pWT PFF-FITC for 24 h and stained with PAb 240-A647. Confocal fluorescence microscopy images of MIA PaCa-2 mutant cells stained with PAb 240-A647 in the absence **(c-e)** and presence of 5 μM pWT PFF **(f-h)** and 5 μM pWT PFF-FITC **(i-l).** The data shows the mean, and the error bars represents the s.e.m. (n= 3 independent experiments. ANOVA with Tukey's multiple comparison test was used to perform statistical analysis. *$p<0.05$, **$p < 0.01$, ***$p<0.001$, ****$p < 0.0001$. Source data file was used to provide source data.

p53 DBD-derived aggregation domains (pR248W and pWT). Another proposed experiment is Transmission electron microscopy (TEM) to confirm that the aggregation-prone segment of mutant p53 forms fibrils and to show the disappearance of the fibril inclusions after treatment with OPs. Heteronuclear single quantum coherence spectroscopy (HSQC) maybe conducted to determine the protein-ligand interaction interface.

Also, Proteomics experiments maybe considered for MIA PaCa-2 cell lysates in the absence and presence of ligands to investigate protein upregulation and downregulation and further re-validate the antagonistic activities of the ligands.

References

1. Araki, K. et al. Parkinson's disease is a type of amyloidosis featuring accumulation of amyloid fibrils of α-synuclein. Proc Natl Acad Sci U S A. **116**, 17963–17969 (2019).
2. Ahmed, J. et al. Foldamers reveal and validate therapeutic targets associated with toxic α-synuclein self-assembly. Nat Commun **13**, 2273 (2022).
3. DeMaagd, G. & Philip, A. Parkinson's Disease and Its Management. P T **40**, 504–532 (2015).
4. Doherty, C. P. A. et al. A short motif in the N-terminal region of α-synuclein is critical for both aggregation and function. Nature Structural & Molecular Biology **27**, 249–259 (2020).
5. Ray, A., Martinez, B. A., Berkowitz, L. A., Caldwell, G. A. & Caldwell, K. A. Mitochondrial dysfunction, oxidative stress, and neurodegeneration elicited by a bacterial metabolite in a *C. elegans* Parkinson's model. Cell Death Dis **5**, e984–e984 (2014).
6. Pujols, J., Peña-Díaz, S., Pallarès, I. & Ventura, S. Chemical Chaperones as Novel Drugs for Parkinson's Disease. Trends Mol Med **26**, 408–421 (2020).
7. Guichard, G. & Huc, I. Synthetic foldamers. Chem. Commun. **47**, 5933–5941 (2011).

8. Kumar, S. et al. Islet amyloid-induced cell death and bilayer integrity loss share a molecular origin targetable with oligopyridylamide-based α-helical mimetics. Chem Biol **22**, 369–378 (2015).
9. Kumar, S. et al. Foldamer-mediated manipulation of a pre-amyloid toxin. Nat Commun **7**, 11412 (2016).
10. Kumar, S., Henning-Knechtel, A., Chehade, I., Magzoub, M. & Hamilton, A. D. Foldamer-Mediated Structural Rearrangement Attenuates Aβ Oligomerization and Cytotoxicity. J. Am. Chem. Soc. **139**, 17098–17108 (2017).
11. Kumar, S. & Hamilton, A. D. α-Helix Mimetics as Modulators of Aβ Self-Assembly. J. Am. Chem. Soc. **139**, 5744–5755 (2017).
12. Kumar, S., Henning-Knechtel, A., Magzoub, M. & Hamilton, A. D. Peptidomimetic-Based Multidomain Targeting Offers Critical Evaluation of Aβ Structure and Toxic Function. J. Am. Chem. Soc. **140**, 6562–6574 (2018).
13. Palanikumar, L. et al. Protein mimetic amyloid inhibitor potently abrogates cancer-associated mutant p53 aggregation and restores tumor suppressor function. Nat Commun **12**, 3962 (2021).
14. Hubbard, R. E. Fragment approaches in structure-based drug discovery. J Synchrotron Radiat **15**, 227–230 (2008).
15. Wasko, M. J., Pellegrene, K. A., Madura, J. D. & Surratt, C. K. A Role for Fragment-Based Drug Design in Developing Novel Lead Compounds for Central Nervous System Targets. Frontiers in Neurology **6**, (2015).

16. Moiola, M., Memeo, M. G. & Quadrelli, P. Stapled Peptides—A Useful Improvement for Peptide-Based Drugs. Molecules **24**, 3654 (2019).
17. Zhu, M. & Fink, A. L. Lipid binding inhibits α-synuclein fibril formation. J Biol Chem **278**, 16873–16877 (2003).
18. Riddle, D. L., Blumenthal, T., Meyer, B. J. & Priess, J. R. Introduction to *C. elegans*. *C. elegans* II (eds. Riddle, D. L., Blumenthal, T., Meyer, B. J. & Priess, J. R.) (Cold Spring Harbor Laboratory Press, 1997).
19. Zhang, S. Genetic analyses of lipid metabolism pathways involved in alpha-synuclein-induced neurodegeneration using a *Caenorhabditis elegans* model of Parkinson's disease. (University of Alabama Libraries, 2017).
20. Cao, S., Gelwix, C. C., Caldwell, K. A. & Caldwell, G. A. Torsin-mediated protection from cellular stress in the dopaminergic neurons of *C. elegans*. J Neurosci **25**, 3801–3812 (2005).
21. Hamamichi, S. et al. Hypothesis-based RNAi screening identifies neuroprotective genes in a Parkinson's disease model. Proc Natl Acad Sci U S A **105**, 728–733 (2008).
22. Singleton, A. B. et al. α-Synuclein locus triplication causes Parkinson's disease. Science **302**, 841 (2003).
23. Anbalagan, C. et al. Transgenic nematodes as biosensors for metal stress in soil pore water samples. Ecotoxicology **21**, 439–455 (2012).

24. van Ham, T. J. et al. Towards multiparametric fluorescent imaging of amyloid formation: studies of a YFP model of α-Synuclein aggregation. J Mol Biol **395**, 627–642 (2010).

25. van Ham, T. J. et al. *C. elegans* model identifies genetic modifiers of α-Synuclein inclusion formation during aging. PLoS Genet **4**, e1000027 (2008).

26. Godini, R., Handley, A. & Pocock, R. Transcription Factors That Control Behavior—Lessons From *C. elegans*. Front Neurosci **15**, 745376 (2021).

27. Kozlowski, H., Luczkowski, M., Remelli, M. & Valensin, D. Copper, zinc and iron in neurodegenerative diseases (Alzheimer's, Parkinson's and prion diseases). Coordination Chemistry Reviews **256**, 2129–2141 (2012).

28. Bharathi, null, Indi, S. S. & Rao, K. S. J. Copper- and iron-induced differential fibril formation in α-synuclein: TEM study. Neurosci Lett **424**, 78–82 (2007).

29. Guo, S., Bezard, E. & Zhao, B. Protective effect of green tea polyphenols on the SH-SY5Y cells against 6-OHDA induced apoptosis through ROS–NO pathway. Free Radical Biology and Medicine **39**, 682–695 (2005).

30. Lau, Y. H. et al. Functionalised staple linkages for modulating the cellular activity of stapled peptides. Chem. Sci. **5**, 1804–1809 (2014).

31. Harrington, A. J., Yacoubian, T. A., Slone, S. R., Caldwell, K. A. & Caldwell, G. A. Functional Analysis of VPS41-Mediated Neuroprotection in *C. elegans* and Mammalian Models of Parkinson's Disease. J. Neurosci. **32**, 2142–2153 (2012).

32. Brenner, S. The Genetics of *C. Elegans.* Genetics **77**, 71–94 (1974).

33. Chaudhuri, J., Parihar, M. & Pires-daSilva, A. An Introduction to Worm Lab: from Culturing Worms to Mutagenesis. JoVE 2293 (2011) doi:10.3791/2293.

34. Chemotaxis in C.elegans (ARENA system) - Phylumtech.

35. Margie, O., Palmer, C. & Chin-Sang, I. *C. elegans* Chemotaxis Assay. JoVE 50069 (2013) doi:10.3791/50069.

36. Garcia-Moreno, J. C., Porta de la Riva, M., Martínez-Lara, E., Siles, E. & Cañuelo, A. Tyrosol, a simple phenol from EVOO, targets multiple pathogenic mechanisms of neurodegeneration in a *C. elegans* model of Parkinson's disease. Neurobiology of Aging **82**, 60–68 (2019).

37. Currey, H. N., Malinkevich, A., Melquist, P. & Liachko, N. F. ARENA-based activity profiling of tau and TDP-43 transgenic *C. elegans*. MicroPubl Biol **2020**.

38. Habchi, J. et al. An anticancer drug suppresses the primary nucleation reaction that initiates the production of the toxic Aβ42 aggregates linked with Alzheimer's disease. Sci Adv **2**, e1501244 (2016).

39. Yoon, D. S., Lee, M.-H. & Cha, D. S. Measurement of Intracellular ROS in Caenorhabditis elegans Using 2',7'-Dichlorodihydrofluorescein Diacetate. Bio-protocol **8**, e2774–e2774 (2018).

40. Kalmankar, N. V., Hari, H., Sowdhamini, R. & Venkatesan, R. Disulfide-Rich Cyclic Peptides from Clitoria ternatea Protect against β-Amyloid Toxicity and Oxidative Stress in Transgenic Caenorhabditis elegans. J Med Chem **64**, 7422–7433 (2021).

41. Polinski, N. K. et al. Best Practices for Generating and Using α-Synuclein Pre-Formed Fibrils to Model Parkinson's Disease in Rodents. J Parkinsons Dis **8**, 303–322.

42. Wördehoff, M. M. & Hoyer, W. α-Synuclein Aggregation Monitored by Thioflavin T Fluorescence Assay. Bio Protoc **8**, e2941 (2018).

43. Nowakowski, A. B., Wobig, W. J. & Petering, D. H. Native SDS-PAGE: High Resolution Electrophoretic Separation of Proteins With Retention of Native Properties Including Bound Metal Ions. Metallomics **6**, 1068–1078 (2014).

44. Raja, S. M. et al. A novel mechanism for protein delivery: granzyme B undergoes electrostatic exchange from serglycin to target cells. J Biol Chem **280**, 20752–20761 (2005).

45. Revankar, C. M., Cimino, D. F., Sklar, L. A., Arterburn, J. B. & Prossnitz, E. R. A transmembrane intracellular estrogen receptor mediates rapid cell signaling. Science **307**, 1625–1630 (2005).

46. Walther, D. M. et al. Widespread Proteome Remodeling and Aggregation in Aging *C. elegans*. Cell **168**, 944 (2017).

47. Lassalas, P. et al. Structure Property Relationships of Carboxylic Acid Isosteres. J. Med. Chem. **59**, 3183–3203 (2016).

48. Bieschke, J. et al. EGCG remodels mature α-synuclein and amyloid-β fibrils and reduces cellular toxicity. Proceedings of the National Academy of Sciences **107**, 7710–7715 (2010).

49. Ngo, S. T., Truong, D. T., Tam, N. M. & Nguyen, M. T. EGCG inhibits the oligomerization of amyloid beta (16-22) hexamer: Theoretical studies. Journal of Molecular Graphics and Modelling **76**, 1–10 (2017).

50. Stillman, N. H. et al. A 2D Fragment-Assisted Protein Mimetic Approach to Rescue α-Synuclein Aggregation Mediated Early and Post-Disease Parkinson's Phenotypes. 2022.07.11.499659 Preprint at https://doi.org/10.1101/2022.07.11.499659 (2022).

51. Juárez Olguín, H., Calderón Guzmán, D., Hernández García, E. & Barragán Mejía, G. The Role of Dopamine and Its Dysfunction as a Consequence of Oxidative Stress. Oxid Med Cell Longev **2016**, 9730467 (2016).

52. Auten, R. L. & Davis, J. M. Oxygen Toxicity and Reactive Oxygen Species: The Devil Is in the Details. Pediatr Res **66**, 121–127 (2009).

53. Jan, A., Gonçalves, N. P., Vaegter, C. B., Jensen, P. H. & Ferreira, N. The Prion-Like Spreading of α-Synuclein in Parkinson's Disease: Update on Models and Hypotheses. International Journal of Molecular Sciences **22**, 8338 (2021).

54. Luk, K. C. et al. Intracerebral inoculation of pathological α-synuclein initiates a rapidly progressive neurodegenerative α-synucleinopathy in mice. Journal of Experimental Medicine **209**, 975–986 (2012).

55. Meyer-Luehmann, M. et al. Exogenous Induction of Cerebral ß-Amyloidogenesis Is Governed by Agent and Host. Science **313**, 1781–1784 (2006).

56. Sandhof, C. A., Hoppe, S. O., Tittelmeier, J. & Nussbaum-Krammer, C. *C. elegans* Models to Study the Propagation of Prions and Prion-Like Proteins. Biomolecules **10**, 1188 (2020).

57. Masuda-Suzukake, M. et al. Prion-like spreading of pathological α-synuclein in brain. Brain **136**, 1128–1138 (2013).

58. Steiner, J. A., Quansah, E. & Brundin, P. The concept of α-Synuclein as a prion-like protein: ten years after. Cell Tissue Res **373**, 161–173 (2018).

59. Ma, J., Gao, J., Wang, J. & Xie, A. Prion-Like Mechanisms in Parkinson's Disease. Frontiers in Neuroscience **13**, (2019).

60. Haass, C. & Selkoe, D. J. Soluble protein oligomers in neurodegeneration: lessons from the Alzheimer's amyloid beta-peptide. Nat Rev Mol Cell Biol **8**, 101–112 (2007).

61. Iwatsubo, T. et al. Visualization of Amyloid beta 42(43) and Amyloid beta 40 in senile plaques with end-specific Amyloid beta monoclonals: evidence that an initially deposited species is Amyloid beta 42(43). Neuron **13**, 45–53 (1994).

62. Hahnel, S. R., Roberts, W. M., Heisler, I., Kulke, D. & Weeks, J. C. Comparison of electrophysiological and motility assays to study anthelmintic effects in Caenorhabditis elegans. Int J Parasitol Drugs Drug Resist **16**, 174–187 (2021).

63. Hafner, A., Bulyk, M. L., Jambhekar, A. & Lahav, G. The multiple mechanisms that regulate p53 activity and cell fate. Nat Rev Mol Cell Biol **20**, 199–210 (2019).

64. Bieging, K. T., Mello, S. S. & Attardi, L. D. Unravelling mechanisms of p53-mediated tumour suppression. Nat Rev Cancer **14**, 359–370 (2014).

65. Sorrell, A. D., Espenschied, C. R., Culver, J. O. & Weitzel, J. N. Tumor protein p53 (TP53) testing and Li-Fraumeni syndrome : current status of clinical applications and future directions. Mol Diagn Ther **17**, 31–47 (2013).

66. Joerger, A. C. & Fersht, A. R. The tumor suppressor p53: from structures to drug discovery. Cold Spring Harb Perspect Biol **2**, a000919 (2010).

67. Ghosh, S. et al. Investigating the intrinsic aggregation potential of evolutionarily conserved segments in p53. Biochemistry **53**, 5995–6010 (2014).

68. Silva, J. L., De Moura Gallo, C. V., Costa, D. C. F. & Rangel, L. P. Prion-like aggregation of mutant p53 in cancer. Trends Biochem Sci **39**, 260–267 (2014).

69. Wang, G. & Fersht, A. R. First-order rate-determining aggregation mechanism of p53 and its implications. PNAS **109**, 13590–13595 (2012).

70. Baugh, E. H., Ke, H., Levine, A. J., Bonneau, R. A. & Chan, C. S. Why are there hotspot mutations in the TP53 gene in human cancers? Cell Death Differ **25**, 154–160 (2018).

71. Reumers, J., Maurer-Stroh, S., Schymkowitz, J. & Rousseau, F. Protein sequences encode safeguards against aggregation. Hum Mutat **30**, 431–437 (2009).

72. Xu, J. et al. Gain of function of mutant p53 by coaggregation with multiple tumor suppressors. Nat Chem Biol **7**, 285–295 (2011).

73. Hishiya, A. & Takayama, S. Molecular chaperones as regulators of cell death. Oncogene **27**, 6489–6506 (2008).

74. Shadfan, M., Lopez-Pajares, V. & Yuan, Z.-M. MDM2 and MDMX: Alone and together in regulation of p53. Transl Cancer Res **1**, 88–89 (2012).

75. Chène, P. Inhibiting the p53–MDM2 interaction: an important target for cancer therapy. Nat Rev Cancer **3**, 102–109 (2003).

76. Silva, J. L., Cino, E. A., Soares, I. N., Ferreira, V. F. & A. P. de Oliveira, G. Targeting the Prion-like Aggregation of Mutant p53 to Combat Cancer. Acc. Chem. Res. **51**, 181–190 (2018).

77. Jucker, M. & Walker, L. C. Self-propagation of pathogenic protein aggregates in neurodegenerative diseases. Nature **501**, 45–51 (2013).

78. Aguzzi, A. & Rajendran, L. The Transcellular Spread of Cytosolic Amyloids, Prions, and Prionoids. Neuron **64**, 783–790 (2009).

79. Forget, K. J., Tremblay, G. & Roucou, X. p53 Aggregates penetrate cells and induce the co-aggregation of intracellular p53. PLoS One **8**, e69242 (2013).

80. Soragni, A. et al. A Designed Inhibitor of p53 Aggregation Rescues p53 Tumor Suppression in Ovarian Carcinomas. Cancer Cell **29**, 90–103 (2016).

81. Cummings, C. G. & Hamilton, A. D. Disrupting protein-protein interactions with non-peptidic, small molecule α-helix mimetics. Curr Opin Chem Biol **14**, 341–346 (2010).

82. Azzarito, V., Long, K., Murphy, N. S. & Wilson, A. J. Inhibition of α-helix-mediated protein-protein interactions using designed molecules. Nat Chem **5**, 161–173 (2013).

83. Ghosh, S. et al. p53 amyloid formation leading to its loss of function: implications in cancer pathogenesis. Cell Death Differ **24**, 1784–1798 (2017).

84. Woldetsadik, A. D., Vogel, M. C., Rabeh, W. M. & Magzoub, M. Hexokinase II-derived cell-penetrating peptide targets mitochondria and triggers apoptosis in cancer cells. FASEB J **31**, 2168–2184 (2017).

85. Palanikumar, L., Al-Hosani, S., Kalmouni, M., Saleh, H. O. & Magzoub, M. Hexokinase II-derived Cell-Penetrating Peptide Mediates Delivery of MicroRNA Mimic for Cancer-Selective Cytotoxicity. BIOCHEM.J. **59**, 2259–2273 (2020).

86. Smith, P. K. et al. Measurement of Protein Using Bicinchoninic Acid'. 10.

87. Rai, Y. et al. Mitochondrial biogenesis and metabolic hyperactivation limits the application of MTT assay in the estimation of radiation induced growth inhibition. Sci Rep **8**, 1531 (2018).

88. Ang, H. C., Joerger, A. C., Mayer, S. & Fersht, A. R. Effects of common cancer mutations on stability and DNA binding of full-length p53 compared with isolated core domains. J Biol Chem **281**, 21934–21941 (2006).

89. Bouaoun, L. et al. TP53 Variations in Human Cancers: New Lessons from the IARC TP53 Database and Genomics Data. Hum Mutat **37**, 865–876 (2016).

90. Pawar, A. P. et al. Prediction of ‘aggregation-prone’ and ‘aggregation-susceptible’ regions in proteins associated with neurodegenerative diseases. J Mol Biol **350**, 379–392 (2005).

91. Hidalgo, M. Pancreatic cancer. N Engl J Med **362**, 1605–1617 (2010).

92. Bray, F. et al. Global cancer statistics 2018: GLOBOCAN estimates of incidence and mortality worldwide for 36 cancers in 185 countries. CA Cancer J Clin **68**, 394–424 (2018).

93. Cohen, S. I. A., Vendruscolo, M., Dobson, C. M. & Knowles, T. P. J. From macroscopic measurements to microscopic mechanisms of protein aggregation. J Mol Biol **421**, 160–171 (2012).

94. Khurana, R. et al. Mechanism of thioflavin T binding to amyloid fibrils. J Struct Biol **151**, 229–238 (2005).

95. Biancalana, M. & Koide, S. Molecular Mechanism of Thioflavin-T Binding to Amyloid Fibrils. Biochim Biophys Acta **1804**, 1405–1412 (2010).

96. Eisenberg, D. S. & Sawaya, M. R. Structural Studies of Amyloid Proteins at the Molecular Level. Annu Rev Biochem **86**, 69–95 (2017).

97. Navalkar, A. et al. Prion-like p53 Amyloids in Cancer. Biochemistry **59**, 146–155 (2020).